SANDIA REPORT
SAND2007-7307
Unlimited Distribution
Printed September 2007

Operational Aspects of an Externally Driven Neutron Multiplier Assembly Concept Using a Z-Pinch 14-MeV Neutron Source (ZEDNA)

Edward J. Parma, Curtis D. Peters, David L. Smith,
Ahti J. Suo-Anttila, Terence J. Heames

Prepared by
Sandia National Laboratories
Albuquerque, New Mexico 87185 and Livermore, California 94550

Sandia is a multiprogram laboratory operated by Sandia Corporation,
a Lockheed Martin Company, for the United States Department of Energy's
National Nuclear Security Administration under Contract DE-AC04-94AL85000.

Issued by Sandia National Laboratories, operated for the United States Department of Energy by Sandia Corporation.

SAND2007-7307
Unlimited Release
Printed September 2007

Operational Aspects of an Externally Driven Neutron Multiplier Assembly Concept Using a Z-Pinch 14-MeV Neutron Source (ZEDNA)

Edward J. Parma, Curtis D. Peters, David L. Smith
Sandia National Laboratories
P.O. Box 5800
Albuquerque, NM 87185-1136

Ahti J. Suo-Anttila, Terence J. Heames
Alion Science and Technology
6000 Uptown Blvd. NE, Suite 300
Albuquerque, NM 87110

Abstract

This report documents the key safety and operational aspects of a Z-pinch Externally Driven Nuclear Assembly (ZEDNA) reactor concept which is envisioned to be built and operated at the Z-machine facility in Technical Area IV. Operating parameters and reactor neutronic conditions are established that would meet the design requirements of the system. Accident and off-normal conditions are analyzed using a point-kinetics, one-dimensional thermo-mechanical code developed specifically for ZEDNA applications. Downwind dose calculations are presented to determine the potential dose to the collocated worker and public in the event of a hypothetical catastrophic accident. Current and magnetic impulse modeling and the debris shield design are examined for the interface between the Z machine and the ZEDNA. This work was performed as part of the Advanced Fusion Grand Challenge Laboratory Directed Research and Development Program. The conclusion of this work is that the ZEDNA concept is feasible and could be operated at the Z-machine facility without undue risk to collocated workers and the public.

Acknowledgements

The authors wish to thank the Laboratory Directed Research and Development (LDRD) Program sponsors for their support of this task under the Advanced Fusion Grand Challenge. Sandia is a multiprogram laboratory operated by Sandia Corporation, a Lockheed Martin Company, for the United States Department of Energy's National Nuclear Security Administration under Contract DE-AC04-94AL85000.

Contents

Figures

Tables

1 Executive Summary

Pulse neutron radiation fields are needed for Defense Programs' requirements and for the definition and certification of weapons systems. The Sandia Pulsed Reactor III (SPR-III) at Sandia National Laboratories (SNL) is a fast-burst reactor (FBR) used for weapons effects testing. However, SPR-III has significant security costs because it uses highly-enriched uranium (HEU) which is at high risk for proliferation. The SPR-III has been shut down permanently as of October 2006. One other FBR exists at the White Sands Missile Range, but falls short of the capabilities of SPR-III. A low-enriched uranium (LEU) FBR would overcome the security cost issues, but this type of reactor has a significantly larger pulse width and is susceptible to pre-initiation from spontaneous neutrons generated in the uranium-238 (U-238).

A potential solution is to use an LEU reactor as a prompt neutron multiplier driven with an external pulsed-neutron source. This externally-driven nuclear assembly (EDNA) is a class of reactor concepts that has been proposed with various drivers. One concept uses a short-pulse electron beam impinging on a high-Z target to produce the neutron pulse. Another uses very high-energy protons (near 1 GeV) hitting a high-Z target (or the reactor itself). This report describes a concept that uses a pulsed-neutron source from a Z-pinch inertial confinement fusion (ICF) device being developed at SNL (the Z machine). The reactor concept that uses this source is called a Z-pinch Externally Driven Nuclear Assembly (ZEDNA). In principle, a strong enough Z-pinch fusion source would be all that is needed for radiation testing. But in practice, the neutron multiplication that occurs within the reactor allows the use of a Z-pinch source that is hundreds of times smaller than would otherwise be needed. This feature makes the ZEDNA concept an attractive option for replacing the SPR-III in the near term.

This report follows a previous document (Parma, et al., 2007) that described the details of the ZEDNA concept, its potential capabilities, and its ability to meet the same neutronic testing requirements imposed on the SPR-III. This report describes additional work performed in the third year of the Advanced Fusion Grand Challenge LDRD. It documents some of the key safety and operational aspects of the ZEDNA reactor concept which is envisioned to be built and operated at the Z-machine facility in Technical Area IV (TA-IV). Operating parameters and reactor neutronic conditions are established that would meet the design requirements of the system. Accident and off-normal conditions are analyzed using a point-kinetics, one-dimensional thermo-mechanical code developed specifically for ZEDNA applications. Downwind dose calculations are presented to determine the potential dose to the collocated worker and public in the event of a hypothetical catastrophic accident. Current and magnetic impulse modeling and the debris shield design are examined for the interface between the Z machine and the ZEDNA. The conclusion of this work is that the ZEDNA concept is feasible and could be operated at the Z-machine facility without undue risk to collocated workers and the public.

Although this work is primarily focused on Defense Programs needs for certification of weapons systems, the ZEDNA machine could play an important role in developing advocacy for a future nuclear waste transmutation application, since it would produce vital data on fission-fusion hybrid systems. The ZEDNA would provide testing capabilities to validate transmutation kinetics models (Cipiti, et al., 2006).

2 Introduction

The needs for an EDNA device and the proposed ZEDNA concept have been described in detail in a previous report (Parma, et al., 2007). The basic premise is that there is a need for a short pulse neutron source that can deliver neutron fluences on the order of 6.1×10^{14} nvt with a pulse width of about 75 μs. The SPR-III reactor is an FBR at SNL that can meet these requirements but has been permanently shut down due to the security cost associated with protecting the HEU fuel. An LEU FBR would not be capable of meeting the pulse-width requirement and would not be reliable due to an inherently high pre-initiation probability. An EDNA concept would use an external pulse neutron source to generate the initial population of neutrons that would then be multiplied in a reactor that is in a supercritical state. A concept called the ZEDNA has been proposed that would use the Z-machine located in TA-IV at SNL to produce the initial pulse of neutrons. The ZEDNA reactor would be in close proximity to the source to allow for effective multiplication of the initial neutrons and generate the neutron fluence and pulse widths similar to that which the SPR-III reactor can produce.

This report follows a previous document (Parma, et al., 2007) that described the details of the ZEDNA concept, its potential capabilities, and its ability to meet the same neutronic testing requirements imposed on the SPR-III. This report includes additional work performed in the third year of the Advanced Fusion Grand Challenge LDRD. This report documents some of the key safety and operational aspects of the ZEDNA reactor concept which is envisioned to be built and operated at the Z-machine facility in TA-IV. Operating parameters and reactor neutronic conditions are established that would meet the design requirements of the system. Accident and off-normal conditions are analyzed using a point-kinetics, one-dimensional thermo-mechanical code developed specifically for ZEDNA applications. Downwind dose calculations are presented to determine the potential dose to the collocated worker and public in the event of a hypothetical catastrophic accident. Current and magnetic impulse modeling and the debris shield design are examined for the interface between the Z machine and the ZEDNA. The conclusion of this work is that the ZEDNA concept is feasible and could be operated at the Z-machine facility without undue risk to collocated workers and the public.

The ZEDNA concept is comprised of a small reactor situated just below the fusion target of the Z machine, as shown in Figure 2-1. The reactor fuel consists of annular discs of uranium metal alloyed with 10 percent molybdenum (U-10Mo). The enrichment is slightly less than 20%, which allows ZEDNA to be characterized as LEU and minimal security costs. The center of the reactor core has a cavity 20 cm in diameter to accommodate the test objects. The nominal pulse environment desired within the cavity is a total fluence of 6.1×10^{14} n/cm^2 with a full-width half-maximum (FWHM) of 76 microseconds. These conditions replicate the conditions within the SPR-III reactor. The ZEDNA would be driven by approximately 4×10^{15} 14-MeV neutrons produced by the Z machine with a D-T reaction. Scaling from past Z performance for D-D yields, this requirement does not seem unrealistic for the near future. However, a D-T yield of this magnitude has yet to be demonstrated on Z.

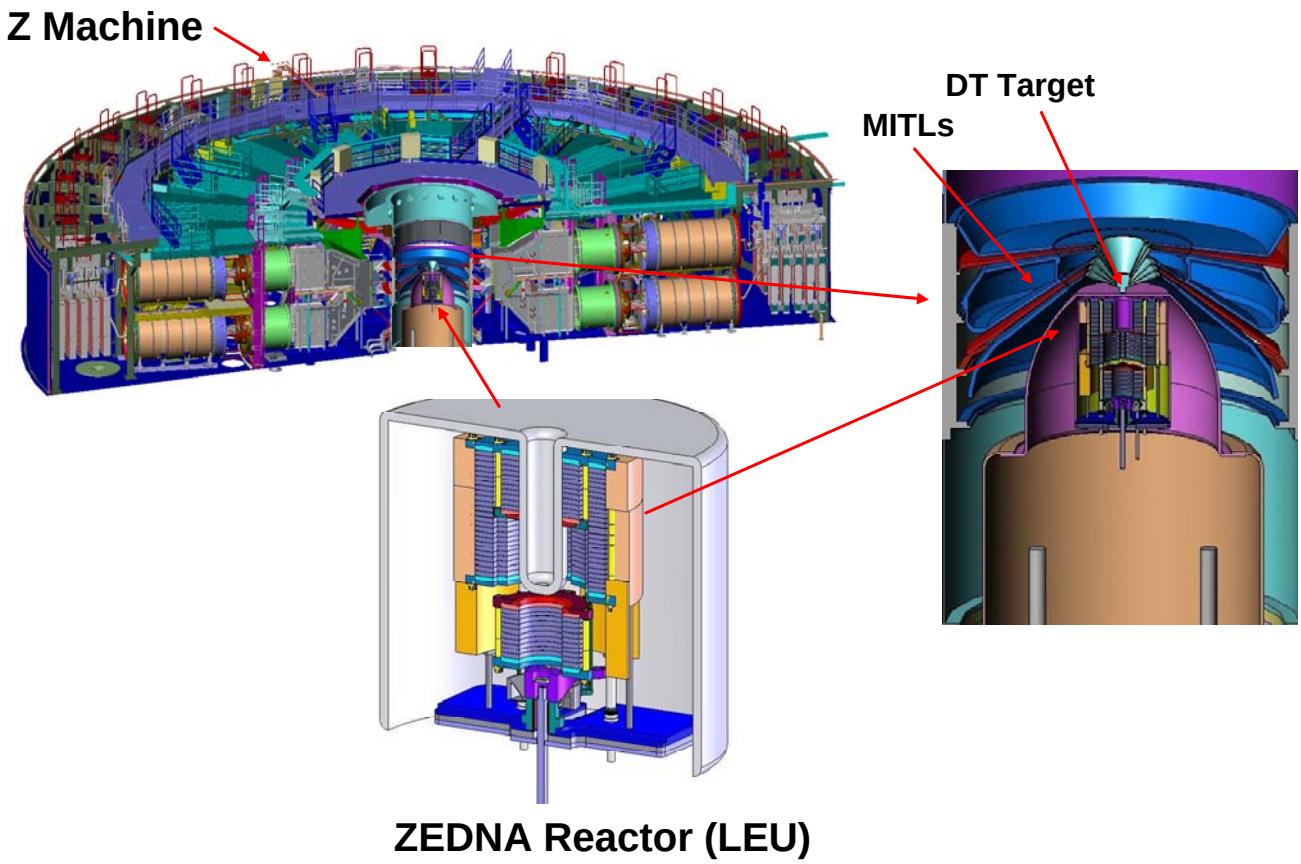

Figure 2-1. Overview of the ZEDNA Concept and the Z Machine.

The reactor would be stored in the basement below the Z facility in a shielded storage vault when not in use. When a test is needed, the experimenters would set up their test article below the Z machine. The experimenters would place the test object into a metal basket supported from a light aluminum table, similar to the method used in SPR-III. After the experimenters left the basement and the area was secured, the reactor would be moved on tracks, via remote handling, until it was below the basket and table. A modified vacuum chamber at the center of the Z machine would allow for the experiment package to be picked up by the reactor and raised to within close proximity to the Z target. A heavy-duty lift would move the reactor upward allowing the basket to enter the reactor cavity and lifting the table. The reactor would continue upward to its final position in close proximity to the target. The reactor would be operated in air within its own confinement vessel. The modified vacuum chamber boundary would be formed by a cylinder and thimble inserted from below to allow access to the Magnetically Insulated Transmission Line (MITL) and fusion target. Only a pumped annular region and the MITL itself would be in a vacuum. The top of the thimble would be thick enough to withstand the impact of debris created from the Z shot.

The Z machine would be charged (charging time approximately three minutes) and the reactor brought to a multiplication (k_{eff}) of 1.006, which is \$0.80 supercritical - equivalent to a reactor period of ~1 second (the reactor period is defined as the time required to change the reactor power by e^1=2.72). The reactor in this reactivity state allows several seconds for the Z machine to fire. The neutrons produced by the shot are multiplied within the reactor by about a factor of

750. The reactor "pulse" is terminated by the depletion of the prompt neutrons, since the reactivity would be below the prompt-critical condition (reactivity equal to $1.00). The reactor would then shut down by moving the control reflector elements to their least reactive state. In addition, an inherent negative reactivity effect from thermal expansion of the fuel ensures reactor shutdown.

After the shot, the reactor would be lowered allowing the table and basket to slide out of the cavity for later access. The reactor would be moved remotely to the shielded storage vault. The experimenters would then have access to the test object after a short wait time, similar to the process in SPR-III.

The results of the calculations for the pulse yield for various values of k_{eff} in the ZEDNA reactor are plotted in Figure 2-2. The source value has been scaled so that the integrated fluence in the central cavity of the reactor is equal to that of the SPR-III (6.1×10^{14} n/cm^2). This summary plot shows the design options for the ZEDNA system. As the capability of the Z machine to produce fusion neutrons increases, the amount of reactivity needed for the reactor can be decreased. Eventually, this could allow operation of the reactor in the subcritical region, if desired. Or, if there is an interest in the difference in pulse width on radiation effects, the pulse width can be changed while the total fluence is kept fixed simply by adjusting the Z yield and the reactor k_{eff}.

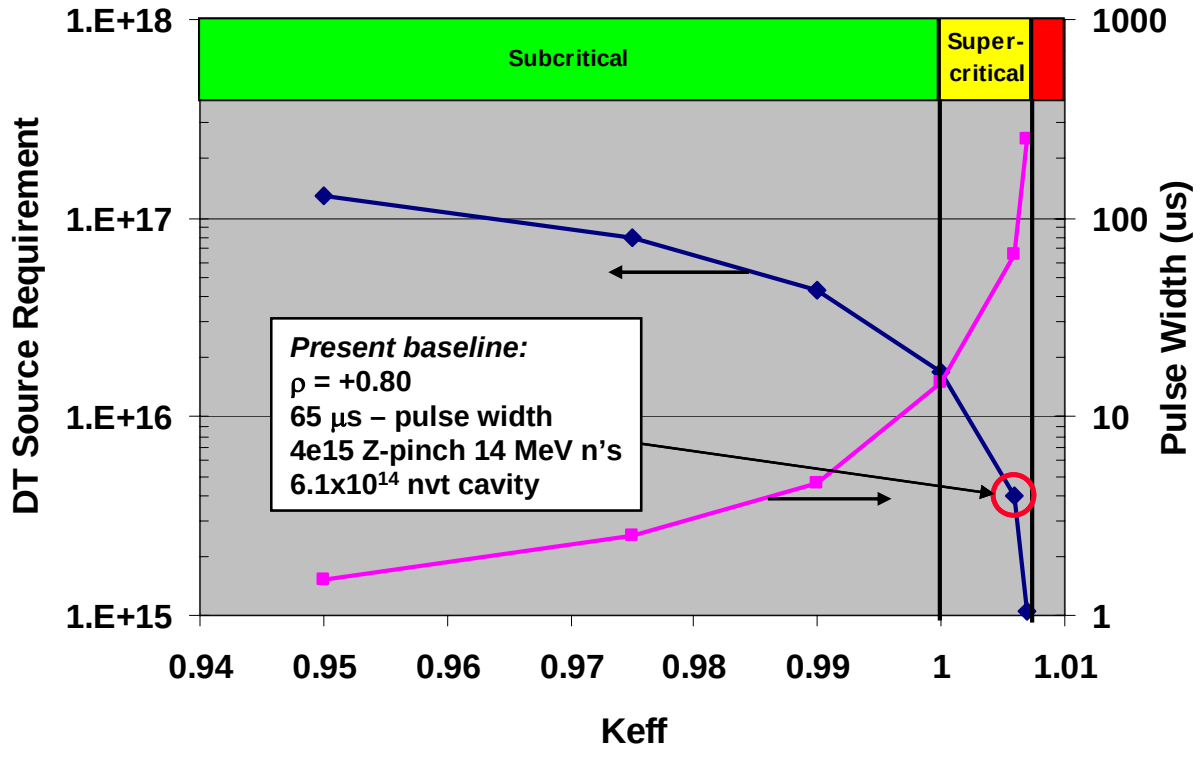

Figure 2-2. Pulsed Source Requirement vs. k_{eff} to Yield 6.1×10^{14} n/cm^2.

The ZEDNA concept is technically feasible. The purpose of this work was to examine the safety and operational conditions of the concept in greater detail. This investigation allows for the safety risk associated with the construction and operation of the ZEDNA device to be more fully understood.

3 Operation and Control of the ZEDNA

The pulse operation of an EDNA device is different than that of an FBR. An FBR must operate in the super-prompt critical regime to generate a pulse and must maintain the weak source conditions, prior to the rapid addition of reactivity by the pulse element. An EDNA device operates in a supercritical, critical, or subcritical state with a power level of milliwatts or watts, prior to the external pulse of neutrons. An FBR must have inherent negative reactivity feedback to terminate the pulse excursion. An EDNA device does not require the inherent shutdown to terminate the pulse, since the device operates in a sub-prompt critical condition. Both devices require engineered shutdown and control mechanisms to safely operate and shutdown the reactors.

An EDNA device can operate in a supercritical, critical, or subcritical state, depending on the required prompt neutron multiplication to attain the desired neutron fluence. The pulse of initial, externally-produced neutrons can be external or internal to the core (within the fuel or cavity region), and can have any energy spectrum. The effectiveness of the initial neutrons in fission production of the first generation of prompt neutrons is dependent on the source geometry and initial neutron energy spectrum. The external neutron pulse must be of short duration compared to the desired pulse duration for the reactor. For a desired pulse width on the order of 80 μs, the external pulse neutron duration must be less than ~5 μs. A Z-machine neutron pulse is on the order of a few nanoseconds in width.

The prompt neutrons, produced by fission caused by the initial external neutrons, are multiplied in the reactor depending on the reactivity state of the reactor. Since the reactor is sub-prompt critical, it cannot sustain itself using the prompt neutrons alone, as it can for an FBR that is super- prompt critical. Hence, for an EDNA device, the initial set of neutrons creates a subsequent set of prompt fission neutrons that, in turn, creates another generation of prompt fission neutrons. However, the quantity of prompt neutrons in each subsequent generation is less than the preceding one, and in time, eventually decreases to zero. This process creates a pulse which has a rise time equal to the duration of the initial external neutron pulse and a fall time which has an exponential decay that is characteristic of the reactivity state of the reactor.

Figure 3-1 shows an example comparing a typical EDNA-type pulse with a SPR-III FBR pulse. The plot shows reactor power as a function of time. The reactor power is proportional to the neutron population in the system. The sharp rise in power (at time equal to zero) and exponential decay is apparent in the EDNA pulse. The SPR-III pulse is more symmetric because it takes time for the chain reaction of the super-prompt critical reactor to build up the neutron population, and then thermal feedback drives the reactor sub-prompt critical. It is not clear which shape is better for weapons effects testing, EDNA or SPR-III. It depends on the scenario being considered. In general, the test community considers the total fluence and pulse width to be the most important factors, so the difference in pulse shape is not considered very important.

Note that the SPR-III FBR pulse is to the right of the EDNA pulse. For the SPR-III calculation, the reactivity was added at time equal to zero and the initial power level was assumed to be 1 watt, but ~20 e-folding periods are required before a significant power level is achieved. Starting at 1 watt, and using a reactor period of 18 μs, a power level of 1×10^9 watts (1000 MW) is not achieved until ~360 μs. For the EDNA device, the reactor is on a positive period (supercritical), and the pulse occurs immediately upon the injection of the external source neutrons.

The total neutron fluence (neutron flux times time, sometimes referred to as nvt - neutrons times velocity times time) generated within the EDNA or FBR cavity will be directly proportional to the integral under the pulse curve. The fluence and energy deposited in the EDNA increase with the external neutron source strength and the multiplication of the reactor. The pulse width for the EDNA varies with the multiplication of the reactor. This gives some flexibility to the EDNA device in simulating radiation environments of interest. The pulse width can be changed while keeping the total fluence fixed by adjusting the external source intensity.

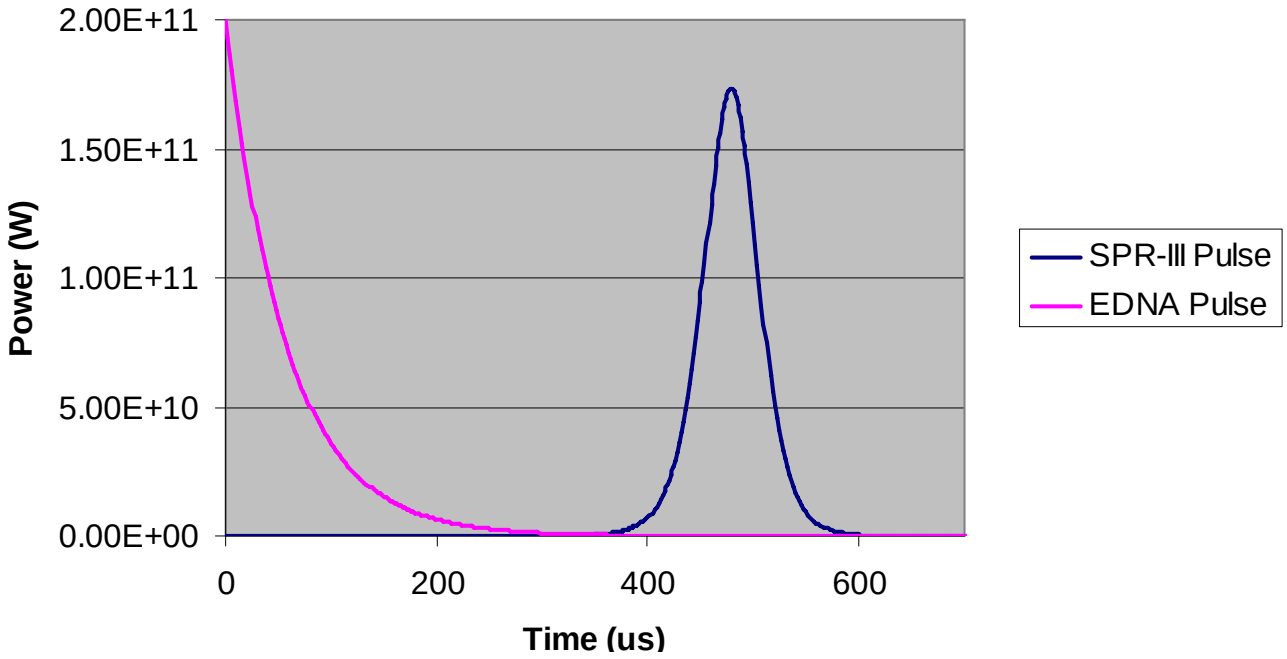

Figure 3-1. ZEDNA Pulse (left) and SPR-III Pulse (right).

3.1 ZEDNA Design and Reactivity Control

The ZEDNA reactor design concept is shown in Figure 3-2. The concept is shown with and without the reflector elements and containment shroud to allow for a more visual representation of the design. The reactor itself is made up of individual metallic fuel plates that are very similar to the SPR-III reactor fuel plates. The fuel plates are U-10Mo with uranium enriched to less than 20% (as compared to SPR-III with uranium enrichment of 93%). The plates are stacked and held together using high-strength steel rods.

For the ZEDNA design, there are essentially three sets of stacked plates to form three regions of the core. The outer region and upper/inner region of the core are fixed in place. A gap separates the inner and outer core regions. The lower/inner region is movable, which allows it to be mated or separated from the upper/inner region. This is similar to the SPR-III design which has two core regions. The lower portion, known as the safety block, is movable to allow for a large reactivity reduction, when desired. The movable lower/inner region would operate using a drive mechanism and electromagnet which allows it to couple to the upper/inner region. The drive mechanism, electromagnet, and coupling mechanisms are below the core support plate. The two inner core regions have their own mounting fixtures and steel rod supports. The core is designed with segmented fuel plates, rather than large diameter fuel plates, to facilitate manufacturability

and allow for the decoupling of the radial and tangential stresses that develop during a pulse. The inner portion of the core has roughly the same outer diameter as the SPR-III reactor. The lower/inner movable region is moved up and down by remote operations at the control room. During a SCRAM,[1] the movable region is dropped by gravity from its "full up" position to its "full down" position by de-energizing the electromagnet. For a large pulse, the expansion of the core in the axial dimension would also cause enough separation from the electromagnetic coupling to break the magnetic flux and drop the lower core region. When this occurs, the lower region is essentially "pushed" away from the upper region due to the rapid axial expansion.

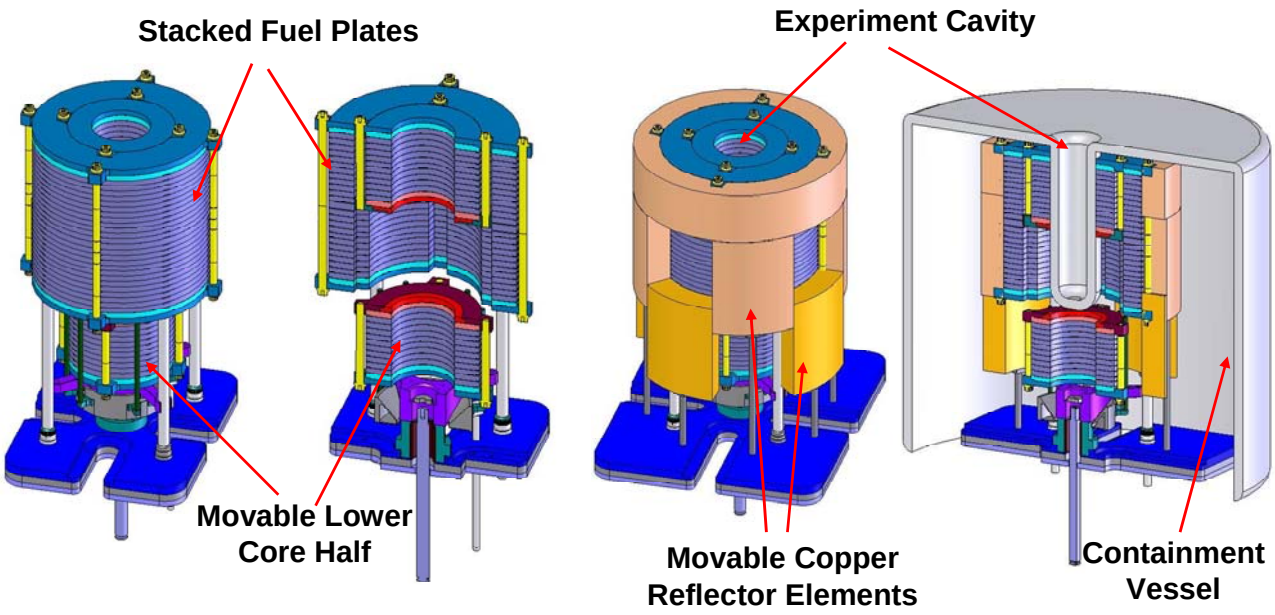

Figure 3-2. ZEDNA Reactor Design Concept.

The control of the ZEDNA is established by using copper reflector elements that surround the core and can be moved up and down using electromagnetically-coupled drive mechanisms. Four movable reflector elements are depicted in Figure 3-2. The movable elements can be positioned at any location between "full up" and "full down" and are dropped by gravity to their "full down" position during a SCRAM. The SPR-III operates in a similar manner using movable copper reflector elements. The SPR-III also includes an aluminum pulse element that can be inserted rapidly using a pneumatic drive system. This type of rapid insertion is not required for the ZEDNA reactor since it does not pulse in the same manner as an FBR.

[1] SCRAM is a term used in nuclear engineering to denote the rapid shutdown in the power level of a reactor core by a mechanical means with the addition of negative reactivity. The original term, SCRAM, stood for Safety Control Rod Ax Man. Today it is used to denote a fast mechanical shutdown mechanism that inserts large amounts of negative reactivity quickly allowing for a rapid drop in the power level. The signal to deploy this mechanism could be initiated manually or by instrumentation that detects a condition outside of the normal operating range.

Reactivity control for the ZEDNA would be only through remote operations at the control room. The control system would be made up of neutronic instrumentation and automatic and manual shutdown (SCRAM) systems. The reactivity would controlled by the operation of the movable lower portion of the core, and by raising and lowering the copper reflector elements.

A containment or confinement vessel that surrounds the core region is shown in Figure 3-2. SPR-III does maintain a shroud that allows for nitrogen gas cooling after a pulse, but SPR-III does not maintain a containment or confinement barrier around the core region. Fission products are thus allowed to escape from the core and contaminate the internal surfaces of the SPR-III room. For ZEDNA, a barrier would be required, since it would not be acceptable to contaminate the basement and lower portion of the Z vacuum stack with fission products.

3.2 Operating Sequence

The operation of the ZEDNA device would be as follows. Once the Z-machine was set up for a pulse and the experiment package was in place on a spider arrangement, the basement and high bay zones of the Z facility would be cleared of all personnel and placed in a secured condition. ZEDNA would be moved from its storage vault in the basement to below the experiment package and source/vacuum stack region of the Z machine using a specially-designed track and remote-control mechanism. The ZEDNA would include all of the mechanical, electrical, and instrumentation components to move and operate from the control room. The ZEDNA control room would be located near the current Z-machine control room. The ZEDNA would be raised from its carriage using a hydraulic or scissor-jack mechanism, and mated with the experiment package and then the Z source. With the ZEDNA mechanically coupled to the pulse source, the reactor would be ready to operate.

Certified reactor operators would coordinate the startup and pulse sequence with the Z-machine operators. Neutronic instrumentation and shutdown systems would be fully functional and operating during the startup sequence of ZEDNA. A startup procedure would be followed by the reactor operators to ensure the proper operation of all instrumentation, equipment, alarms, etc. When ready to operate, the operating sequence would commence. A small, steady-state neutron source (such as an AmBe or PuBe source) would be raised near the fuel to ensure a sufficient neutron population during startup. The movable lower portion of the core would be raised and electromagnetically coupled to the upper portion of the core. The reactor would be brought to the delayed critical condition using the reflector elements. The neutron source would then be removed and the reactor power would be adjusted to a very low level, for example, 1 watt or less. When the Z-machine was within a few seconds of pulsing, the reactivity would be added by adjusting the control reflectors to the required positive reactivity addition, for example, \$0.80. The reactivity would not need to be added rapidly. At an addition rate of \$0.05/sec, \$0.80 of reactivity would be added in 16 seconds. Once the \$0.80 of reactivity was added, the reactor power level would be increasing exponentially with a period (e folding time) of ~0.9 seconds. This means that the power level of the reactor would be increasing by e^1 (2.72) every 0.9 seconds.

Assuming an initial power level of 1 kW, and a total reactivity addition of \$0.80, the reactor power level 5 seconds following the addition would be ~260 kW. The amount of energy deposited in 5 seconds would be about 0.23 MJ. This is a trivial quantity compared to ~25 MJ of energy that will be generated in the reactor following the pulse from the multiplied neutron source. After the pulse occurs, a SCRAM signal would initiate the reactor shutdown. This

would occur by de-energizing the electromagnets, which are part of the element drive mechanisms. The movable reflector elements and the inner movable core region would fall by gravity to their least reactive positions. Negative reactivity would also be added by inherent negative temperature effects, similar to SPR-III. These effects are analyzed in Section 5 of this report.

The EDNA reactor would be required to maintain both inherent and engineered mechanical safety features to ensure the reactor could be shut down rapidly by adding negative reactivity. The reactor and control system will need to be over designed with excess capacity and redundant safety features to account for potential accident conditions, such as the addtion of too much reactivity, or the production of too many pulse neutrons by the Z source.

3.3 Reactivity Calculations

The control of the ZEDNA prior to the initiation of the external pulse source is described in this section. Section 5 describes the feedback of the ZEDNA during and after the pulse, as well as accident conditions that could be postulated for the ZEDNA. Prior to the external neutron pulse, the reactor must be super critical with the correct amount of reactivity such that the desired prompt neutron multiplication is achieved. Although ZEDNA would be at a very low power level during this operation prior to the pulse, the reactor must still be controlled to ensure that the reactivity addition is limited, and that the power level does not exceed a significant value. This is achieved by using trained and certified operators, administrative procedures, and engineered control and safety features. The engineered control features would include a limit on the reactivity addition rate and a "rod block" that would not allow addition of more reactivity if the reactor period became too short. Safety equipment would include instrumentation that would provide reactor trip or SCRAM, if conditions exceed the operating range. Safety features would include a period trip (SCRAM if the reactor period becomes too small) and a power level trip (SCRAM if the reactor power becomes too high). In addition, other safety features would be included such as a time-out trip (SCRAM if the neutron pulse is not initiated within a given time interval following a "ready-to-fire" signal from the reactor console). Parametric analysis must be performed to ensure that the delay time between initiation of a SCRAM signal and the start of gravity fall of the control reflectors is acceptable.

The transient behavior of ZEDNA prior to the pulse can be modeled using point-reactor kinetics with delayed neutrons. A fundamental issue that must be addressed for a control/shutdown system is if the reactor can be controlled and shut down without adding too much energy to the system that could jeopardize the integrity of the fuel. The following analysis will be used to determine: 1) the limit that should be imposed on the control element reactivity addition rate; 2) the effectiveness in using a "rod block" condition and the value of the limiting period; 3) the proposed period trip condition; 4) the proposed power level trip condition; and 5) the maximum delay time from SCRAM initiation to control element release.

In order to achieve the desired goal of the ZEDNA cavity fluence, using the projected D-T neutron source potentially available in Z, the ZEDNA must be super critical with a reactivity of \$0.80 or more, as shown in Figure 2-2. Once the critical condition is established at a low power level for the reactor, the reactivity must be added either by adjusting the control reflector positions, or possibly, by inserting a pulse-type element similar to that used in SPR-III. The stable period associated with the addition of \$0.80 is 0.9 seconds. This implies that the reactivity must be added relatively quickly, and the pulse must occur within a few seconds following the

addition. Although most research reactors and no power reactors operate with this short of a period, it is not necessarily unsafe to do so, given that enough safety features are in place to ensure that the fuel cannot be overheated by the addition of too much energy. In fact, the SPR-III reactor is routinely operated in this fashion, in what is commonly known as the mini-pulse mode. For the ZEDNA, the safety issues include limiting the total amount of reactivity added and the total energy deposited prior to the external neutron pulse. It is desirable to add the reactivity with a relatively slow ramp rate (tens of cents per second, compared to dollars per second), to ensure that the addition of $0.80 will not be exceeded. However, if the reactivity is added too slowly, the energy deposited during the ramp could become too large and unacceptable.

Figures 3-3 and 3-4 show the result of power versus time for ramp reactivity addition rates of $0.05/s, $0.10/s, $0.20/s and $30/s, an initial starting power level of 1.0 W, and total reactivity additions of $0.80 and $0.90, respectively. The $30/s ramp is shown for perspective if a pneumatically driven reflector element was used to add the reactivity after the critical condition was established. The other values represent typical reactivity addition rates for control elements.

In Figure 3-3, reactivity of $0.80 is added and a stable period of ~0.9 seconds results. For the ramp reactivity a addition of $0.05/s, the reactor power is ~300 W when all of the $0.80 is added (at 16 s). The amount of energy deposited is the integral under the power curve. Again, for the $0.05/s case, the energy deposited at 16 s is ~300 J. Three seconds after the reactivity is added (19 s), the power level is 9.3 kW and the energy deposited is 8.1 kJ. Five seconds after the reactivity is added (21 s), the power level is 93.5 kW and the energy deposited is 81.3 kJ. Seven seconds after the reactivity is added (23 s), the power level is 937 kW and the energy deposited is 913 kJ. These results indicate that the reactivity can be added at a relatively low rate ($0.05/s) and can achieve acceptable conditions for the Z-machine timing. Under this scenario, the ZEDNA control system would send a signal to the Z-machine control system when the full $0.80 of reactivity was added. The Z-machine would be given 5 seconds in which to pulse. This should be achievable for the Z machine. If the Z machine did not fire within this time interval, the timer shut down would SCRAM the reactor. Faster ramp rates would also achieve this goal. However, the faster rates could lead to the potential for the addition of too much reactivity. For the SPR-III reactor, reactivity is added at $30/s to within one cent every time the reactor pulses. Therefore, using a pulse element to add the $0.80 of reactivity is acceptable. Specific operating procedures, similar to that used for SPR-III operations, would be followed to ensure the reactivity of the pulse element is known.

Figure 3-4 shows the same calculations but with a reactivity addition of $0.90. For the ramp rate of $0.05/s, $0.90 is added in 18 seconds. At 18 seconds, the power level is 26.8 kW and the energy is 9.1 kJ. Three seconds later (21 s), the power level is 311 MW and the energy is 99.9 MJ. These values would not be acceptable and would require a smaller time-out interval. A one-second interval would be more appropriate. Increasing the ramp rate would not allow for a longer time-out interval, since the period for a $0.90 addition is ~0.3 seconds.

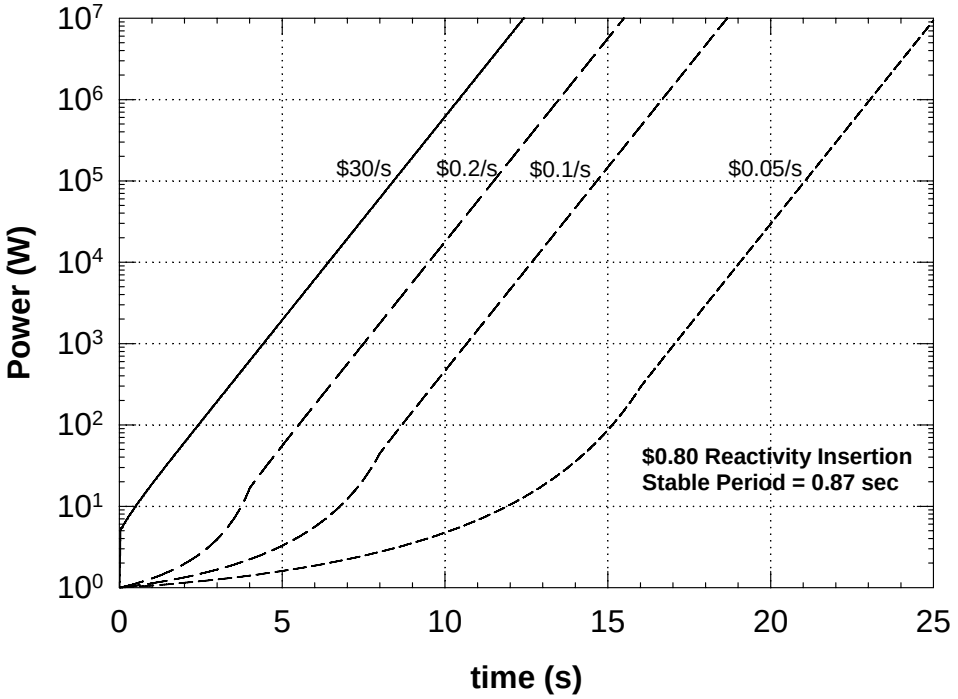

Figure 3-3. Power Versus Time for a $0.80 Reactivity Addition and Different Ramp Rates.

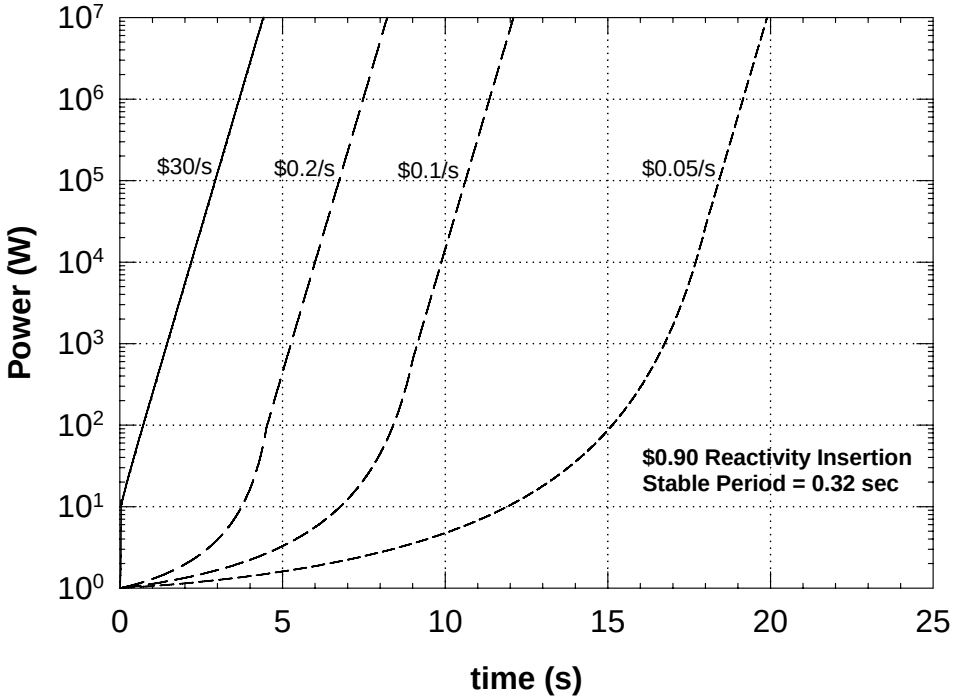

Figure 3-4. Power Versus Time for a $0.90 Reactivity Addition and Different Ramp Rates.

Increasing the reactivity addition beyond $0.90 would not be practical for an EDNA type device for two reasons. One: although the prompt multiplication increases with increasing reactivity, the pulse width also increases with reactivity. From Figure 2-2, the pulse width for a $0.80 reactivity addition is ~64 μs, which is an acceptable value. However, the pulse width for a $0.90 reactivity addition is ~300 μs, which is an unacceptable value in meeting the SPR-III like goals. However, larger pulse widths may be desirable for testing applications currently unavailable for SPR-III. If this were the case, then a larger reactivity addition could be an important design consideration. Two: the reactor period becomes very short above $0.90 (less than 0.3 seconds), which does not allow a very large time window for the Z pulse to occur prior to the reactor overheating. For larger reactivity additions, a pulse element would probably be required with more precise timing with the Z-machine firing.

Figures 3-5 and 3-6 show similar calculations using a rod block feature built into the control system. Using this approach, the control element reactivity addition would be limited by the reactor period. If the period became too short, the system would not allow the control rod drives to operate. This would not apply to a pulse element driven system, if used. The results show that for a rod block period limitation of 0.7 seconds (Figure 3-5), $0.83 of reactivity can be added to the system. For a 0.5 second period block (Figure 3-6), $0.86 of reactivity can be added. If the control elements were used to add the reactivity prior to a pulse, the rod block feature would ensure that the reactivity addition was limited to within these values.

Figures 3-7 and 3-8 show results for a SCRAM initiation if the period becomes too short. This safety feature would be in place if the rod block did not perform properly or if reactivity was added by another means unintentionally, such as inadvertent movement of the ZEDNA during the operation sequence. Figure 3-7 shows the results for a 0.5 second period trip and Figure 3-8 for a 0.3 second period trip for ramp addition rates of $0.05/s, $0.10/s, and $0.20/s. Since some amount of time is required to allow for the trip signal to reach the magnet power supply, the magnetic flux to diminish, and the control elements to begin to fall, delay times of 0.25 and 0.5 seconds are analyzed. The results show that for these ramp rates, both period values and delay times are acceptable.

In addition to these safety features, a power level trip would be used to SCRAM the reactor if the power level exceeded a set value. A power level trip will ensure not only a limit on the reactor power prior to the pulse, but will ensure that a SCRAM signal is initiated during the pulse. The delay in the signal will allow for the pulse and prompt multiplication to occur, but will ensure that negative reactivity is added to the system by a mechanical means immediately following the pulse. A value of 1 MW with a delay time of 0.5 seconds would be acceptable.

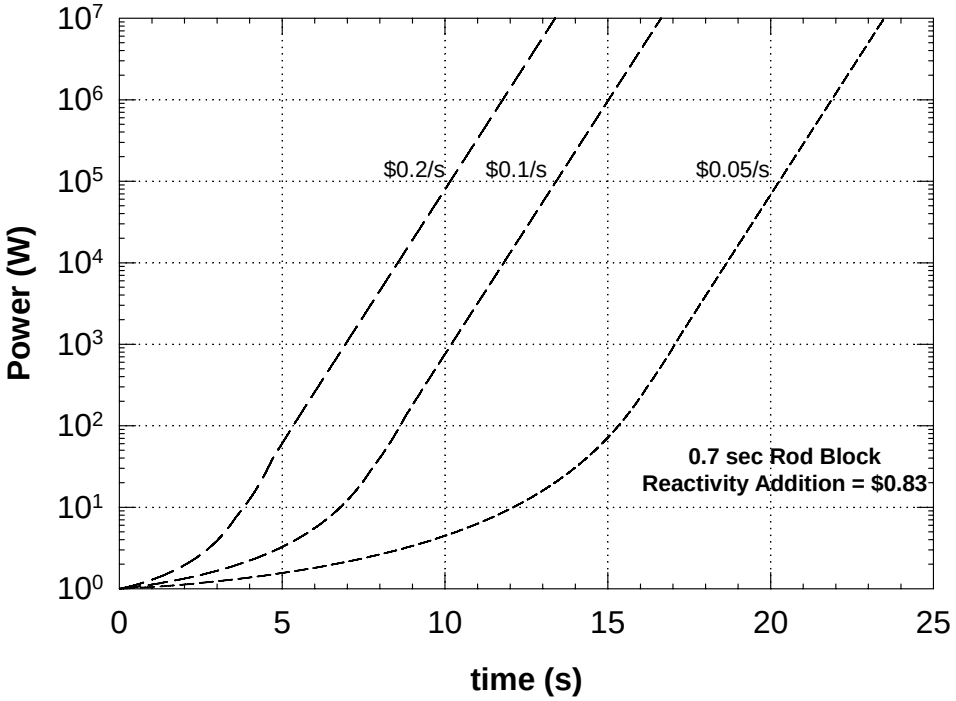

Figure 3-5. Power Versus Time for a 0.7 Second Rod Block and Different Ramp Rates.

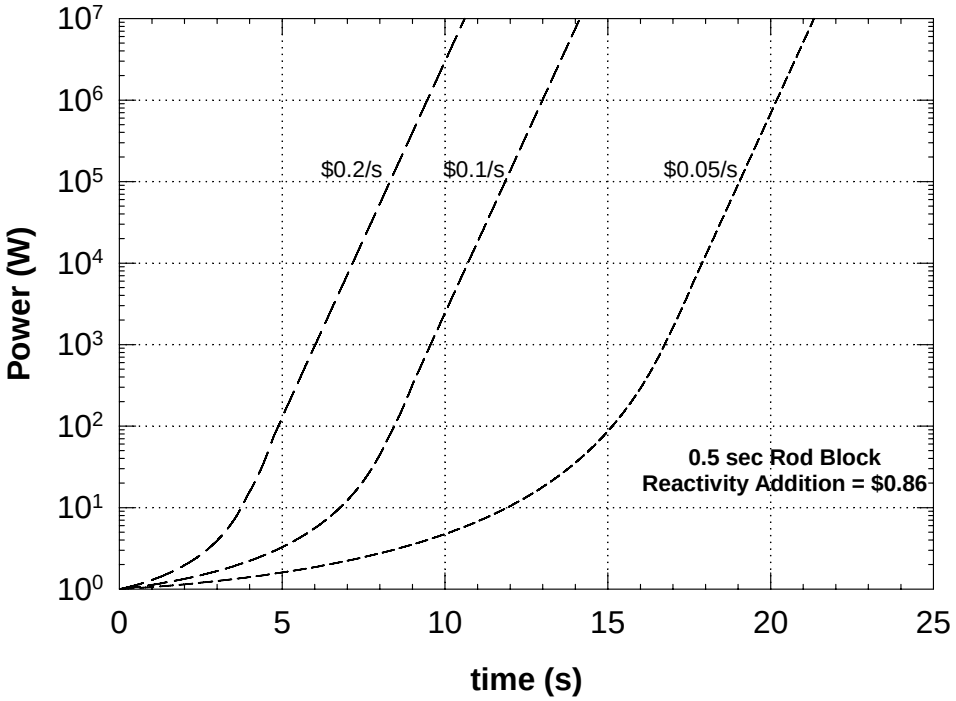

Figure 3-6. Power Versus Time for a 0.5 Second Rod Block and Different Ramp Rates.

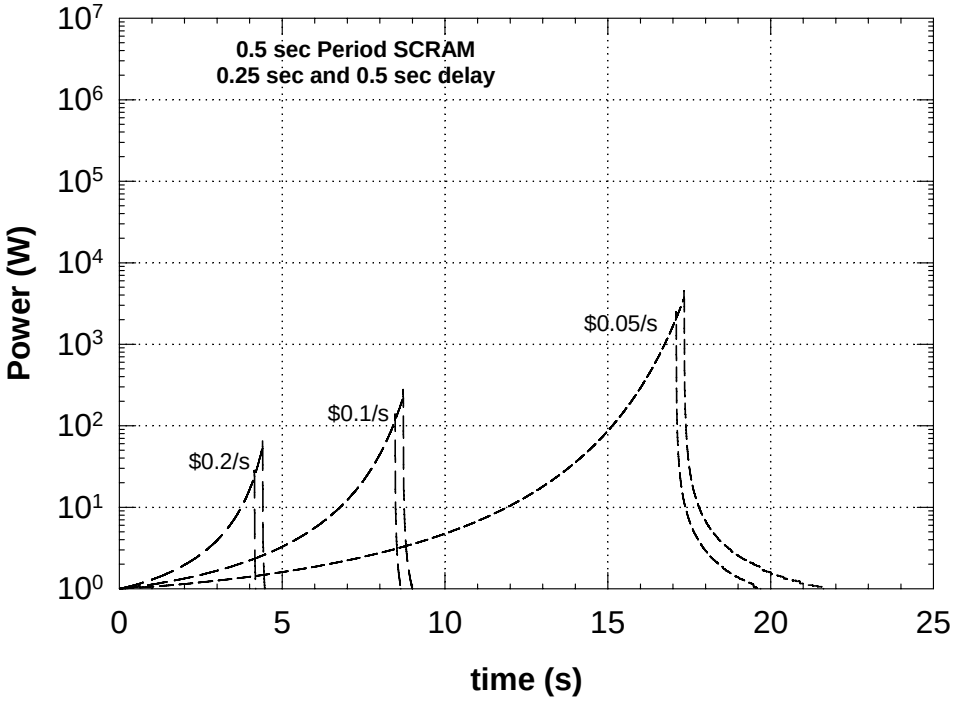

Figure 3-7. Power Versus Time for a 0.5 Second Period Scram and Different Ramp Rates.

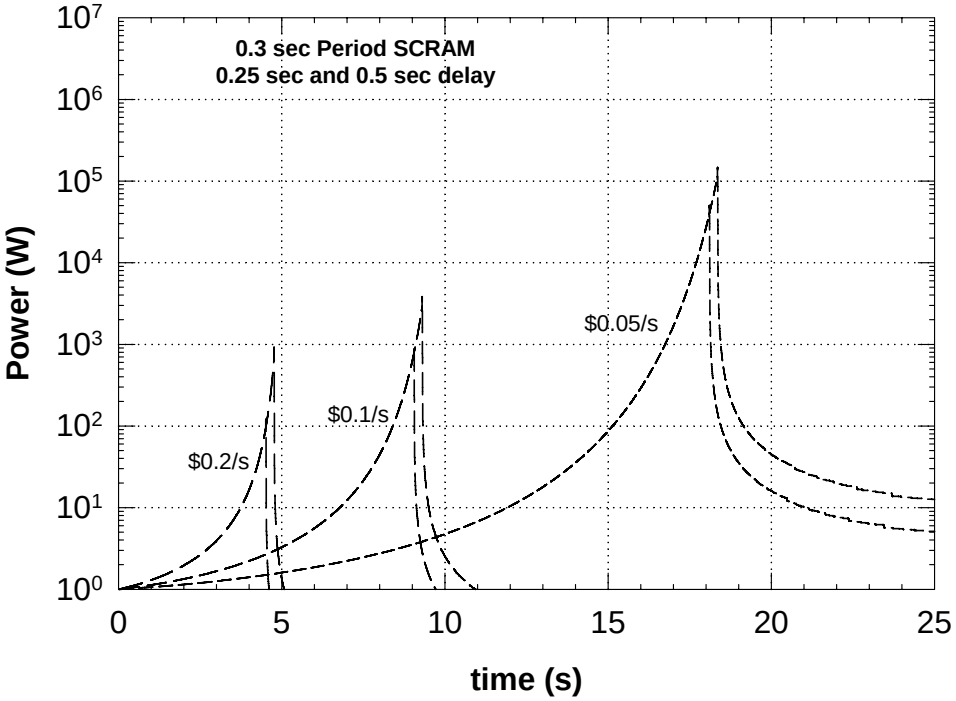

Figure 3-8. Power Versus Time for a 0.3 Second Period Scram and Different Ramp Rates.

3.4 ZEDNA Control Parameters Summary

From the previous analysis, a number of control and safety parameters were derived for the ZEDNA to control reactivity addition. Prior to the Z pulse, the ZEDNA will be brought to a delayed critical configuration at a low power level (10 W or less). The delayed critical condition will be established by certified reactor operators using the following proposed methodology.

1. The Z facility basement and high bay will be cleared and secured.
2. Ventilation and the control console will be operating.
3. ZEDNA will be remotely moved from its storage location in the basement to below the experiment package and pulse source.
4. ZEDNA will be raised to mate with the Z source.
5. The startup procedure will be performed to ensure all equipment and control and safety channels are functioning properly.
6. The steady-state neutron source will be raised to provide a source of neutrons for establishing a delayed critical condition.
7. The movable portion of the reactor will be raised and electromagnetically coupled to the upper region of the core.
8. The control reflector elements will be raised and adjusted to reach the delayed critical condition.
9. The steady-state neutron source will be lowered since it is no longer required once the delayed critical condition is established.
10. The power level of ZEDNA will be adjusted to below 10 W.
11. A signal will be sent to the Z machine operators to begin charging procedure.
12. A signal will be sent from the Z machine to the ZEDNA console when the Z machine is charged and ready to fire.
13. The required additional reactivity ($0.80) will be added to the ZEDNA either by the control elements or a pulse element.
14. A “fire” signal will be sent to the Z-machine console.
15. A time-out interval will SCRAM the reactor if the Z-machine fails to fire within the time period.
16. A successful firing of the Z machine will result in a pulse. Temperature and neutronic instrumentation will record the event.
17. During the pulse, a high power SCRAM will be initiated. The control elements and movable core region will drop after the pulse ensuring reactor shutdown.
18. The reactor will be lowered and moved back into the shielded storage vault.
19. The Z facility high bay and basement will be cleared by radiation health physics personnel.

Two methods are proposed for adding the $0.80 of reactivity prior to the pulse. The same control reflector elements used to establish the delayed critical condition can be used to add the reactivity, or a pulse-type element that is pneumatically driven can be employed. Either method would be acceptable and would work satisfactorily for this application. Using a pulse element would require additional procedural steps to ensure the reactivity worth prior to insertion. The following limits have been analyzed in the previous section assuming the control elements are used to add the reactivity.

- Reactivity limit $0.80 to $0.90 depending on desired multiplication and pulse width
- Control element ramp reactivity addition limit = $0.05/s
- Rod block period = 0.5 s (limits reactivity addition to $0.86)
- Period SCRAM = 0.3 s
- Delay time limit (time between SCRAM initiation and start of element drop) < 0.5 s
- Time-out interval < 5 s
- Power level SCRAM < 1 MW

These parameters are the proposed values that would allow for the ZEDNA reactor to operate in a safe and reliable manner. A documented safety analysis (DSA) would be used to further investigate the operational control and limits of the system.

4 MITL Design

The ZEDNA interface options with the Z machine were presented in detail in the previous ZEDNA report (Parma, et al., 2007). Two of the key elements of the interface design are the MITL and debris shield. The MITL, debris shield, and source configuration must be designed to allow for close proximity of the source with the ZEDNA to allow for the greatest effectiveness of the source neutrons with minimal risk of energetic debris impinging on the reactor. The MITL efficiency, in terms of current-to-source transmission, must be evaluated to ensure that a contorted MITL is acceptable with minimal technical risk. This section summarizes the continued work performed in this area during the past year.

Understanding the mechanics of how the offset-extended MITL fails and breaks apart following the power generating pulse in a full scale ZR shot scenario is an important issue for ZEDNA. Containing, collecting, and safely removing the resulting dust, debris, and shrapnel are important steps that must be proceduralized, among many others, in order to have a successful and smoothly operating test facility. Beryllium handling and neutron activation of materials within the vacuum stack are also important considerations in the facility.

In this section the model of the current and the dynamic pressure pulse along the offset MITL is presented. The results can be used as inputs to other models, such as CTH and ALEGRA, that will aid in characterizing the debris shield and containment wall impacts. The primary software tool used in this analysis is the Micro-Cap network solving code applied innovatively to represent different configurations and different degrees of resolution. The following discussion uses the ZR Z-pinch expected nominal parameters which are 26 MA, 6 MV, and 100 ns. The current trapped in the vacuum section and the associated pressure pulse are assumed to gradually decay over tens of microseconds. This modeling approach was also employed to support the ZIPS Task 3.4 of the LDRD Grand Challenge, in the design of a demonstration containment vessel.

4.1 Current and Magnetic Impulse Modeling Assumptions

1. The ZR pulsed power driver model is similar technology as the Z oil/water configuration. The Z machine is currently undergoing a refurbishment upgrade (ZR). It is expected that existing models used for the Z machine will remain valid for the ZR.
2. The MITL consists of perfectly aligned concentric cylinders with no less than a 3-mm operating gap between them. This avoids non-uniform currents around the MITL.
3. A 6-MV rated vacuum insulator stack (VIS) separates the water dielectric feed lines from the vacuum power flow inside the MITLs.
4. After the Z-pinch event, the VIS flashes over, undamaged, on the vacuum side, effectively trapping residual energy in the MITL sections. This effect is routine for Z operations.

5. Magnetic forces on larger diameter coaxial MITLs can be estimated by using the parallel strip-line formula:

$$F(b) = [b/2]\,[\mu o/4.448]\,[I(b)/b]^2 \quad \text{- total repulsive force per length on plates (lbf/m),}$$

$$P(b) = F(b)\,[0.0254]2 / b \quad \text{- pressure on parallel plates in (psi),}$$

where

b = strip-line width (i.e. coax circumference) (m),

I(b) = load current for the MITL associated with b (amps).

6. A coaxial correction is needed for the parallel formula when it is no longer true that the radius is much greater than the gap.

7. The pressure is uniform over the full length of a cylinder. This is not true for conical MITL geometry, which can approximated with a series of cylinders.

Note that, other than for a time-varying inductance, Z-pinch physics is not included in the circuit model load. Also, relying heavily on the waveform data after the time of peak current is not desired, because the timing spread of the VIS flash-over can result in quite large variations in trapped energy.

4.2 Optional MITL Configurations

A number of configurations have been considered in trade-off studies for the purpose of offsetting the Z-pinch load to a source location where it can most effectively generate neutrons in close proximity to the ZEDNA with minimal losses. Two options will be presented that represent the most feasible configurations; an inverted post-hole convolute option and an extended coaxial offset MITL extension option.

A vertical cut-away perspective of the Z machine center vacuum section in Figure 4-1 illustrates the re-entrant chamber concept for positioning ZEDNA close to the source but without having to be inside the evacuated region of the stack. The ZEDNA would be raised and lowered within its own containment/confinement barrier (not shown) and be capable of being moved into a storage vault during non operational periods. This sequencing and experiment package interfacing was described in detail in the previous report (Parma, et al., 2007).

Figure 4-2 is an enlarged view of the Z-pinch/reactor interface that shows how the fusion target is placed near a debris shield container by inverting the center-most section of the four ZR conical MITLs and converging them onto the vacuum post-hole convolute (PHC), which has also been lowered from its normal position. The reactor is as close as possible to the neutron source in order to capture the maximum number of neutrons for multiplication. Replacing the center set of conical MITLs with an inverted assembly does not appreciably affect the total inductance of the system. However, any coaxial extension for the wire array offset does add inductance which would degrade the overall performance.

The extended coaxial option is shown in Figure 4-3. This configuration maintains the conical MITL and PHC in their original orientation but uses a longer, more inductive coaxial offset MITL. The advantages of this case include less complexity and cost and easier alignment. The reduced current may be more than compensated by a potentially closer proximity of the source within the reactor cavity, thus increasing the overall performance. In this configuration, the four parallel inverted conical MITLs shown in Figure 4-2 have been replaced by the single coaxial MITL which also adds inductance. A compromise between the two configurations would be to shorten the longer coaxial extension from 80 cm to about 56 cm where the fusion target is just above the debris shield as in Figure 4-2.

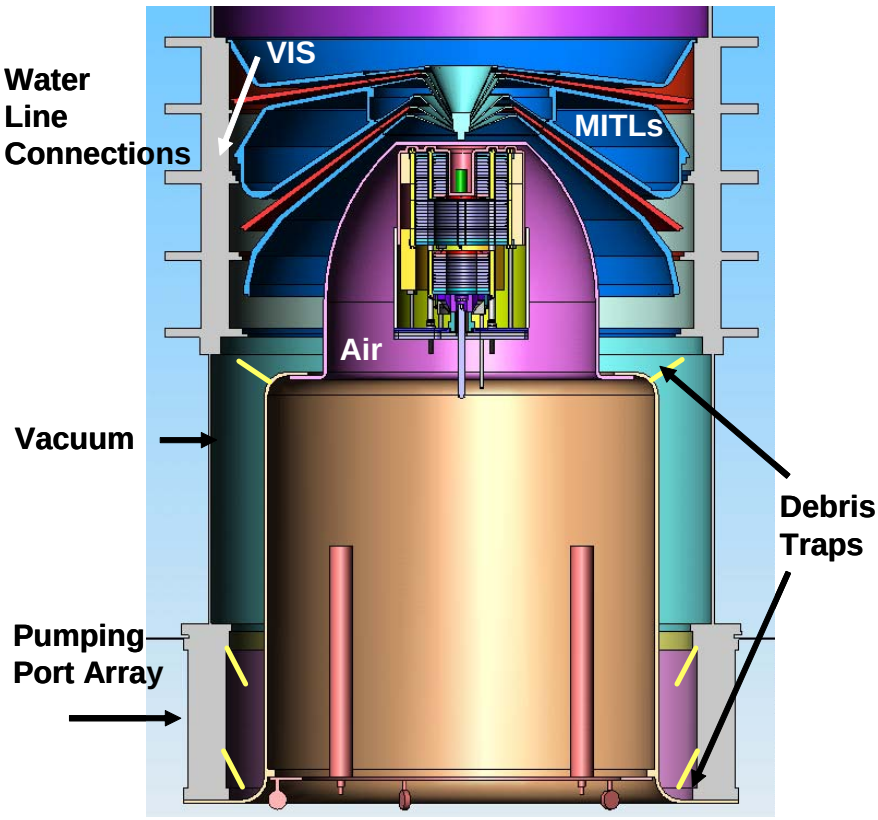

Figure 4-1. Vacuum Center Section Showing the Inverted PHC/MITL and Re-entrant Air Chamber for Loading the ZEDNA From Below.

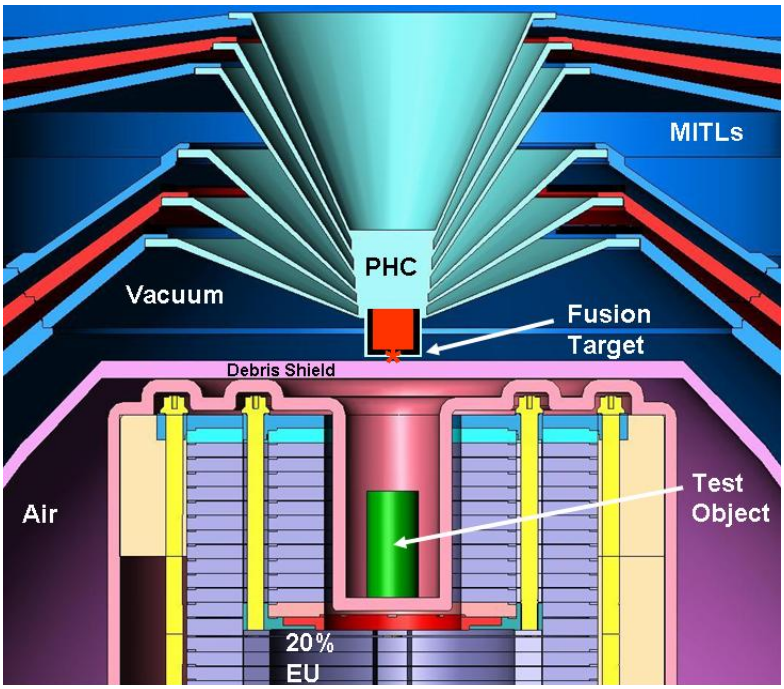

Figure 4-2. Expanded View of Source Region Showing the Inverted MITL Interface.

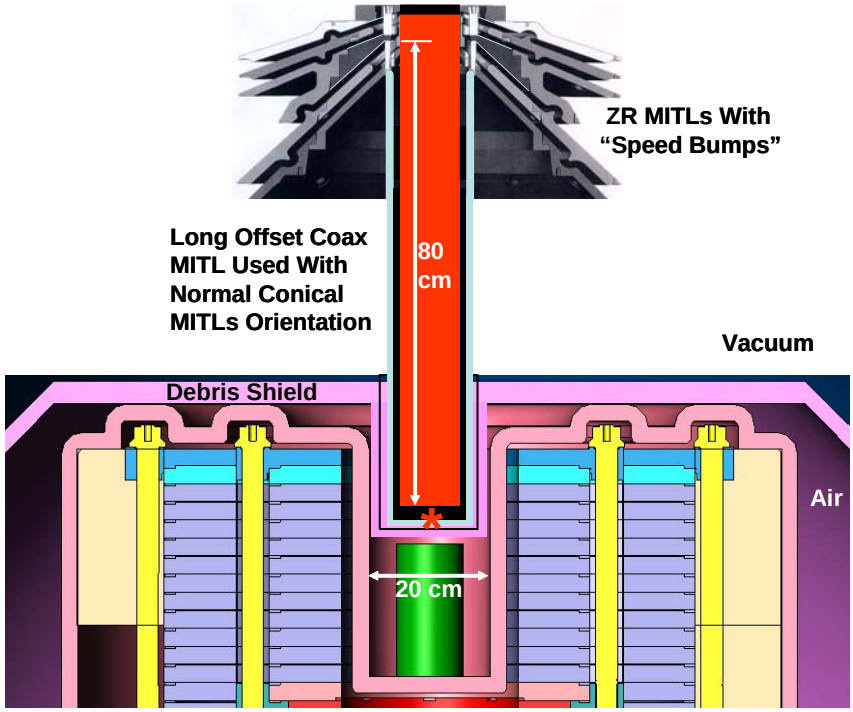

Figure 4-3. Extended Coaxial MITL From Within the Post Hole Convolute Ring With the ZR Conical MITLs in the Standard Configuration.

The sensitivity of the load current on inductance near the load is plotted in Figure 4-4. For typical ZR parameters, the peak current has a nearly linear dependence on the load inductance over a 10-nH range resulting in a 20% reduction in peak current. This corresponds to an average sensitivity of 0.5 MA/nH loss. The estimated inductance is shown in Table 4-1. There exists 5 to 6 nH of additional inductance in the normal center/extended coaxial case as compared to the inverted MITL. The Table 4-1 values in parentheses represent the shorter 56 cm extension. In both cases the nominal vacuum gap in the conical MITLs is assumed to be about 1 cm. The vacuum gap along the ~18-cm outer diameter coaxial extension is assumed at 0.5 cm. The reduction of current may be acceptable for demonstration purposes due to the potential significant cost savings for the simpler coaxial configuration.

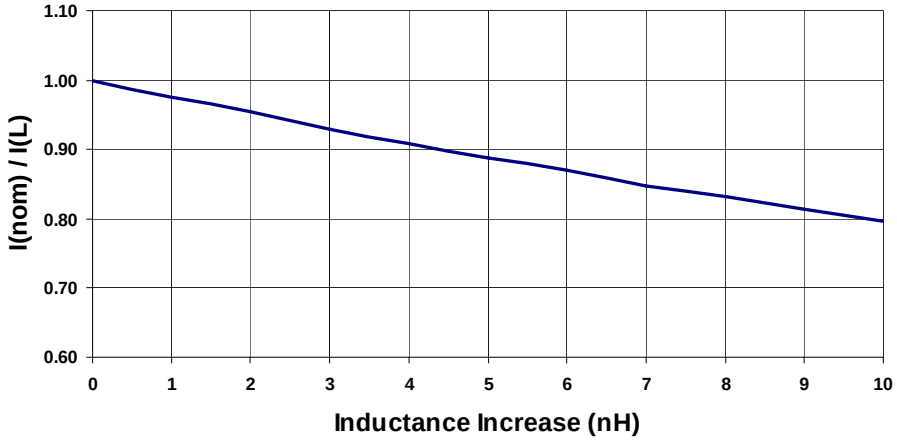

Figure 4-4. Relative Peak Z-Pinch Current as a Function of Inductance.

Table 4-1. Conical MITL and Extended Coaxial MITL System Inductance.

	Normal Center	Inverted Center	Δ
Center Section (nH)	0.7	0.6	0.1
Extended MITL (nH)	7.3 (5.1)	1.8	5.5 (3.3)
System Total (nH)	8.0 (5.8)	2.4	5.6 (3.4)

The center section inductance outside of the PHC is small because it is farther off axis and there are four MITLs in parallel, thus reducing the total effective value for the inductance.

4.3 Current and Efficiency Model for ZR

The assumptions and current/pressure relationships of section 4.1 remain valid for this discussion. The primary differences between the current ZR MITL and that for a future fusion power plant are that the inner offset portion of the MITL, or Recyclable Transmission Line (RTL), is mostly coaxial for ZR instead of conical for the power plant scale, and it is one-quarter or less of the total length. Some flaring to a slightly larger diameter below the PHC should help stiffen the extension and reduce its inductance. Likewise, rounding or tapering at the bottom would be appropriate to more smoothly match the load geometry. These model results are based on a coaxial MITL effective operating gap of 4 mm, which is probably the smallest reasonable value based upon some Z-machine experience.

The same Micro-Cap circuit model configuration used to represent the Z machine was used with the modified ZR component parameters. The separate reference and test models are shown in Figure 4-5. The primary power is provided by the Marx generator models on the left side of the circuit, and the load representing the Z-pinch wire array is on the right. The lower test model is the same as the upper reference model, but with the addition of one transmission line model (Xmitl) that has the impedance and one-way propagation time for the offset extension RTL. It is a straight forward calculation to vary parameters for the different coaxial dimensions considered in this analysis.

Results of the analysis are shown in Figures 4-6 to 4-10. The time scale for plots is 50 ns/division. The estimated magnetic pressure pulses will follow the same shape as the current waveforms, with a fast rise of about 100 ns and a slower fall off for many microseconds. Although this time period is short with respect to mechanical response times, we can probably assume that even short pressure impulses above some threshold value (e.g. 30 ksi yield strength for stainless steel) will lead to the violent disruption of the MITLs.

A 20-cm (or 0.67-ns) long coaxial RTL is about the shortest extension for any of the ZR experiments. The current and pressure waveform results are shown in Figure 4-6 for this reference case with an outer diameter of 18 cm and a gap spacing of 4 mm. The short RTL causes a reduction of peak current by only 3%, not including MITL corner losses, which are assumed to be small. The average pressure across the whole RTL is about 184 ksi at the peak of ~1.57 μs.

Figure 4-7 shows the effect of lengthening the extended coaxial RTL to 80 cm (or 2.67 ns). The extension reduces the peak current by about 11% from the reference case. The average pressure waveform peaks at about 155 ksi due to the lower current value.

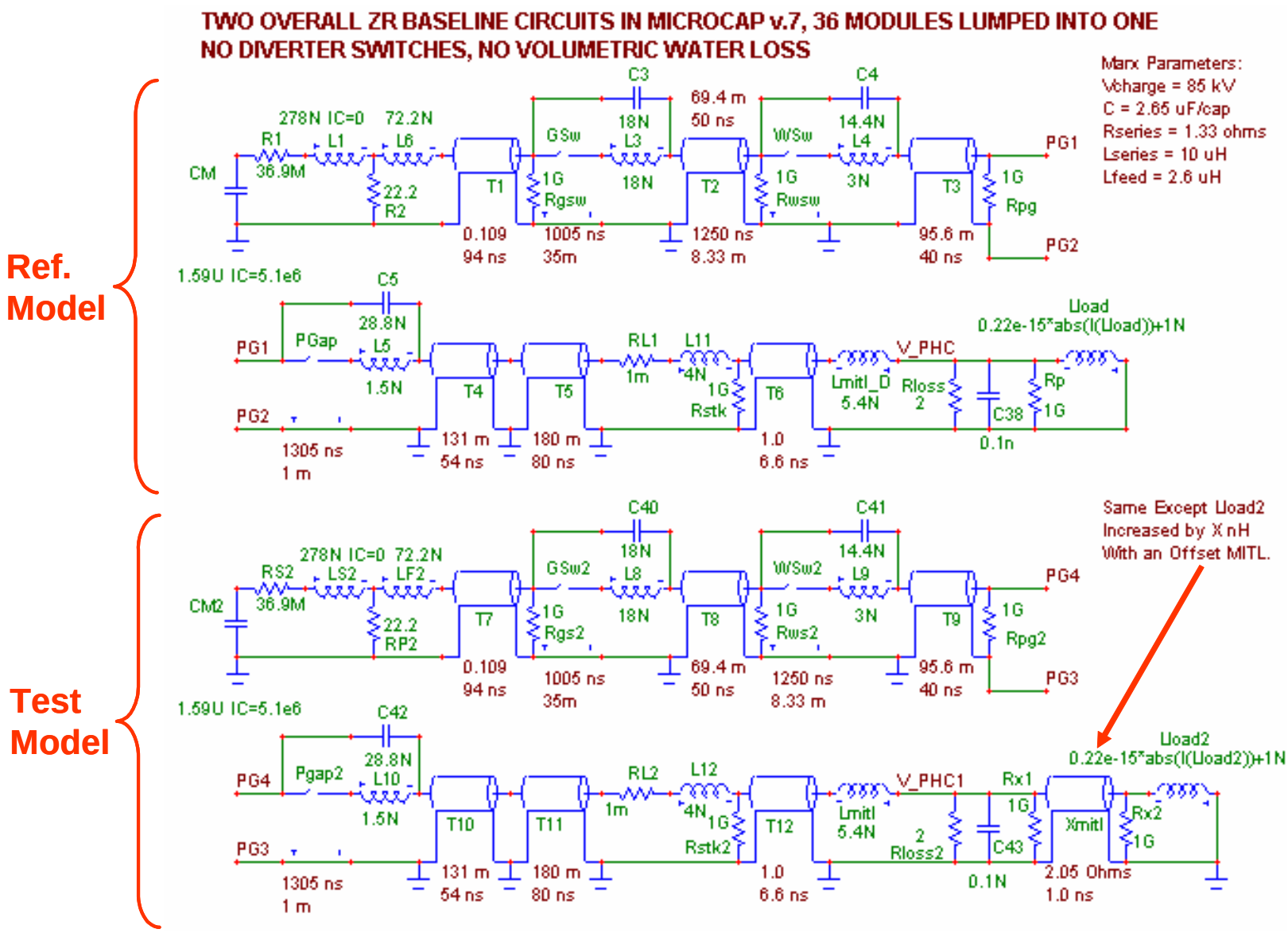

Figure 4-5. ZR Micro-Cap Dual Circuit Model for Coaxial Extended RTL Comparisons.

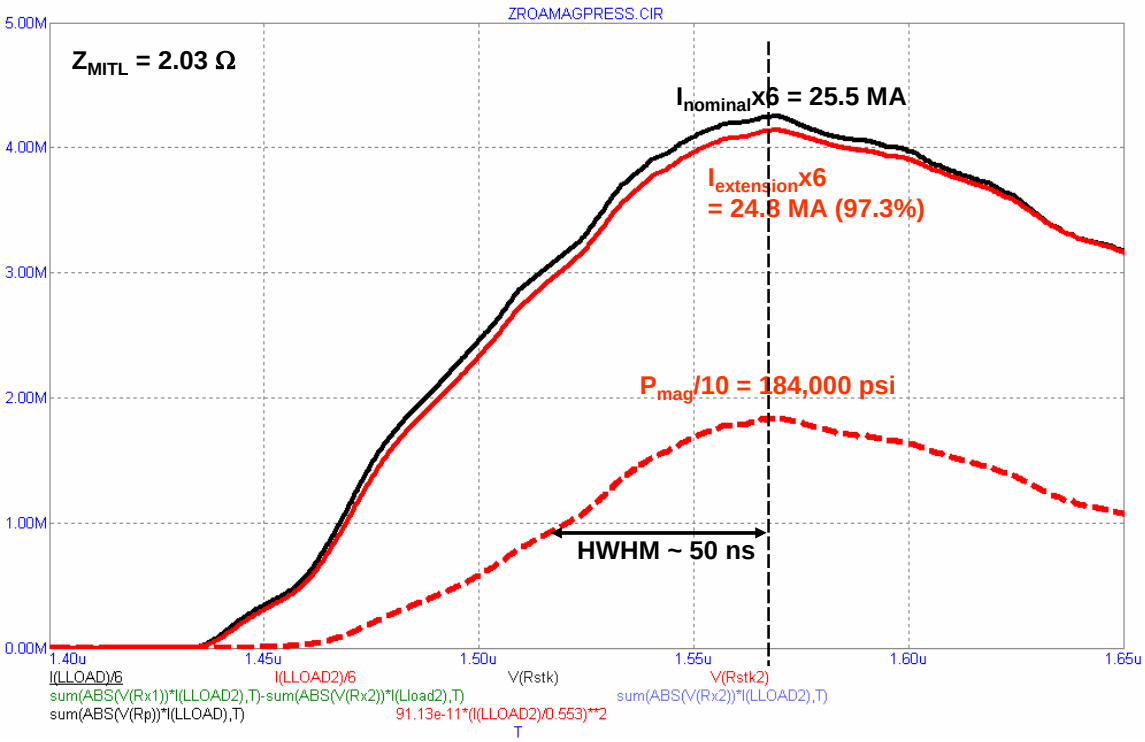

Figure 4-6. Current and Pressure for a 20-cm Long Extended Coaxial RTL.

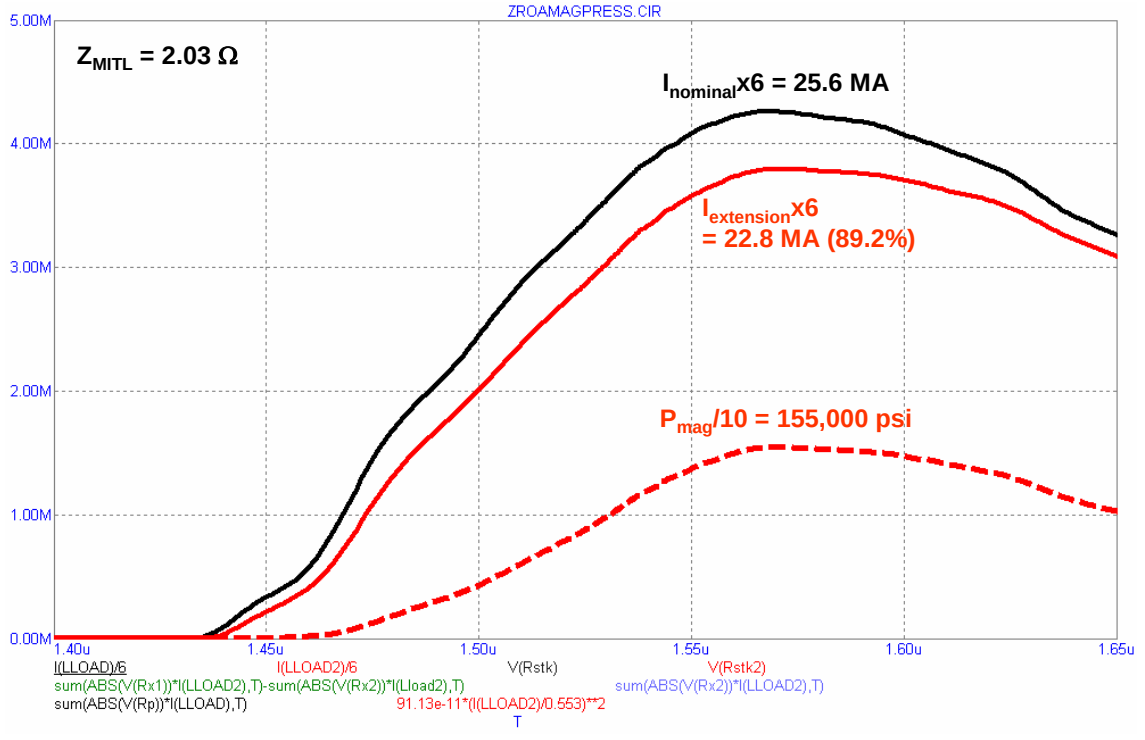

Figure 4-7. Current and Pressure for a 80-cm Long Extended Coaxial RTL.

The results for the compromise MITL length of 56 cm are shown in Figure 4-8. The nominal peak current is reduced by about 7.5% and the pressure waveform peaks at around 166 ksi.

A sensitivity analysis was performed to determine the effect in varying only the outer diameter of the MITL. Figure 4-9 shows the results for a 1 m extended coaxial MITL with a 4 mm gap spacing for the cases of an 18 cm and 44 cm outer diameter. The vertical scale is 30 ksi per division.
A large range of the magnetic peak pressures from ~145 ksi to ~28 ksi, respectively, are the result of the rapidly increasing surface area.

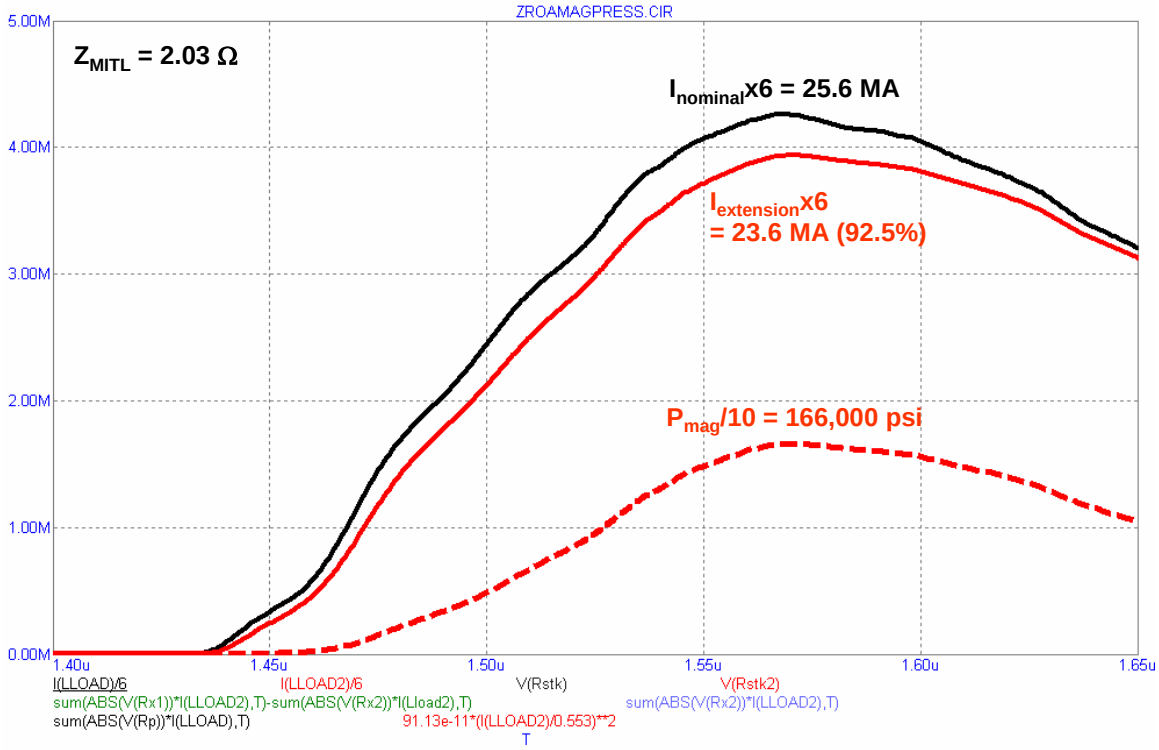

Figure 4-8. Current and Pressure for a 56-cm Long Extended Coaxial RTL.

As shown in Figure 4-10 the fractional electrical energy stored in each component varies with time and other component parameters. The vertical scale is 1 MJ per division. For the smaller diameter RTL, at the time of peak load current, there are almost equal amounts of electrical energy in the Z-pinch load and the RTL. When the RTL diameter is increased and the impedance reduced, more energy is proportionately stored in the load than in the RTL. This condition is desirable because the load performance is optimized, and the lower pressures in the RTL results in less shrapnel, debris, dust, and vapor production. Applying trade-off studies to balance performance against hardware/design cost and development time can determine whether it is realistic or necessary to optimize the current and energy delivered to the load.

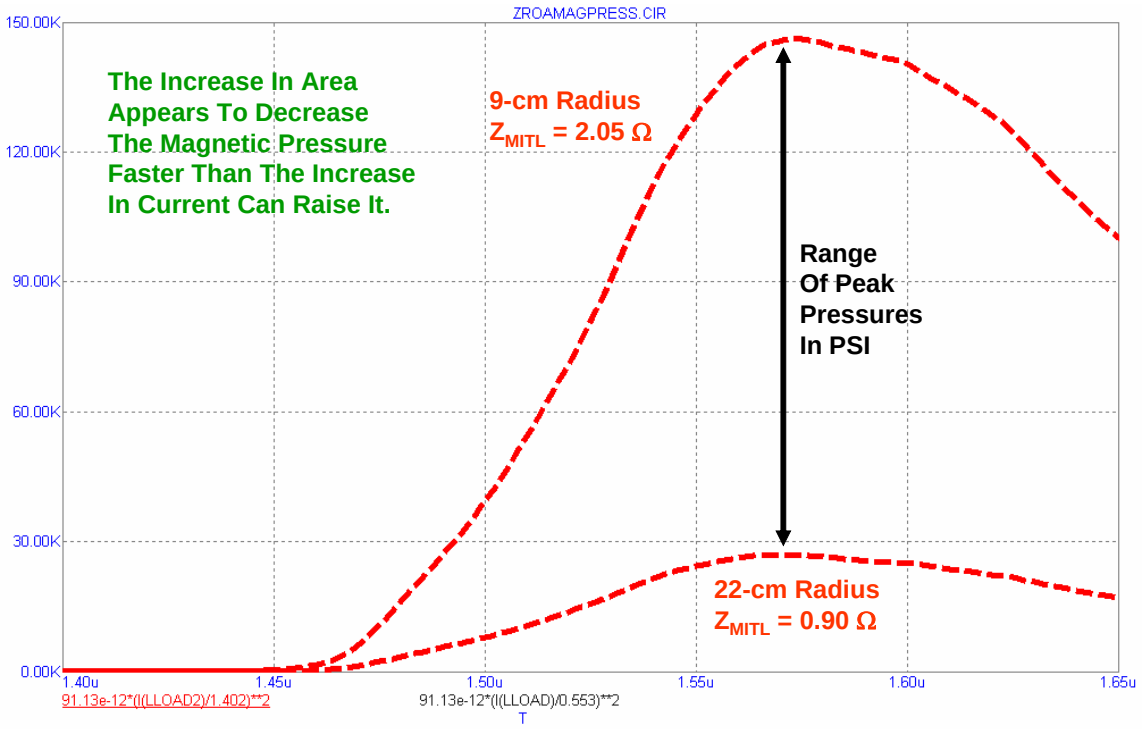

Figure 4-9. Pressure Range for 1-m Long by 4-mm Gap Extended Coaxial RTLs With Outer Diameters of 18 cm and 44 cm.

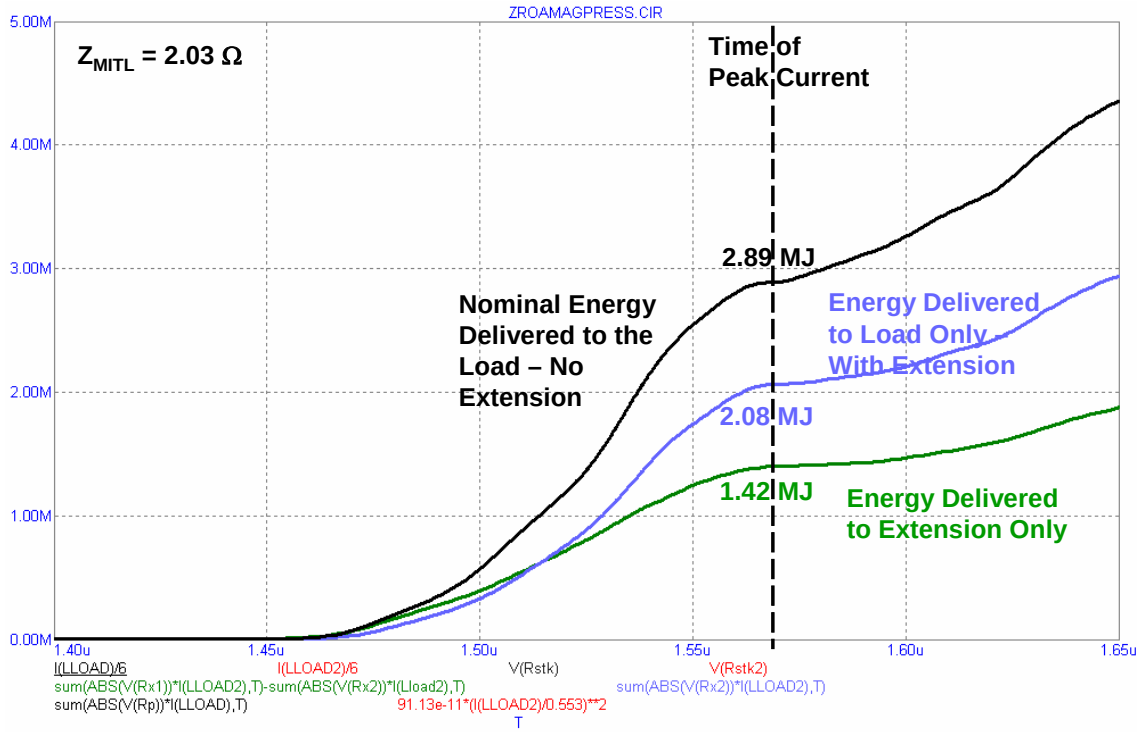

Figure 4-10. Accumulative Energy for the 80-cm Long Extended RTL with 18-cm Outer Diameter and 4-mm Gap.

4.4 Application for a Typical Scenario

An example of a possible design approach is presented assuming that a minimum peak current of 22 MA (from a 26-MA capable ZR machine) is necessary to produce the desired kinetic, thermal, pressure impulse, and/or neutronic response from the Z-pinch load. This places a limit on the allowable current loss and maximum inductance that can be added to the circuit by the RTL extension. One method of satisfying this load current requirement with a practical design follows.

RTL Design

The design approach involves estimating the inductance that can be added to the center section while maintaining current at 22 MA minimum, then determining the longest RTL of a reasonable diameter which matches that inductance (or less). A starting point is the plot of Figure 4-4 where it can be seen that the inductance associated with the relative reduced current (22 MA/26 MA = 0.846) is approximately 7.0 nH. Arbitrarily chosen are the typical coaxial MITL dimensions of 18 cm outer diameter and 4 mm vacuum gap spacing. Smaller diameters or larger gaps would increase the inductance penalty, and larger diameters would complicate the connection hardware. Now the vacuum impedance, Zo, and the MITL operating impedance, Zmitl, can be determined. The latter is based on a gap that is 75–80% of the vacuum gap (~3 mm) due to the presence of the electron sheath flowing along the cathode surface. This was determined for ZR parameters and similar geometries in a separate effort as

$Zo = 60 \ln(18/17.2) = 2.73\ \Omega$

$Zmitl \sim 60 \ln(18/17.4) = 2.03\ \Omega.$

Using a basic transmission line relationship, the one-way propagation time through the RTL can be calculated from the ratio of the inductance to the operating impedance as

$\tau = Lmax / Zmitl = 7.0\ nH / 2.03\ \Omega = 3.45\ ns.$

Since the electromagnetic wave can travel at approximately 30 cm/ns in a vacuum, the maximum length that this coaxial RTL could be is 103.4 cm. Now a decision can be made regarding the acceptable size and proximity of a reactor or the containment vessel to be tested. Using this RTL length in the configuration of Figure 4-3 would limit the vessel radius to around 50 cm or less, due to the shape and angle of the outer MITL section. Alternatively, the inverted center section MITLs of Figure 4-2 provide an additional offset of about 66 cm, so a test chamber radius of around 1 m would be possible. The power-flow performance and circuit model simulation will not differ significantly for either case, unless the MITL corner losses, assumed to be small, are deemed important and need to be included in the inverted case.

Impact on ZR Efficiency

The values for $Zmitl = 2.03\ \Omega$ and $\tau = 3.45$ ns were entered as transmission line model parameters in the Micro-Cap circuit schematic shown in Figure 4-5. The component representing the coaxial RTL is located near the bottom right corner of the layout and is labeled "Xmitl." The results of this simulation are shown in the Figure 4-11. The peak load current is 22.1 MA and the corresponding peak magnetic pressure in the RTL is 146 kpsi. These values could decrease slightly when MITL corner losses are properly included in the analysis. The additional loss can be compensated for by lowering the RTL inductance, which implies reducing the extended length or increasing the diameter.

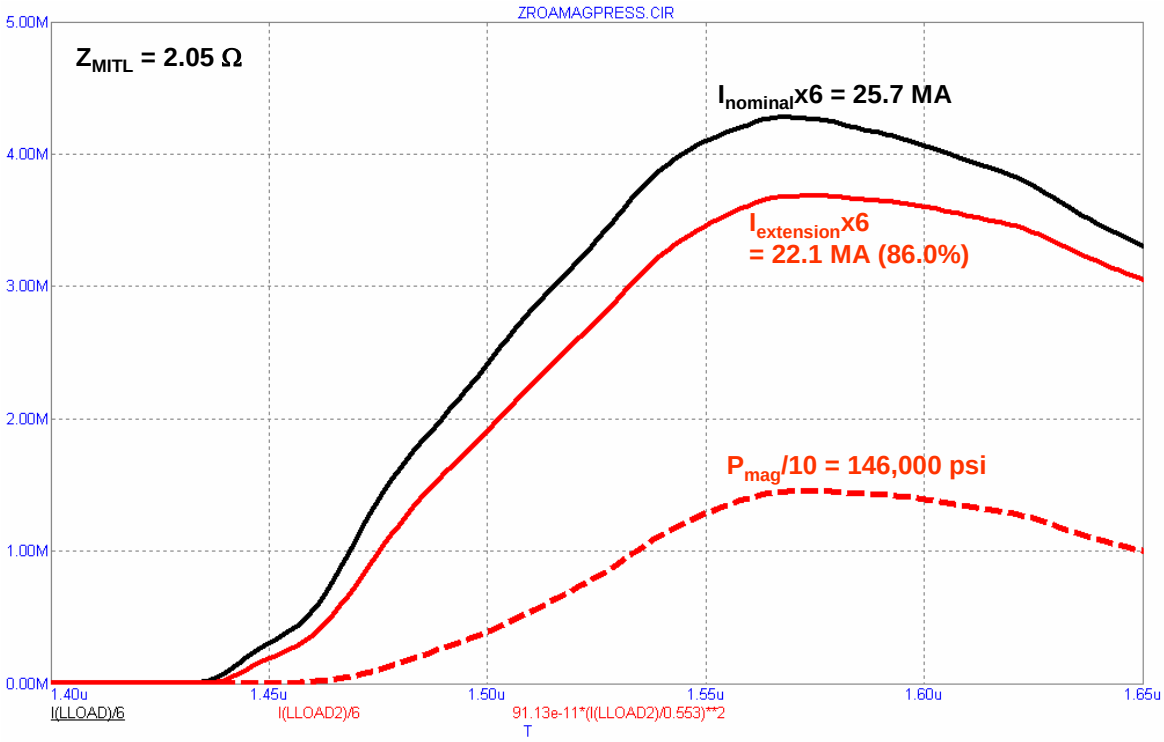

Figure 4-11. Peak current and pressure results for the 103-cm long by 18-cm OD by 4-mm gap extended coaxial RTL.

Another effect on the pulsed power driver from the added inductance is an increase in voltage across the vacuum insulator stack (VIS). This particular set of parameters results in a 7% increase in the VIS voltage peak from about 5.56 to 5.94 MV, according to the modeling results shown in Figure 4-12. The ZR stack design should have enough safety margin to accommodate this added voltage change, but a vacuum side, non-surface flashover would serve to further protect the stack. The primary goal would always be to design for the least inductance in the load area, both to maximize the energy to the load and to protect the machine hardware.

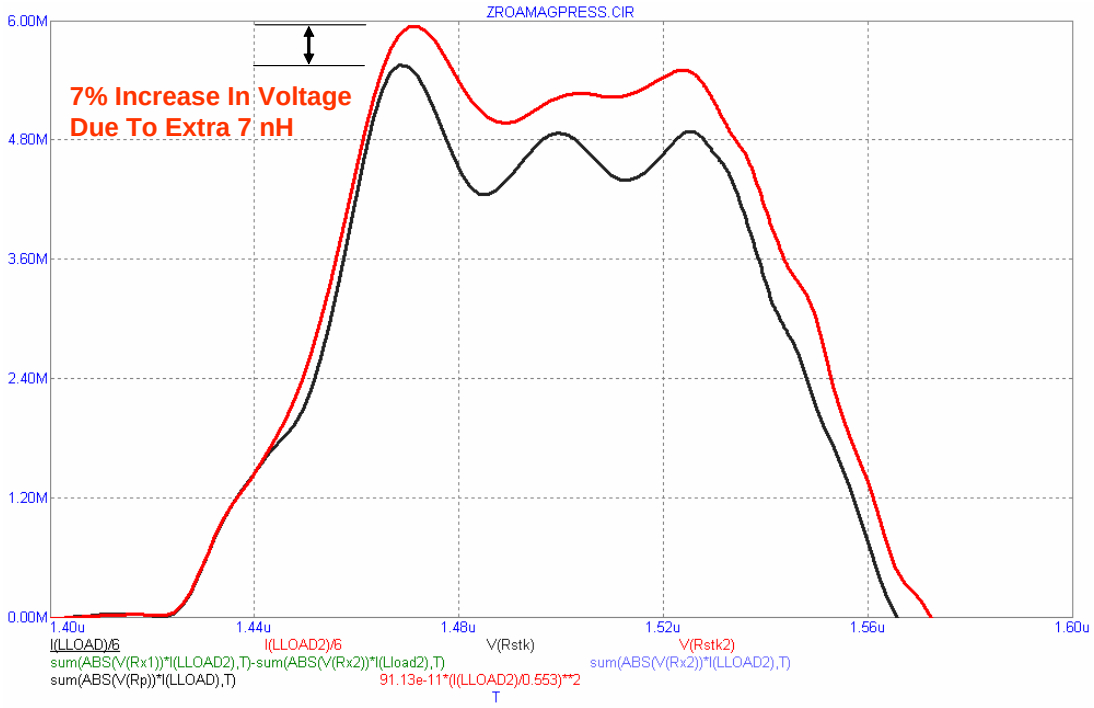

Figure 4-12. VIS voltage waveform results for the 1-m long by 18-cm OD by 4-mm gap extended coaxial RTL. The horizontal scale is 40 ns per division.

4.5 Summary of MITL Design

The additional work presented is complementary to that presented in the previous ZEDNA report (Parma, et al., 2007). Two design options have been developed that could work with the ZEDNA, an inverted post-hole convolute option and an extended coaxial offset MITL extension option. Both options are technically feasible and allow for optimization from a neutron production level, source to ZEDNA proximity, shrapnel and debris production, cost, manufacturability, and replacement. Further work would include fabrication and testing of the options in the ZR machine to determine source effectiveness, optimization, and determine other design, fabrication, maintenance, and operational issues.

5 Overpower and Reactivity Initiated Accident Analysis

A documented safety analysis would be developed to analyze potential off-normal events and hypothetical accidents involving the ZEDNA reactor operating at the Z facility. Hazard tables would be constructed that would investigate qualitatively, every possible initiating event in accordance with DOE-STD-3009. For FBR systems, the most important accidents are those that could end up disrupting the core with the potential release of fission products to the environment. These accidents are always hypothetical-type events driven by either overpower conditions or are reactivity initiated.

This report will investigate a few of the major hypothetical accidents postulated for ZEDNA. Since ZEDNA uses U-10Mo plate-type fuel and reflector elements similar to the SPR-III, the inherent reactivity feedback mechanisms are similar to SPR-III. SPR-III does not maintain a fuel temperature feedback due to Doppler broadening of the neutron cross sections, but it does maintain a significant temperature feedback effect due to expansion of the core that increased the neutron leakage. This is the inherent shutdown mechanism that allows the SPR-III to pulse. ZEDNA will have a Doppler broadening effect, due to the large amount of U-238 present, and a leakage effect due to geometric changes due to temperature. The reactivity feedback will not be as large as for SPR-III due to the larger size and the fully reflected geometry. Although the negative shutdown characteristic of the core are not required for normal operations of the ZEDNA, the reactivity feedback effects will play a large role in the inherent shutdown characteristics in the event of an overpower or reactivity driven accident.

5.1 Modeling Technique

A dynamic reactor modeling code was developed to simulate the pulse operation of SPR-III and the ZEDNA (Suo-Anttila, 2007). SPR-III was modeled first to determine if the computational technique could be validated using experimental results from SPR-III shots. Once the code was validated using SPR-III, it was then applied to the ZEDNA system. The code solves the point reactor kinetics equations with a one-dimensional thermo-mechanical model developed by Reuscher (1969, 1972). The feedback terms are incorporated in the code as lookup tables constructed using MCNP (2003). The SPR-III and ZEDNA reactors were modeled in detail using MCNP. Reactivity changes were calculated as the temperature or geometry of the reactor was differentially modified. This technique allows the reactor pulse to be simulated using only first principle modeling and with no additional assumptions. The results of the code are power profiles, temperature profiles, and radial and tangential stresses as functions of time.

The major design differences between SPR-III and ZEDNA consist of the fuel enrichment and geometrical differences. ZEDNA maintains fuel plates with similar dimensions and U-10Mo fuel enriched to 20% U-235. The ZEDNA is significantly larger than SPR-III, with a height of 62 cm, a diameter of 30.5 cm, and a cavity diameter of 20 cm. ZEDNA also maintains a two radial region core with a 1-cm gap between the inner and outer fuel plates. There also exist some neutronic differences between the SPR-III and ZEDNA. The neutron lifetime for ZEDNA is 73 ns, the delayed neutron fraction is 0.0073, and a Doppler temperature coefficient exists as compared to SPR-III.

An MCNP model of ZEDNA was constructed and variations on fuel temperature, outer radius, inner radius, axial expansion, and inner movable core position, were studied to determine changes in reactivity. Significant neutron histories were run to ensure precision of results.

Tables 5-1 to 5-5 show the results of the analysis for the fuel temperature feedback, outer radial expansion, inner radial contraction, axial expansion, and inner movable core position, respectively. This tabular data was then used as lookup tables in the dynamic modeling code to determine the reactivity feedback as a function of the fission heating in the core. Linear interpolation was used in the tabular data to generate a continuous feedback effect.

Table 5-1. ZEDNA Doppler Feedback Coefficient as a Function of Temperature.

Fuel Temperature (K)	Reactivity Change ($) from reference
293 (reference)	0.000
400	-0.064
500	-0.078
600	-0.078
1200	-0.082

Table 5-2. ZEDNA Leakage Feedback as a Function of Outer Radial Expansion.

Outer Radial Expansion (mm)	Reactivity Change ($) from reference
0.0 (reference)	0.000
0.1	-0.004
0.2	-0.023
0.3	-0.035
0.4	-0.049
0.6	-0.072
0.8	-0.109

Table 5-3. ZEDNA Leakage Feedback as a Function of Inner Radial Contraction.

Inner Radial Contraction (mm)	Reactivity Change ($) from reference
0.0 (reference)	0.000
-0.1	+0.002
-0.2	+0.019

Table 5-4. ZEDNA Leakage Feedback as a Function of Axial Expansion.

Axial Expansion (mm)	Reactivity Change ($) from reference
0.0 (reference)	0.000
0.1	-0.0015
0.2	-0.023
0.3	-0.040
0.4	-0.049
0.5	-0.068
0.6	-0.076
0.7	-0.095
0.8	-0.122

Table 5-5. ZEDNA Reactivity Change as a Function of Inner Core Position.

Axial Position (cm)	Reactivity Change ($) from reference
0.0 (reference)	0.000
0.5	-0.157
1.0	-0.214
1.5	-0.285
2.0	-0.420
2.5	-0.505
3.0	-0.651
4.0	-0.912
10.0	-2.532
20.0	-5.266
30.0	-7.620
46.0	-10.91

5.2 Normal ZEDNA Operation

The dynamic modeling code was run for the ZEDNA for a reactivity addition of $0.80 and nominal Z-pulse condition. This calculation allows for a base case for comparison of the off-normal conditions. The nominal condition includes enough initial D-T neutrons to ensure that the cavity fluence meets the requirement of 6.1×10^{14} nvt. Figures 5-1 to 5-3 show the reactor power level, fuel temperature, and total energy yield as functions of time, respectively, for the ZEDNA for a nominal operation. The Z pulse occurs at 0.1 ms (10^{-4} s). The safety block (movable portion of the reactor core) drops at 50 ms (5×10^{-2} s). The timing for the safety block to drop is arbitrarily chosen for the analysis. For a large pulse on the SPR-III reactor, the safety block is actually pushed by the axial expansion of the fuel which, at the same time breaks the electromagnetic coupling. The safety block begins to move immediately with acceleration greater than that of gravity, due the force applied by the axial expansion. For ZEDNA, the electromagnetic field can be adjusted to ensure a timely release of the safety block. However, for all of the analyses presented, the safety block is assumed to be released by gravity at 50 ms.

The initial spike in the power level (Figure 5-1) is due to the initial pulse neutrons causing fission. The initial neutrons are multiplied (prompt multiplication) over the next ~200 μs. Over this time period, the neutron population decreases by five orders of magnitude. This is the portion of the power curve that is desirable for the experimenter. After this period, delayed neutrons drive the system with inherent negative reactivity feedback from the energy deposition in the pulse. A large negative reactivity addition occurs at 55 ms when the safety block falls from the core adding ~$10 of negative reactivity in ~0.2 seconds. The tail portion of the curve (after ~0.3 s) is the continued decrease in power from the delayed neutron contribution. Additional negative reactivity would be added at less than 0.5 seconds with the reactor SCRAM initiation and dropping of the control reflector elements. This effect is not included in the analysis. With significant negative reactivity added to the system, the reactor power would continue to decrease with a period of ~80 seconds due to the decay of the most persistent delayed neutron group.

The average and peak temperature rise in the reactor fuel (Figure 5-2) is not significant for a nominal pulse condition. The peak temperature rise is only ~110°C immediately after the pulse and ~140°C with the additional energy included in the tail following the pulse. The average temperature rise is ~70°C immediately after the pulse and ~100°C with the additional energy included in the tail following the pulse. Compare this with the SPR-III reactor that increases in temperature by a few hundred degrees after a shot. The energy deposited in the ZEDNA following a nominal shot is ~30 MJ compared to ~10 MJ for SPR-III, but ZEDNA has a fuel mass of ~1900 kg, compared to SPR-III with a mass of ~250 kg, a factor of 7.6 times the heat capacity. The temperature is shown in Figure 5-2 to decrease at 250 seconds due to a convective cooling boundary condition included in the analysis.

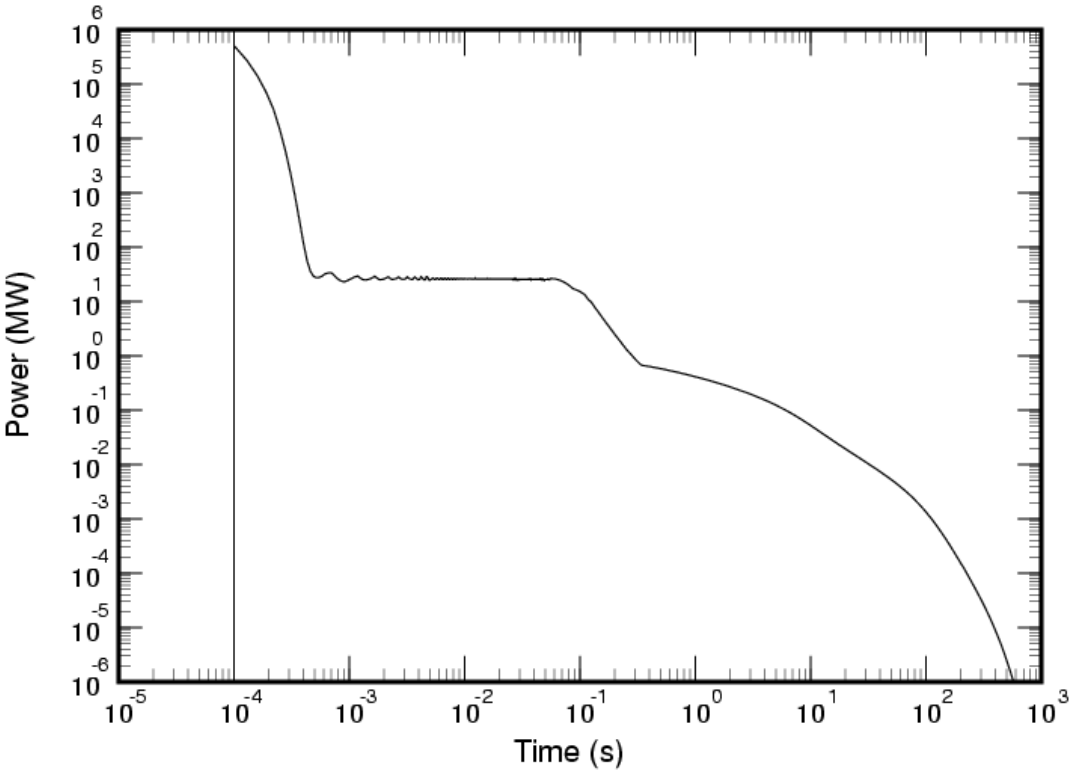

Figure 5-1. Reactor Power as a Function of Time for the Nominal Operating Condition.

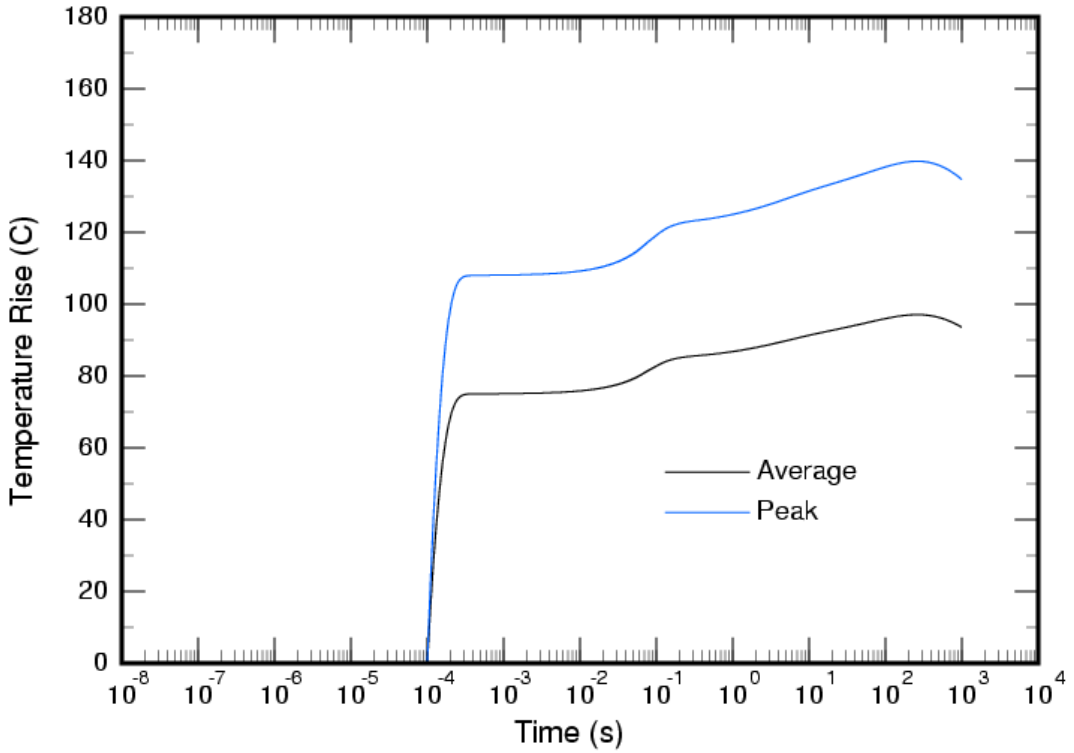

Figure 5-2. Fuel Temperature as a Function of Time for the Nominal Operating Condition.

The energy yield (total fission energy deposited in the fuel) is shown in Figure 5-3 for four different reactivity feedback conditions: 1) with Doppler and expansion (nominal condition); 2) Doppler only; 3) expansion only; and 4) no feedback. The energy scale in Figure 5-3 is from 20 to 35 MJ and the time scale is in milliseconds. The black curve shows the energy yield in the case of no reactivity feedback, except for the safety block drop at 50 ms. Without feedback the neutron pulse is multiplied yielding approximately 25 MJ of energy. If only Doppler feedback is included the energy yield is reduced to approximately 22 MJ. If only expansion feedback is included, there is an increase in initial energy yield because the inner radius expands before the outer radius. And finally, when all feedback effects are included, the net pulse yield is 22.5 MJ, which is a loss of 2.5 MJ (10%) compared to the case of no feedback.

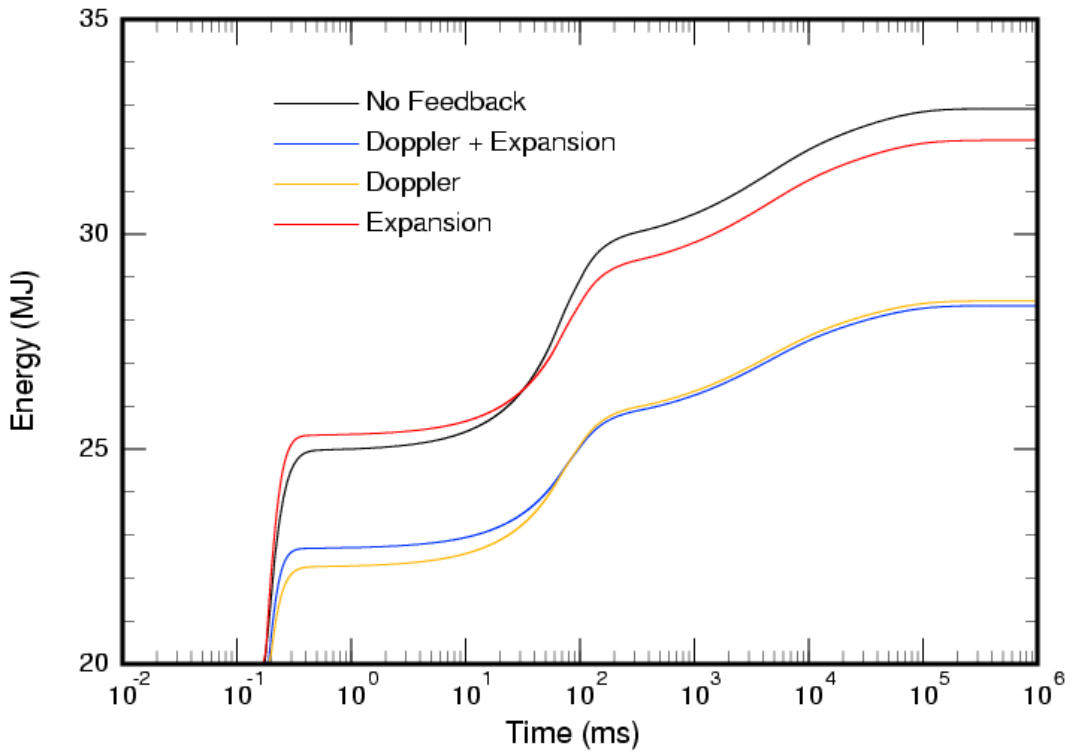

Figure 5-3. Energy Yield as a Function of Time for the Nominal Operating Condition.

5.3 Off-Normal ZEDNA Cases

Three off-normal initiating events or hypothetical accidents are presented that are thought to bound the possible overpower and reactivity driven accident possibilities. The first event assumes that reactivity is added at a ramp rate of \$0.25/s and that reactivity of greater than \$1.00 is added, followed immediately by a Z pulse. The second event assumes that the Z pinch produced a neutron pulse four times greater than a nominal neutron pulse. The third event assumes reactivity greater than \$1.00 is added and that the safety block fails to fall away from the core and the control reflector elements fail to fall.

Case 1: Reactivity Greater Than $1.00 Followed by a Z Pulse

The first off normal event consists of too much initial reactivity, which causes a ZEDNA pulse similar to a SPR pulse. Using the control elements or a pulse element to add the reactivity, it would be highly unlikely that this accident could ever occur. For control element insertion, the initiating event would be that the control element was withdrawing uncontrollably, or that the operator was inadvertently moving the control element. For control element insertion, the rod block and period SCRAM would also have to fail to function properly. For pulse element insertion, the initiating event would be an inaccurate calibration of the pulse element, or a reactivity change in the pulse element prior to insertion.

The calculation consists of reactivity addition of $1.05 (arbitrarily chosen) at $0.25/s followed by the Z pulse 20 ms later, followed by safety block release 50 ms later. Figures 5-4 to 5-7 show the reactor power level for a logarithmic and linear time scale, fuel temperature, and reactivity as functions of time, respectively, for this ZEDNA accident. The first reactor pulse occurs at ~0.23 s because the reactivity has exceeded one dollar. The inherent Doppler and expansion reactivity feedback are all that exist to shut the reactor power down at this point. If there were no negative feedback, the reactor power would continue to rise until enough expansion occurred or the reactor disassembled itself. Since $1.05 was added, only $0.05 of negative reactivity is required to terminate the pulse because the reactor is being driven by prompt neutrons. Note from Table 5-1, that negative $0.06 of reactivity can be added by Doppler for a temperature rise of ~100°C. The second pulse occurs because control hardware was assumed to be unable to stop the Z machine from initiating a pulse. This double pulse causes the maximum energy yield conceivable for this type of accident.

The time scale in Figure 5-4 goes out approximately 15 minutes to give the reader an idea of the full power history. The pulse detail is shown in the Figure 5-5 which is plotted on a linear time scale. The plateau that follows the second pulse is similar to that seen for the nominal case; it is due to multiplication of delayed neutrons. The drop in power after the plateau is due to the safety block drop. The reactor power continues to decrease after this time with a period of ~80 seconds due to the decay of the most persistent delayed neutron group.

The slight rise in power before the safety block drop is a numerical artifact caused by releasing the fixed axial boundary condition at the core mid plane. When the fixed displacement boundary condition is released, the core relaxes, but in the direction of adding reactivity. Thus the two core halves move toward each other at a rate faster than the falling velocity. In reality this effect cannot happen since the two core halves actually push against one another. The slight error introduced by this effect is negligible in terms of the overall modeling behavior, but it appears in some cases when a safety block drop occurs.

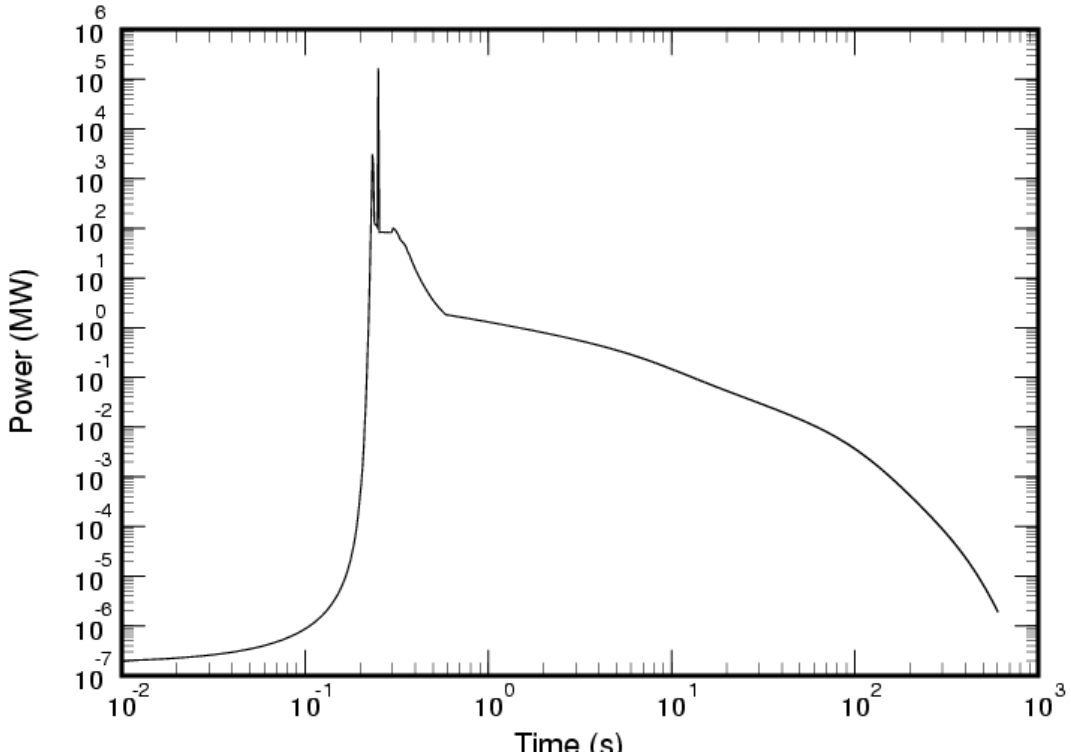

Figure 5-4. Reactor Power as a Function of Time for the $1.05 Addition Followed by a Z Pulse and Safety Block Drop.

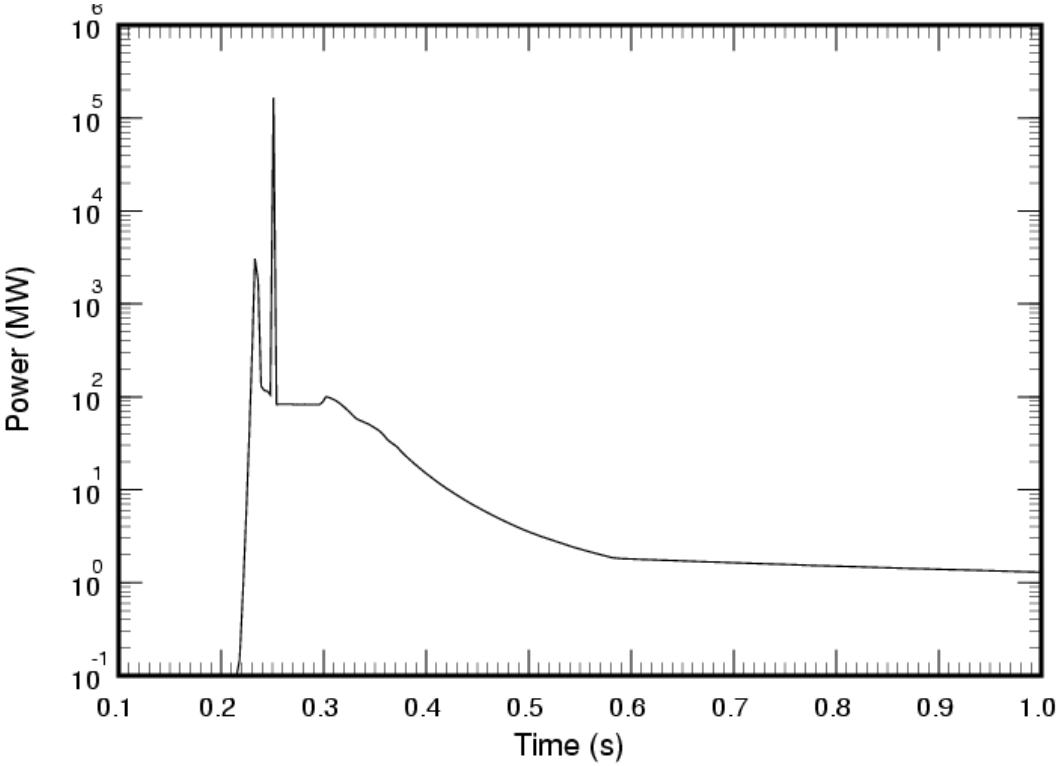

Figure 5-5. Detailed Reactor Power as a Function of Time for the $1.05 Addition Followed by a Z Pulse and Safety Block Drop.

Figure 5-6 shows the average and peak temperature rise in the fuel as a function of time. The peak temperature rise is less than 350°C immediately following the pulse. The average temperature rise is less than 250°C immediately following the pulse. These temperatures are about the same as that for a nominal SPR-III pulse. The amount of energy deposited in the ZEDNA fuel for this accident condition is about three times that of a nominal ZEDNA pulse condition (~70 MJ compared to ~22 MJ). Hence this type of off-normal double pulse event would not jeopardize the integrity of the ZEDNA reactor fuel. Fuel cracking could occur if the fuel plates were not properly segmented, but release of fission products would not be expected since the fuel melt temperature of 1130°C is not approached.

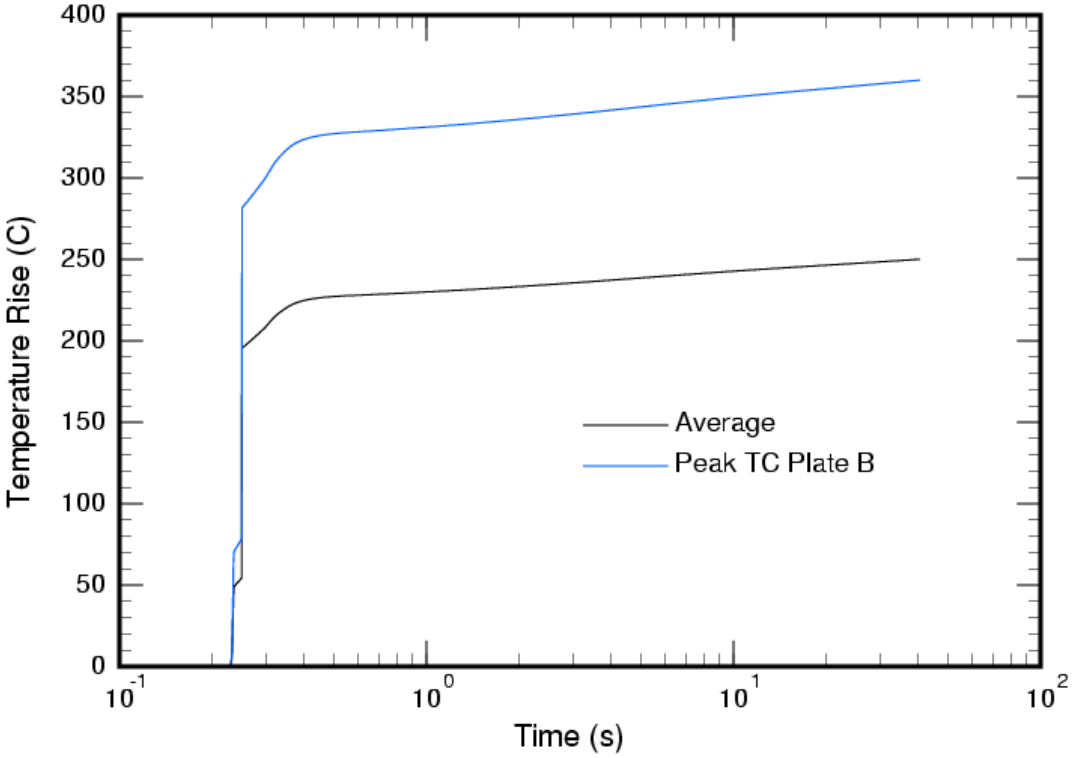

Figure 5-6. Fuel Temperature as a Function of Time for the $1.05 Addition Followed by a Z Pulse and Safety Block Drop.

The reactivity associated with this accident is shown in Figure 5-7. The initial positive slope is due to the $0.25/s reactivity ramp addition. The drop at 0.23 s is due to the first pulse that adds enough negative reactivity to lower the value to below $1.00. The next drop at ~0.25 s is due to the Z pulse and subsequent prompt neutron multiplication, which adds most of the energy yield and causes a significant drop in reactivity – to approximately $0.70 positive. The final drop in reactivity at 0.3 s is due to safety block drop.

Note that although there was a $1.05 reactivity limit in the initial reactivity addition, larger additions could be tolerated without risk to the reactor. Other cases with higher reactivity limits would have similar behavior, but with more total energy yield.

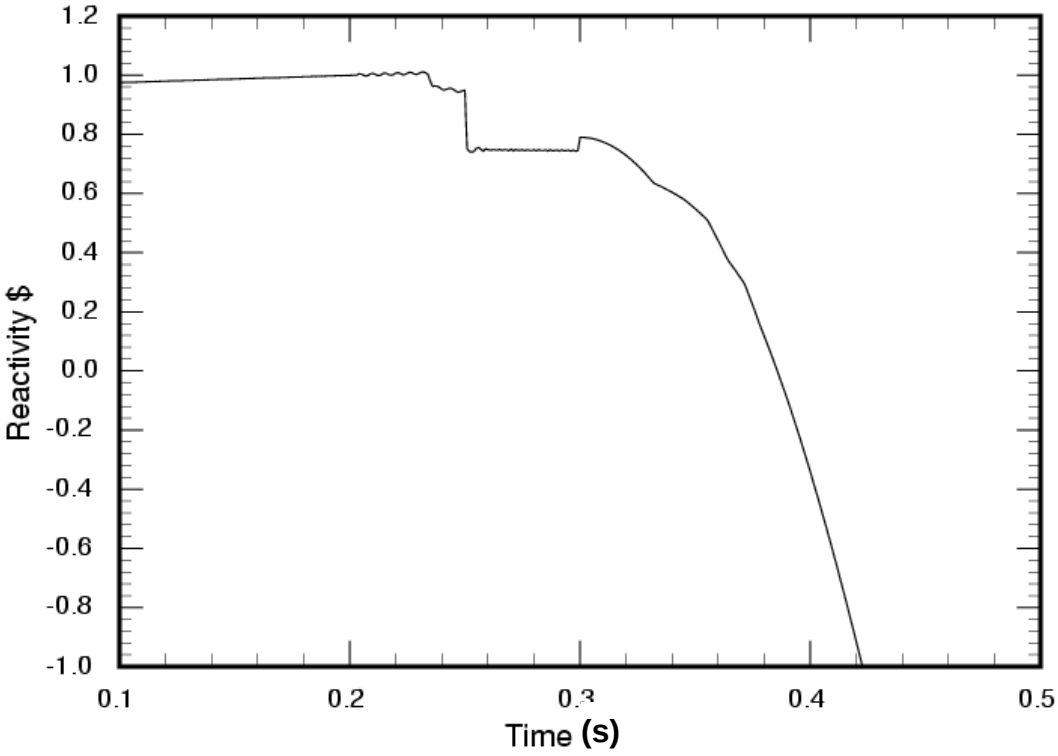

Figure 5-7. Reactivity as a Function of Time for the $1.05 Addition Followed by a Z Pulse and Safety Block Drop.

Case 2: Z Pulse - Four Times Nominal

This off-normal ZEDNA event assumes the nominal conditions, but that the Z pulse is larger by a factor of four. The factor of four was arbitrarily chosen. The increase could only be due to an unexpected increase in the Z machine or source output. How this could happen is unknown and is therefore highly hypothetical. It would be expected that once a source was used for ZEDNA it would be experimentally tested many times to identify the potential source variation. Changes due to the interface geometry of ZEDNA with the source could only have tens of percent changes in the effective source magnitude. Also, any change in the geometry of the source or the proximity to ZEDNA would be expected to result in a decrease in the source magnitude.

The calculation is the same as for the nominal condition, but the initial source for the analysis was multiplied by four. Figure 5-8 to 5-10 show the reactor power level, fuel temperature, and energy yield as functions of time, respectively, for this ZEDNA accident. The resulting power profile shown in Figure 5-8 is very similar to Figure 5-1 for the nominal case, as expected.

Figure 5-9 shows the average and peak temperature rise in the fuel as functions of time. The peak temperature rise is ~350°C immediately following the pulse. The average temperature rise is less than ~250°C. These temperatures are about the same result as found for the previous accident. The energy yield, shown in Figure 5-10, is ~75 MJ immediately after the pulse, and ~87 MJ at ~300 s. This result is about four times the nominal energy yield and is expected since the yield should be directly proportional to the external source magnitude.

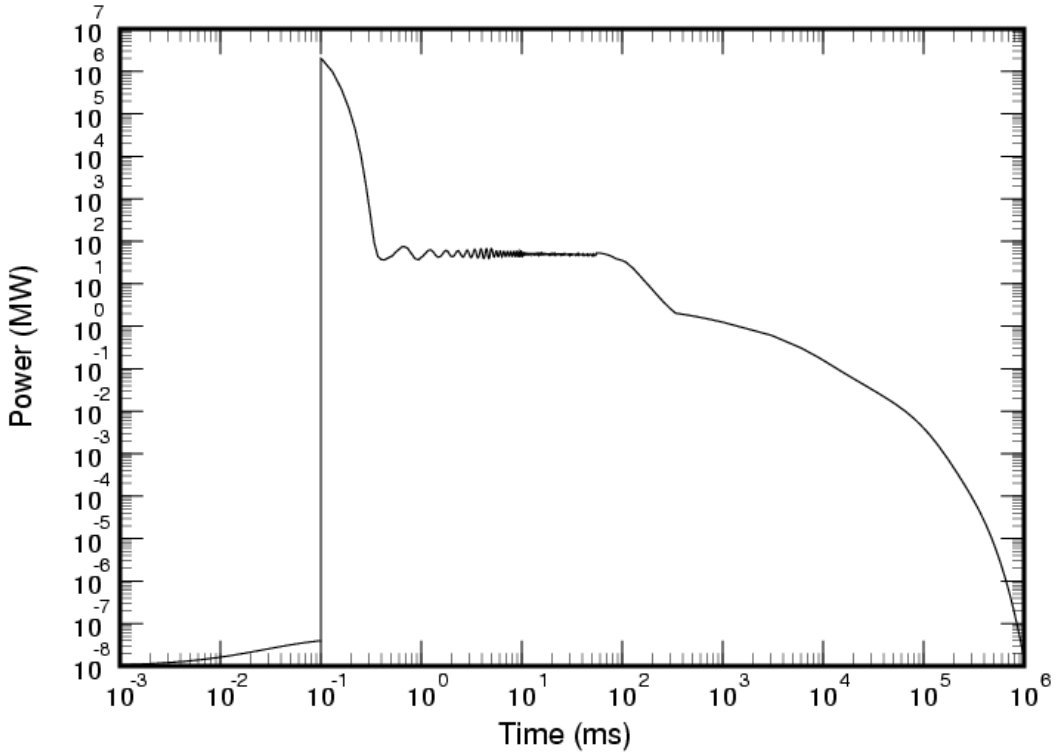

Figure 5-8. Reactor Power as a Function of Time for the Nominal Z Pulse Increased by a Factor of Four and Safety Block Drop.

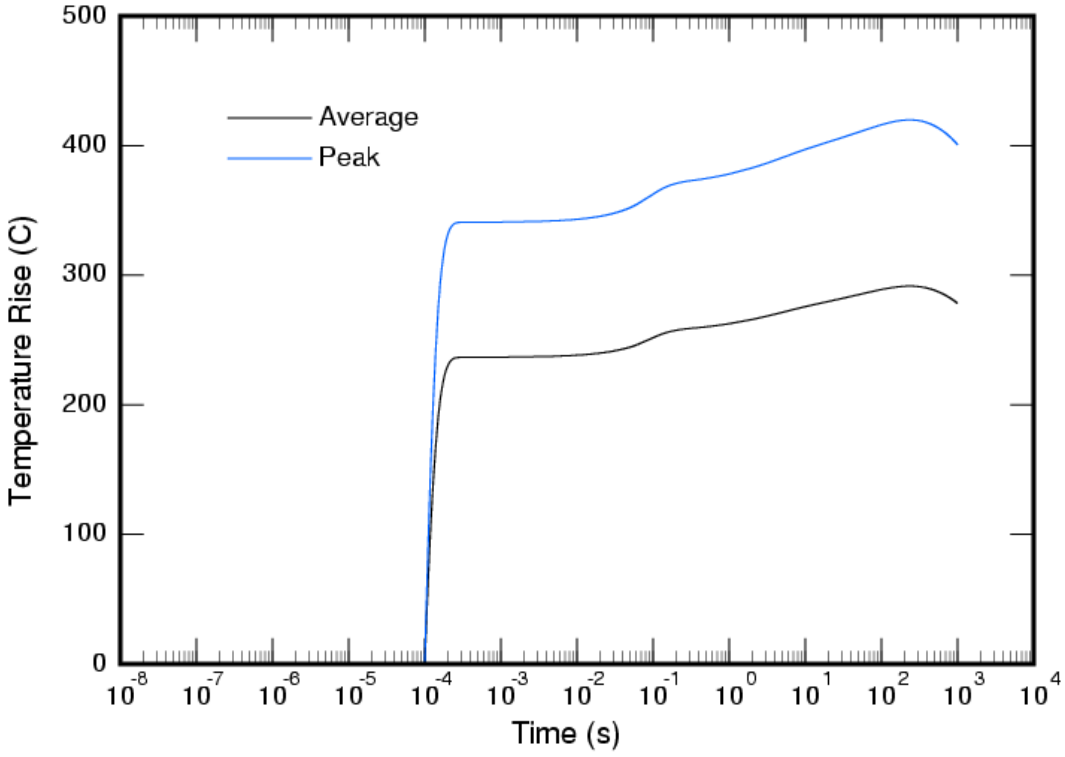

Figure 5-9. Fuel Temperature as a Function of Time for the Nominal Z Pulse Increased by a Factor of Four and Safety Block Drop.

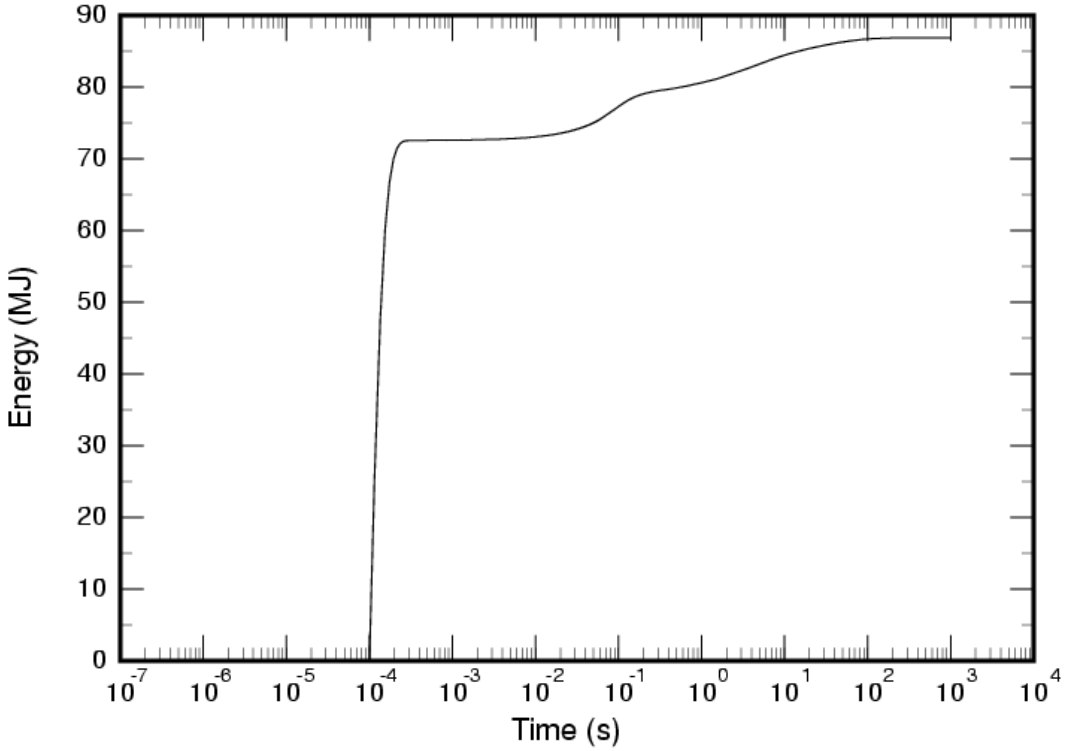

Figure 5-10. Energy Yield as a Function of Time for the Nominal Z Pulse Increased by a Factor of Four and Safety Block Drop.

These results indicate that this type of off-normal event would not jeopardize the integrity of the ZEDNA reactor fuel. Fuel cracking could occur if the fuel plates were not properly segmented, but release of fission products would not be expected since the fuel melt temperature of 1130°C is not approached.

Case 3: Reactivity Greater Than $1.00 Without Shutdown

The most severe hypothetical accident that can be envisioned is that in the event of a nominal pulse or an accident where greater than $1.00 of reactivity was added, the safety block and control elements fail to fall from the core. This event is hypothetical for three reasons: 1) in the event of a large pulse, the safety block will be pushed away from the core and break the electromagnetic coupling, and 2) a SCRAM signal will be initiated automatically following a pulse, de-energizing the power to the electromagnets to the safety block and the control reflector elements, and 3) the operators are trained to manually SCRAM the reactor immediately following a pulse if a SCRAM is not automatically initiated. Hence at least two failures would be required for this event to occur. The SCRAM system must fail and the safety block must be jammed and unable to separate from the upper core. However, for the purpose of safety analysis, this worst possible condition was analyzed. For this analysis the control reflector elements are assumed to add reactivity at the rate of $0.25/s and a maximum reactivity of $1.05 (arbitrarily

chosen) is added. These same “shutdown restricted” conditions for the nominal pulse case would be a less severe accident and would be bounded by this analysis.

This accident condition would severely degrade the core because, although some negative reactivity is added immediately following the pulse, the reactor remains in a supercritical condition and significantly more negative reactivity is required. From Table 5-1, the Doppler reactivity feedback is not significant after the initial 100°C temperature rise. The core must continue to expand until either the neutron leakage is enough to drive the reactor subcritical, or the fuel plates begin to crack or melt and the core disassembles itself. The dynamic code currently only treats expansion with elastic deformation. Hence the analysis is performed with these caveats. The resulting power, fuel temperature, energy yield, and reactivity are shown in Figures 5-11 to 5-14.

The power profile is shown in Figure 5-11. The power following the pulse decreases, due to the added negative reactivity, but the quantity of negative reactivity is insufficient to make the reactor subcritical. The temperature profile (Figure 5-12) shows that the peak temperature would reach 2050°C and the average temperature 1450°C. Since these temperatures are well beyond the fuel melt temperature of 1130°C, the results of the code are not valid. A code that included modeling of the plastic region, and fuel cracking/melting would be required to better predict the core behavior at these conditions. The predictions for this code are based upon large extrapolations of material properties, which have only been measured up to 600°C.

The energy yield (Figure 5-13) shows that at the end of 40 s, ~380 MJ of energy is deposited in the core. The reactivity (Figure 5-14) is less than zero at approximately 6 seconds into the transient. At 6 s, the peak fuel temperature has exceeded the melt point, but the average fuel temperature is still well below the melt point. However, sufficient power decay remains in the core to cause significant additional heating and potential melting of at least a portion of the core.

Again this accident is highly hypothetical. Although more advanced modeling must be developed to determine the actual transient behavior of the core, the results allow an estimate of the total energy yield to be determined. Approximately 380 MJ of energy would be deposited in the fuel. A portion of the core would potentially melt, allowing some fraction of the fission products, especially the gases and volitiles, to escape into the containment vessel and possibly from the building through the ventilation system.

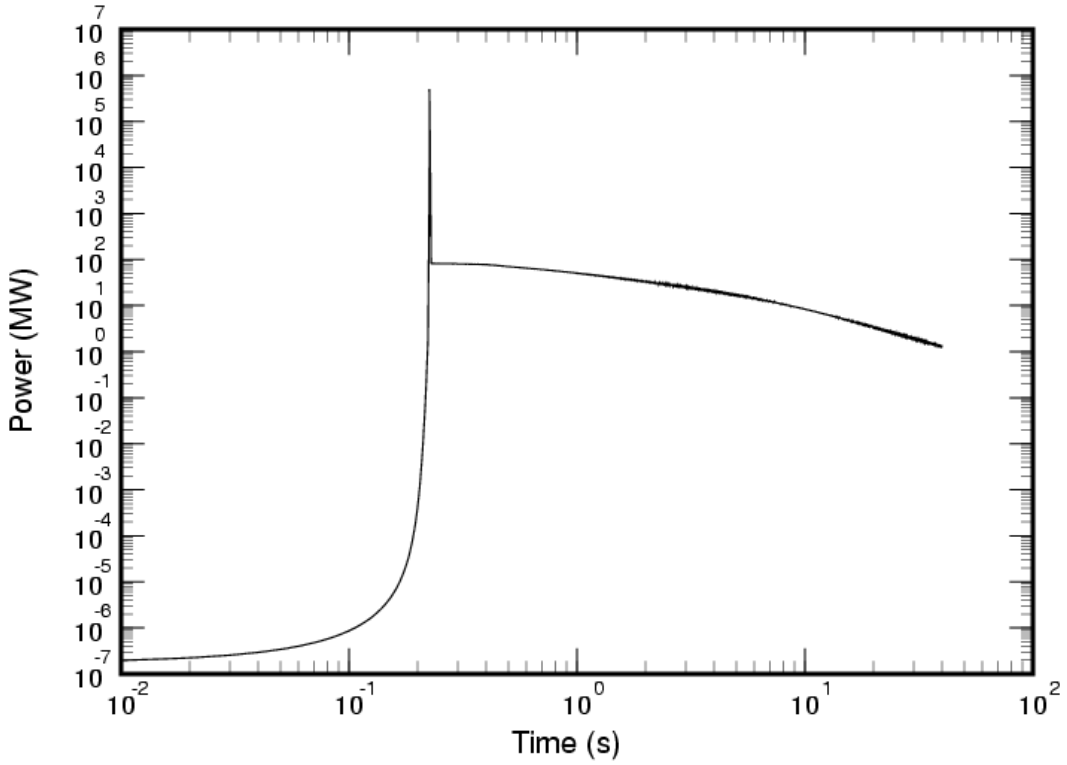

Figure 5-11. Reactor Power as a Function of Time for the $1.05 Addition Without Safety Block Drop or Control Element Drop.

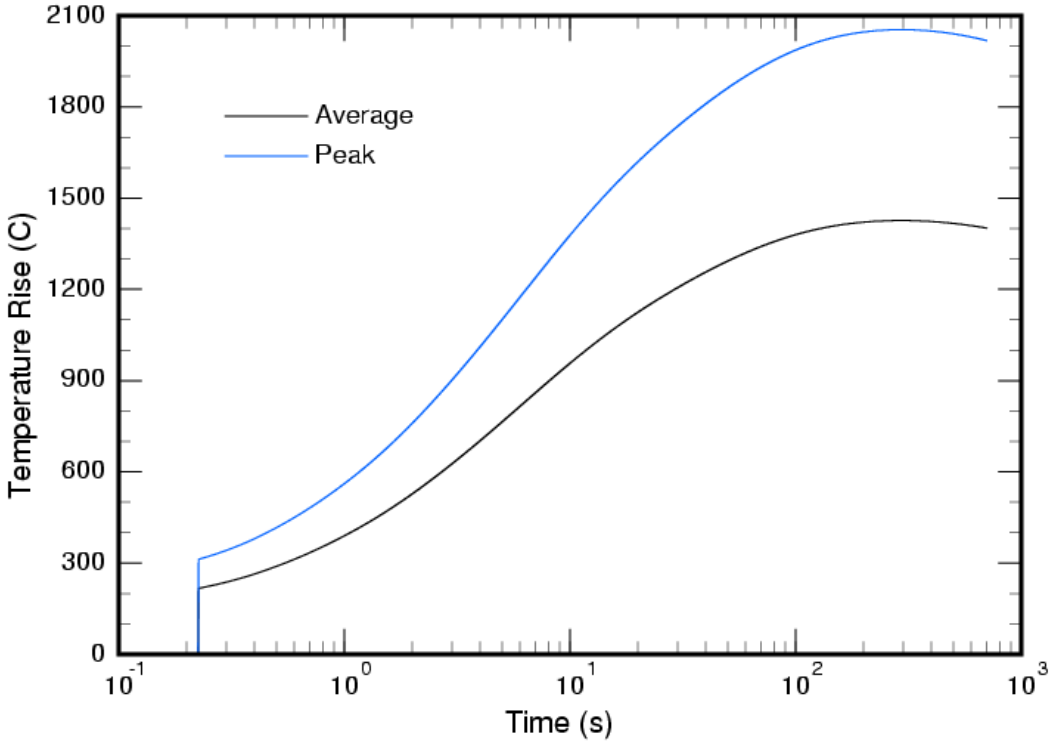

Figure 5-12. Fuel Temperature as a Function of Time for the $1.05 Addition Without Safety Block Drop or Control Element Drop.

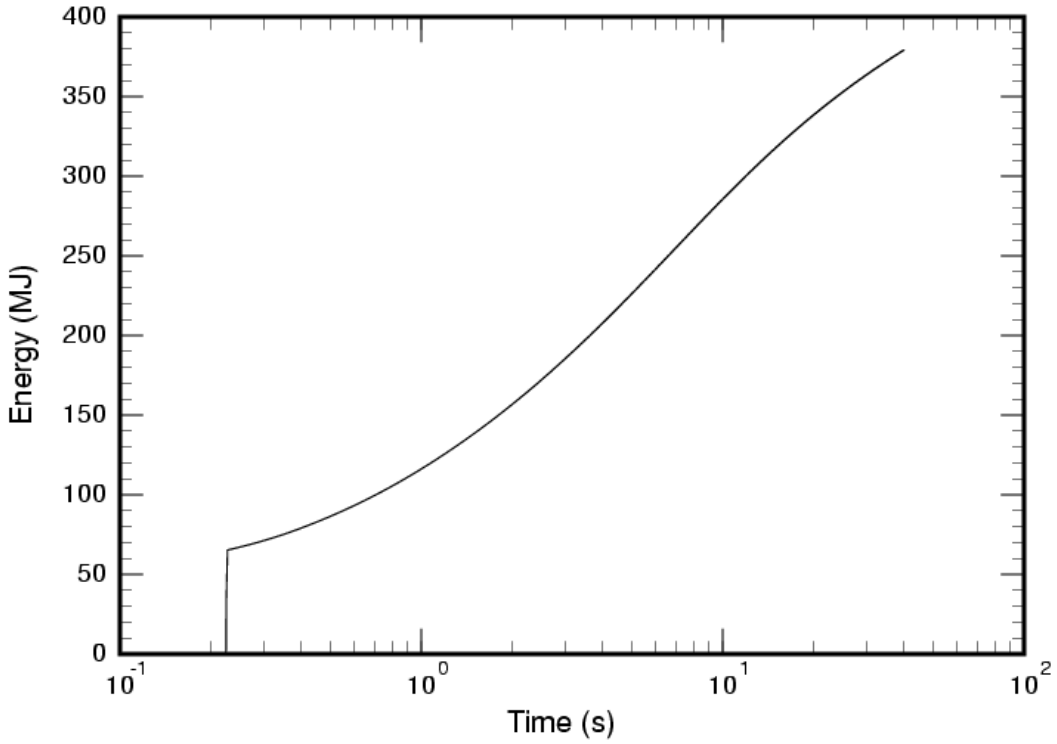

Figure 5-13. Energy Yield as a Function of Time for the $1.05 Addition Without Safety Block Drop or Control Element Drop.

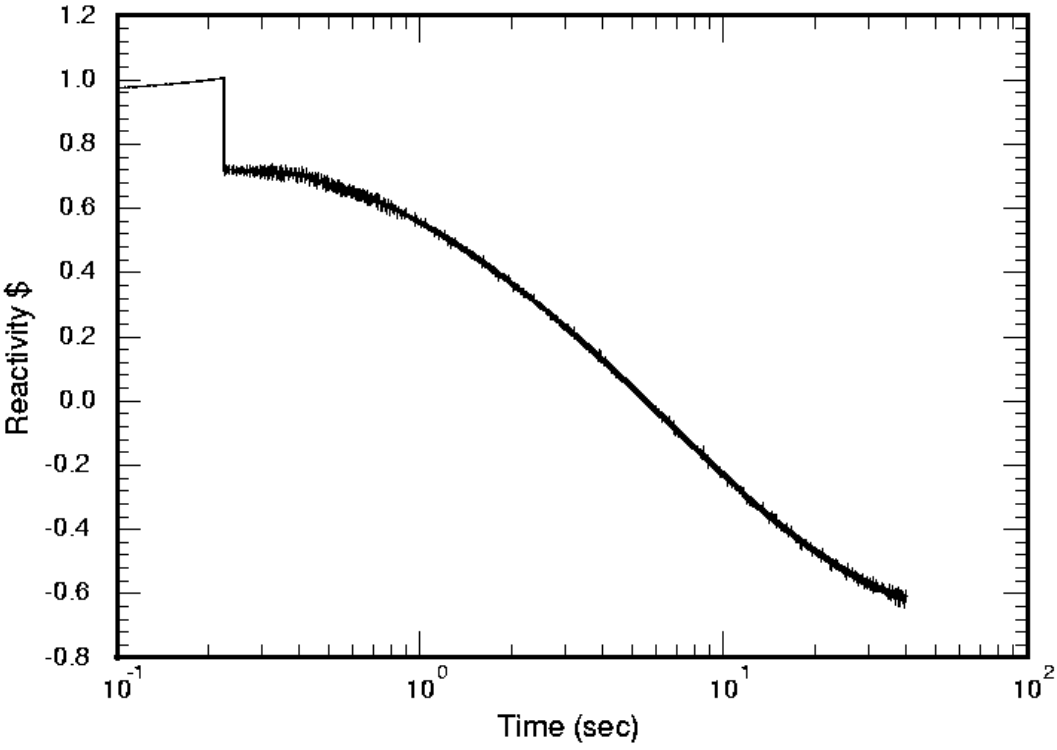

Figure 5-14. Reactivity as a Function of Time for the $1.05 Addition Without Safety Block Drop.

5.4 Summary of Off-Normal Events

The accidents presented are hypothetical and would require several failures in order to occur. However the results using the dynamic modeling code show that if the safety block portion of the core and the control reflector element operate as designed, the integrity of the fuel plates for the ZEDNA is not jeopardized. For these cases, no significant fission product release from the core would be expected. The ZEDNA is designed with enough inherent negative shutdown and heat capacity to mitigate the conditions if too much reactivity or source neutrons were inserted into the core. The condition of excessive reactivity with failure of the safety block and control reflector elements would cause the core to approach the melt temperature. For this hypothetical case, it would be expected that significant fission product release might occur, especially if a portion of the core experienced melt conditions. More advance modeling is required to treat the shutdown mechanisms of this hypothetical accident properly. However, this type of accident is considered in calculating the potential downwind dose estimate in the next section.

6 Downwind Dose Estimates for ZEDNA Accidents

The ZEDNA will not require external cooling during operations. Nitrogen gas cooling may be included in the design of the reactor in a similar way that SPR-III is cooled. SPR-III has a nitrogen gas cooling system to operate in the steady-state mode, and to allow for cooling when multiple pulses per day are required. However the ZEDNA would not operate in a steady-state mode, and would probably only pulse once per day, and would therefore not necessarily require this type of cooling system. Decay heat generated from the fission products is minimal for these types of research reactors and does not require decay heat removal, as does a power reactor. Fuel melting due to decay heat generated is not possible. However, other accident conditions could occur that could cause sufficient heat generation to melt and vaporize some of the reactor fuel. These types of accidents could include reactivity addition accidents, failure of shutdown accidents, or overpower accidents from too large of source neutrons produced from the Z machine. Although more unlikely, a fire in the facility could also potentially, melt or cause fuel vaporization.

For all of these types of accidents, a fraction of the fission products that were generated in previous pulse operations, or in the accident initiating pulse, could be released from the fuel melt and into the containment vessel. The containment vessel could maintain its integrity and not allow any of the fission product to escape, or it could be breached and allow fission products to be released to the environment via exhaust stacks that would be required for the vacuum stack, basement, and high-bay area.

The purpose of this analysis is to provide a quantitative estimate of the potential radiological dose that could be realized to the collocated worker and the public in the event of a catastrophic accident of ZEDNA at the Z-machine facility. The results are intended to be used for scoping purposes. The methodology presented is intended to be conservative and bounding.

6.1 Site and Exclusion Boundary

In order to determine downwind dose estimates, the site and exclusion boundaries must be established for the nuclear facility. The site boundary is identified as the fenced-in area of the facility where a person of the general public or a collocated worker would be restricted from entering. A site boundary would have both fences and security gates that would allow only access-personnel to the site. There is no requirement that the dose at the site boundary be below a given value in the event of a catastrophic accident. Of course, the desire is that the dose at the site boundary be low if a catastrophic accident did occur.

The exclusion boundary encompasses an area significantly larger than the site boundary. The exclusion boundary must be an area where the emergency management team can gain access and control in the event of a catastrophic accident. This may include public and private roads and property. For the SNL nuclear facilities in TA-V, the exclusion boundary is a circle 1350 m in radius with TA-V at the center. This places the edge of the exclusion boundary at Pennsylvania Avenue near the Kirtland Air Force Base riding stables.

TA-IV is located about 1.6 km directly south of the Steve Schiff Auditorium at SNL, Albuquerque. Currently there is no official site boundary or exclusion boundary for TA-IV because the facilities located there are not nuclear facilities. The current security controlled fence boundary of TA-IV, that includes the Z-machine facility (Building 983), is shown in

Figure 6-1. This could become the site boundary if the Z facility was established as a nuclear facility, or a different boundary could be established if necessary to control access to the facility. Currently the south and southeast boundaries are 0.062 km away from the Z-machine building edge. The gate to the parking lot is 0.10 km to the west. The parking lot edge is 0.15 m west northwest. The buildings to the west and northeast are experimental facilities that maintain other pulsed-power machines. The closest office building is Building 980 outside the gate, 0.10 km to the west. The closest permanent office buildings within the boundary are Building 970 located 0.12 km northeast and Building 960 located 0.15 km to the northwest. Building 962 is located 0.3 km to the north northwest.

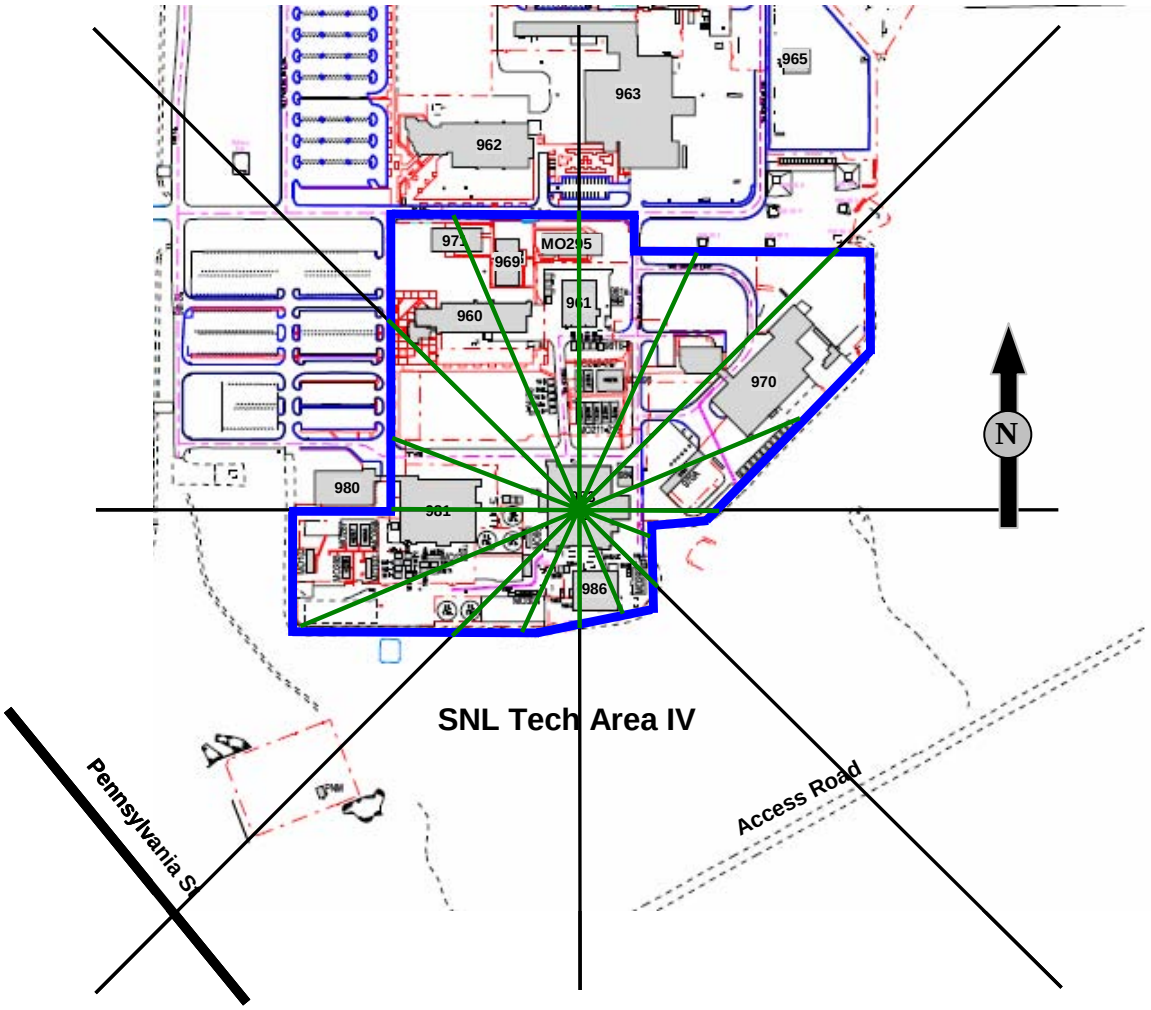

Figure 6-1. Current Fenced Boundary at TA-IV.

Figure 6-2 shows the proximity of various landmarks from the Z-machine facility, Building 983. The numbers identified in Figure 6-2 are delineated as follows:

1. The Steve Schiff Auditorium and Buildings 821, 822, and 823 are 1.6 km north;
2. Building 810 is 2.1 km north north-west;
3. The Manzano Mesa residential area is 3 km north-east;
4. The Kirtland Air Force Base Eubank gate is 2.5 km north-east;
5. The nearest meteorological tower is 1 km north;
6. The Kirtland Air Force Base golf course about 1.8 km south south-east;
7. Pennsylvania Avenue is about 0.5 km South West of the building.

Base housing is greater than 2.1 km north north-west of the facility. Downtown Albuquerque is about 10 km north-west of the facility.

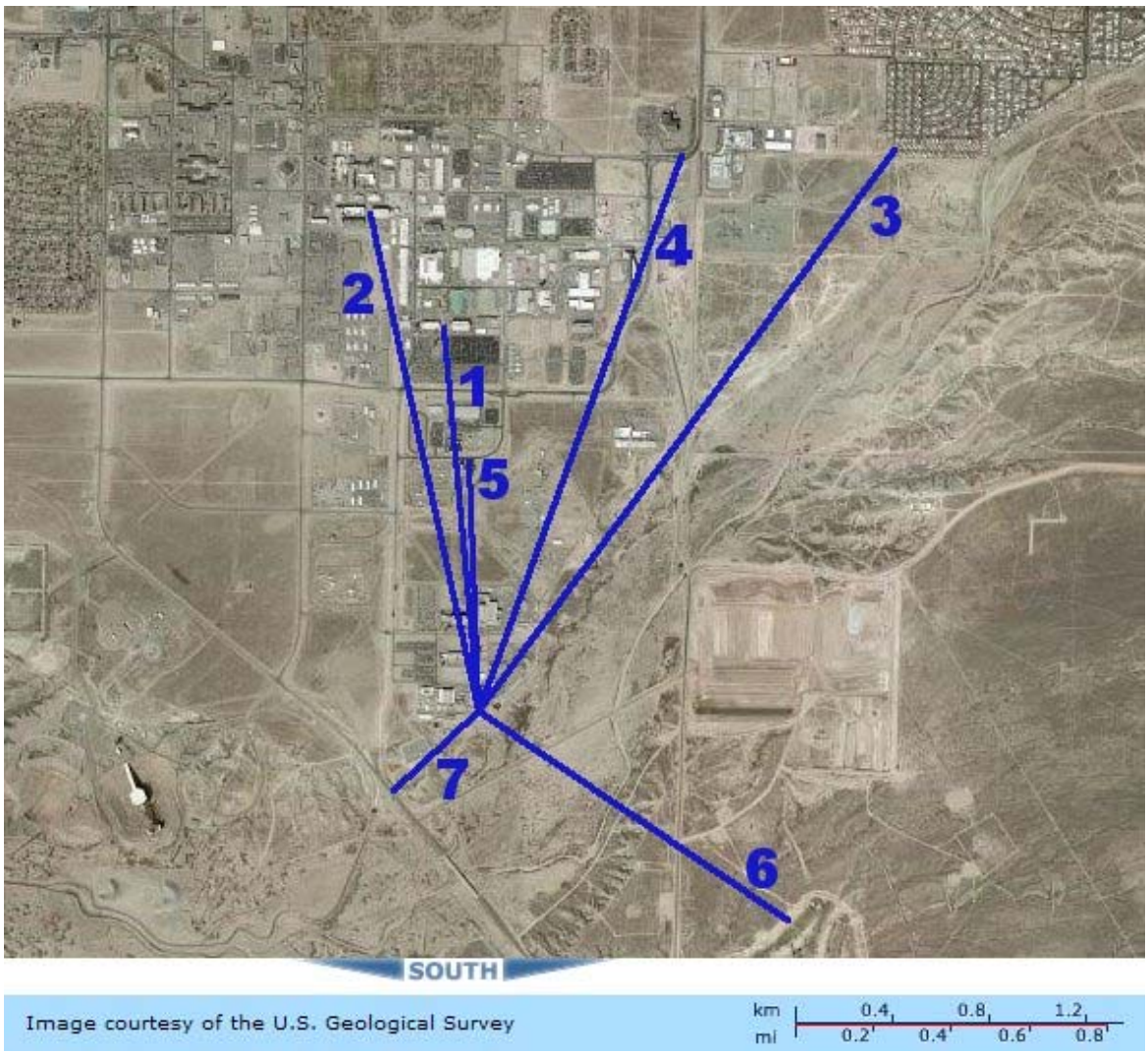

Figure 6-2. Distances to Various Landmarks From the Z-Machine Facility.

Figure 6-3 shows TA-IV with the Z facility at the center of two concentric circles 400 m and 500 m in radius. The 500 m radius circle just touches Pennsylvania Avenue and includes all of the buildings in TA-IV. It does not encompass any portion of TA-I, TA-II, the golf course, pole-line road, or other close proximity base site. This may be a reasonable exclusion boundary that could be well controlled in the event of an emergency.

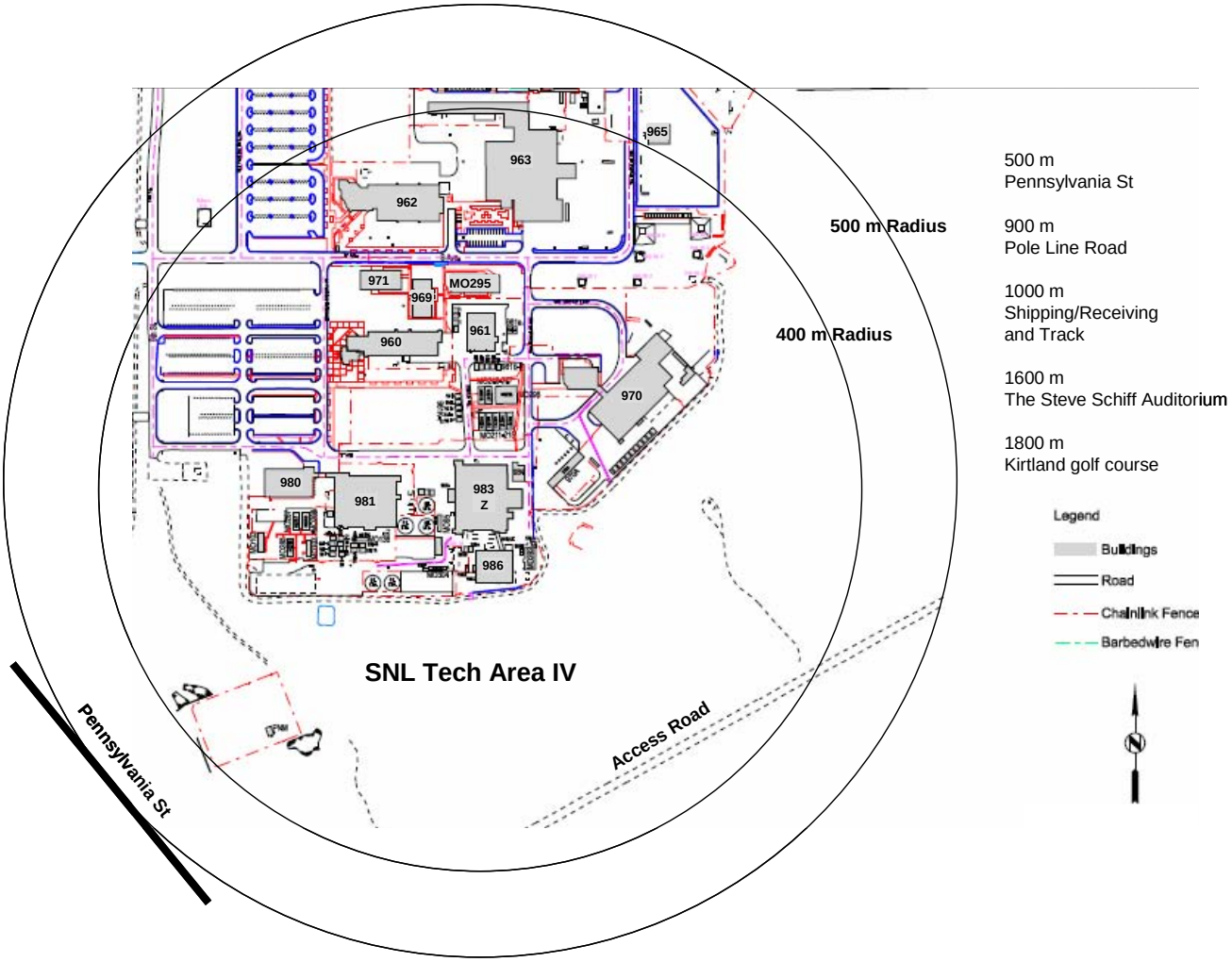

Figure 6-3. Proposed Exclusion Boundary for TA-IV.

6.2 Worker, Collocated Worker, and Member of the Public

For the purpose of this report, a worker is defined as a person who would be located within the site boundary of the facility during operations. A collocated worker is a worker who would be outside of the site, but permanently reside in a nearby building or high bay. A member of the public would be a person who could be living nearby or have access to public and private roads and other facilities.

In the event of a hypothetical catastrophic nuclear accident, it is highly desirable that workers and collocated workers be protected. This protection is ensured by making every effort to have a

well designed and robust reactor system with inherent and automatic shutdown systems, trained and certified reactor operating personnel, trained workers at the facility, and a well managed emergency plan.

The same holds true for members of the public, with the additional requirement that dose estimates be calculated for a hypothetical maximally exposed individual. This person is a member of the public that receives the highest dose at or beyond the exclusion boundary during the passage of the airborne radioactive plume generated as a result of a hypothetical accident. As the plume passes the individual, the individual could receive a radiation dose due to both immersion within the plume and inhalation from breathing the plume. The total effective dose equivalent (TEDE) to the whole body is calculated at the location that includes the dose due to immersion and inhalation from the passing airborne plume of radioactive material. In accordance with DOE-STD-3009-94, slow-developing dose pathways such as the ingestion of contaminated food, water supply contamination, or the inhalation of resuspended material are not included in the calculation. Direct exposure from the radioactive plume is included, but radioactive material deposited on the ground causing direct exposure is not included. The inhalation dose includes direct exposure from the material while in the lung as well as the 50-year committed effective dose equivalent (CEDE) from material remaining in the lung or passing into the body organs.

6.3 Evaluation Guideline

An evaluation guideline is a TEDE value established by the DOE that is used to judge the risk associated with a hypothetical radiological accident. If the calculated dose at the exclusion boundary approaches this value, then more engineered safety features, identified as safety-class structures, systems, and components (SSCs), are required in the design, or a larger exclusion boundary is required. Change Notice 2 to DOE-STD-3009-94 (DOE 2002b) mandates a TEDE of 25 rem (0.25 Sv) at the exclusion boundary for the evaluation guideline. This value is also consistent with the NRC requirement established in 10 CFR 50.67.

6.4 Methodology

DOE-STD-3009-94 requires that estimates of dose consequences be made for comparison with the evaluation guideline. The basic analytical models use a Gaussian plume dispersion model to determine the downwind dose as the plume is transported from the source to the receptor. The basic form of this equation for a ground release of radioactive isotope *i* is as follows (RG 1.145):

$$TEDE_i = RS_i \left[(BR\ CEDE_i) + DC_i \right] \frac{\chi}{Q}$$

where

$TEDE_i$ = Total effective dose equivalent for isotope *i* (rem or Sv),

RS_i = Source term released of isotope *i* (Ci or Bq),

BR = Average breathing rate of receptor (3×10^{-4} m^3/s),

$CEDE_i$ = Committed effective dose equivalent from inhalation for isotope *i* (rem/Ci or Sv/Bq),

DC_i = Dose coefficient for air submersion for isotope *i* (rem-m^3/Ci-s or Sv-m^3/Bq-s)

$$\frac{X}{Q}\ (Chi\ over\ Q) = \frac{1}{\pi\, U\, \sigma_y\, \sigma_z}\ (s/m^3)$$

U = wind speed (m/s),

σ_y = Standard deviation in the crosswind concentration as a function of the atmospheric stability class and downwind distance (m),

σ_z = Standard deviation in the vertical concentration as a function of atmospheric stability class and downwind distance (m).

The lower the wind speed, the greater the concentration of the isotope i at the receptor. The value for the standard deviation is a function of the atmospheric stability class and the downwind distance from the source. Directional wind data and atmospheric stability classes are used to determine the appropriate values for the wind speed and the standard deviations.

A number of computer codes have been written to evaluate the downwind dose for both continuous releases and puff source-term releases. For this analysis, two codes were used to estimate the downwind dose for a ZEDNA hypothetical accident in TA-IV. The Melcor Accident Consequence Code System Version 2 (MACCS2) computer model (Chanin and Young, 1997) was used in the form of an isotopic database as a function of downwind distance. This database was developed for TA-V nuclear facilities (Naegeli, 2003) and is used exclusively for calculating release estimates in the nuclear facilities documented safety analysis. The assumption in using this database is that the directional wind data and atmospheric stability classes for TA-IV are similar to TA-V. This is believed to be true since the two areas are in relatively close proximity to each other.

The other method uses the PAVAN code (Bander, 1982) and wind rose data from the meteorological tower near TA-IV to determine the Chi over Q (X/Q) dispersion coefficient values and the directional dependent maximum values over different time spans. This code allows for the maximum dose as a function of direction and distance to be calculated using actual wind rose data from the site.

The MACCS results include the dose conversion from Ci or Bq to rem or Sv. The PAVAN code uses the X/Q values calculated with the $CEDE_i$ and DC_i to determine the dose. The values for the $CEDE_i$ and DC_i for individual isotopes are found in the Federal Guidance Report 11 (Eckerman, et al., 1989), and Federal Guidance Report 12 (Eckerman and Ryman, 1993), respectively.

6.5 Source Term

For this analysis, only fission products are assumed to be released from ZEDNA in a hypothetical accident. The uranium and other activated materials in the reactor will not contribute significantly to the overall dose estimate. Experiments containing plutonium, tritium or other radioactive materials will not be considered in this analysis, although these materials could contribute overwhelmingly to the dose estimate. For example, a plutonium experiment that was accidentally overheated could cause a large downwind dose effect. The tritium included in the D-T ICF source is also not included in the analysis, but will have a small downwind dose effect. In a full documented safety analysis, the downwind dose contribution from experiments would be required to be analyzed. For this report, we are only concerned about the reactor source term, which is dominated by the fission product inventory.

The quantity of airborne fission products that could leave the Z facility in the event of an accident is referred to as the source term, or release source term (RS). This quantity is dependent on the specific accident in question and other factors, such as decontamination factors in the building ventilation. In the context of DOE-STD-3009-94, as applied to a reactor facility, the airborne release source term can be expressed as:

$$RS = \sum_i RS_i$$

and

$$RS_i = MAR_i \times DR_i \times ARF_i \times RF_i \times LPF_i \times DF_i \qquad (15.2)$$

where

RS = release source term - total source term released from the facility (Ci or Bq),

RS_i = the source term released from the facility of isotope i (Ci or Bq),

MAR_i = material at risk - total inventory of isotope i in the reactor that could potentially be released,

DR_i = damage ratio – the fraction of MAR_i that is available for release from the reactor fuel – e.g. the fraction of fuel melt,

ARF_i = airborne release fraction – the fraction of the released inventory of isotope i that is airborne,

RF_i = respirable fraction – the fraction of isotope i that is respirable,

LPF_i = leak path factor – the fraction of isotope i that is not plated out or retained in ventilation filters on the building,

DF_i = decay factor – the fraction of isotope i that is not decayed prior to release from the facility.

For purposes of this analysis, all releases will be assumed to be unmitigated. The following assumptions apply:

1) No credit is taken for the ventilation system, including filters or plate-out within the building (i.e., $LPF_i = 1.0$).
2) The decay, within the facility, of short-lived radionuclides generated in the accident is ignored (i.e., $DF_i = 1.0$). However a 10 minute decay will be assumed in calculating the radioisotope inventory.
3) The ARF_i and RF_i will be taken as unity (i.e., $ARF_i = RF_i = 1.0$).
4) For fission products, DR_i will be taken to mean that fraction of the radionuclide, *i*, inventory released from the parent material.

In summary, for fission products,

$$RS_i = MAR_i \times MRF_i$$

where MRF_i is the fraction of the released inventory of isotope, *i*, that is airborne and respirable.

For all accidents that involve the reactor, it was assumed that the reactor has been operating in the pulse mode for 30 days prior to the accident. The reactor is assumed to have pulsed every day at 25 MJ per pulse. In order to determine the fission product pre-accident inventory, a power level of 300 W (equivalent to 25 MJ divided by 24 hours per day and 3600 seconds per hour) was assumed over a 29 day period with a 24 hour decay period leading up to the accident condition. The inventory for a 25 MJ pulse was also calculated with a 10 minute decay period. The pulse inventory was then scaled appropriately to reflect the amount of fission energy in the accident event. The fission product inventory was calculated using the computer code ORIGEN2 (Croff 1983). The calculated fission product inventory for the 25 MJ pulse with a 10 minute decay and the 300 W operation for 29 days with a 24 hour decay is included in Appendix A. This inventory represents the MAR_i values used in determining the source term, RS_i.

For sufficient fission energy release in a reactor accident, a portion of the fuel may be melted. In the absence of vaporization, such a melted region would be located near the center of the fuel mass. For a fuel region driven into a molten state (greater than approximately 1150^{o}C), it is expected that essentially all of the solid-species and non-volatile fission products would be retained in the melt. Furthermore, a significant fraction of the volatile (halogens), semi-volatile (selenium, cesium, tellurium, ruthenium) and the noble gas (xenon, krypton) species would also be expected to be retained.

Some NRC-proposed data for the release of fission products from melting (greater than approximately 2860^{o}C) oxide fuel in a pressurized water reactor (PWR) is given in DOE-HDBK-3010-94. The release fractions for noble gases and halogens are given as 0.95 and 0.22, respectively. The release fraction given for semi-volatile species ranges from a high of 0.15 for cesium to a low of 0.002 for lanthanum. DOE-STD-1027, Attachment 1, suggests release fractions of 1.0, 0.5, 0.01, and 0.001, respectively, for gases, volatiles, semi-volatiles, and all other materials, in establishing the hazard category level for facilities.

The time dependence of the release is not given in any of the references, but will vary depending on the diffusion time of the species in the melt. Because the melted fuel region developed in an accident case is surrounded by solid material, it will solidify shortly after the accident and limit the diffusion of any of the fission products.

For purposes of this accident analysis, the MRF_i values suggested in DOE-STD-1027, Attachment 1, and shown in Table 6-1 will be used for both the MACCS and PAVAN calculations. In addition an MRF_i value equal to 1.0 will be used for comparative purposes in the MACCS analysis.

Table 6-1. Material Release Fraction Assumed for Chemical Groups.

Group	Material Release Fraction	Elements
1. Gases	1.0	Nobles
2. Volatiles	0.5	Halogens
3. Semi-Volatiles	0.01	Se, Rb, Sn, Te, Cs
4. Non-Volatiles	0.001	Ge, As, Sr, Y, Zr, Nb, Mo, Tc, Ru, Rh, Pd, Ag, Cd, In, Ba, La, Ce, Pr, Nd, Pm, Sm, Eu

In the event of a hypothetical catastrophic accident, the amount of energy deposited in the fuel is directly proportional to the fission product inventory in the pulse. The amount of energy deposited must be estimated in order to determine the potential source term. It could be envisioned that for some reactivity driven accidents, the fuel melting would be the ultimate shutdown mechanism. Even for these conditions, melting the complete core would not be very likely. Instead, melting in the peak flux regions would be more expected. Table 6-2 shows the energy requirements for various conditions for the full ZEDNA core, with a mass of 1950 kg. The total enthalpy required to reach melt (1130°C), go through melt (heat of fusion), to vaporization, and through vaporization (heat of vaporization) are shown. The scaling factor compared to a 25 MJ nominal pulse is also shown. In order to reach the melting point for the complete ZEDNA core, about 15 times the nominal 25 MJ pulse would be required.

Table 6-2. Enthalpy Required to Melt and Vaporize ZEDNA.

Condition	Enthalpy (J/g)	Energy Required for ZEDNA (1951 kg) (MJ)	Multiple of Nominal 25 MJ Pulse
1. to melt (1130°C)	200.9	392.0	15
2. through melt	259.5	506.3	20
3. to vaporization	694.9	1355.7	54
4. through vaporization	2570.2	5014.3	200

For this analysis, it will be assumed that a hypothetical, worst-case accident could include a pulse with an energy deposition 15 times the nominal 25 MJ operation. This is consistent with the accident scenario results presented in Chapter 5. This result is believed to be a bounding condition for the ZEDNA.

6.6 Downwind Dose Results Summary

The downwind dose results are presented for the MACCS database and the PAVAN calculations. The MACCS results are calculated using the source term inventory included in Appendix A with the release fractions and MACCS database dose conversion factors included in Appendix B. The PAVEN results are calculated using the same source term inventory included in Appendix A, the X/Q values calculated using PAVAN in Appendix C, and the $CEDE_i$ and DC_i values from the Federal Guidance Reports 11 and 12.

The MACCS results are shown in Table 6-3 using the material release fractions in Table 6-1, and Table 6-4 using a material release fraction of one. Results were analyzed for downwind distances of 0.35 to 0.55 km, 0.95 to 1.05 km, and 1.30 to 1.40 km. The results show that using the release fractions from Table 6-1, the downwind dose for a 15 times nominal pulse inventory is 0.82 rem at the proposed exclusion boundary of 500 m. The dose decreases by more than a factor of 2.5 at 1 km, and a factor of 4 at 1.35 km. The dose is dominated by the fission product inventory generated in the accident initiating pulse. The dose fraction attributed to the accident initiating pulse is more than 25 times greater than that from the fission product build up from previous operations.

Table 6-4 shows the results if all of the inventory is released from the reactor. These results are about a factor of 10 greater than the results using the more realistic release fractions. Releasing all of the inventory is not realistic but is presented to inform the reader on what the upper bound dose could be.

The PAVAN results are shown in Table 6-5 using the material release fractions in Table 6-1. Downwind dose estimates are presented for 0.1 km, 0.5 km, and 1.6 km. These values represent the possible site boundary, exclusion boundary, and distance to the Steve Schiff auditorium, respectively. The results show that using the release fractions from Table 6-1, the downwind

dose for a 15 times nominal pulse inventory is 15.5 rem at the proposed site boundary of 100 m. The dose at the proposed exclusion boundary of 500 m is 1.03 rem, which is close to the value found using MACCS. The dose estimate at the Steve Schiff auditorium is 0.19 rem. Just as for MACCS, the PAVAN dose result is dominated by the fission product inventory generated in the accident initiating pulse. The dose fraction attributed to the accident initiating pulse is more than 50 times greater than that from the fission product build up from previous operations.

Table 6-3. Downwind Dose Estimates Using MACCS and Material Release Fractions.

Condition	Dose (Rem) at 0.35 – 0.55 km	Dose (Rem) at 0.95– 1.05 km	Dose (Rem) at 1.30 – 1.40 km
Pulse 25 MJ with 10 min decay	0.055	0.021	0.013
15 x Pulse 25 MJ with 10 min decay	0.82	0.31	0.20
300 W for 29 days with 1 day decay	0.030	0.0058	0.0042

Table 6-4. Downwind Dose Estimates Using MACCS Assuming Complete Release.

Condition	Dose (Rem) at 0.35 – 0.55 km	Dose (Rem) at 0.95– 1.05 km	Dose (Rem) at 1.30 – 1.40 km
Pulse 25 MJ with 10 min decay	0.56	0.14	0.082
15 x Pulse 25 MJ with 10 min decay	8.42	2.09	1.22
300 W for 29 days with 1 day decay	0.30	0.070	0.042

Table 6-5. Downwind Dose Estimates Using PAVAN and Material Release Fractions.

Condition	Dose (Rem) at 0.1 km W	Dose (Rem) at 0.5 km SW	Dose (Rem) at 1.6 km N
Pulse 25 MJ with 10 min decay	1.04	0.069	0.013
15 x Pulse 25 MJ with 10 min decay	15.5	1.03	0.19
300 W for 29 days with 1 day decay	0.25	0.016	0.0031

These results conclude that the ZEDNA reactor could be sited at the TA-IV Z-machine facility and maintain low downwind dose levels at the site boundary and proposed exclusion boundary in the event of a hypothetical accident. The dose at 500 m using the MACCS and PAVAN results is approximately 1 rem for a hypothetical accident where 15 times the nominal energy is deposited in the fuel as the initiating event for the accident. This result is significantly below the 25 rem evaluation guideline. This result indicates that no safety-class SSCs would be required for the reactor containment or ventilation systems. This analysis did not include any downwind dose estimates associated with experiments that may be performed in ZEDNA. It would be expected that potential accidents using experiments containing plutonium could result in much higher downwind dose results and that these types of experiment capsules could require the use of safety-class SSCs. The downwind dose results presented assumed unmitigated release of the fission products from the containment vessel and building. These results would be much higher than the actual values since the containment vessel and building would maintain filtered exhaust that would allow for plate-out and capture of most of the volatile and semi-volatile elements.

7 Conclusions and Major Issues

FBRs have played a major role in neutron radiation testing over the past decades. However, since these types of reactors require HEU fuel to operate reliably, they are being shutdown due to security costs and protection issues. The SPR-III is the only high-fluence FBR left in the US and is no longer available (since October 2006). If fast, pulsed neutron irradiation testing is required in the future, these capabilities will not exist. LEU fueled reactors are not conducive for pulsed operations. However, an LEU fueled reactor with an external pulsed neutron source (EDNA device) is technically viable in achieving neutron fluences and pulse widths similar to the SPR-III capability. No large EDNA device to perform this task has ever been built. The reason for this is that none were needed while FBRs were available. There are no technical reasons that such a system could not be built and operated reliably. Several types of pulsed neutron sources exist or could be developed to provide a sufficient number of initial source neutrons to reach the SPR-III capabilities. The reactor design is relatively straightforward and can be similar to the SPR-III design except for using LEU fuel. This report has focused on using the ZR machine and a D-T target to produce the initial burst of neutrons. Other device drivers could be envisioned using the same reactor design presented in this report.

An EDNA concept using the ZR machine is technically feasible. Initial scoping calculations show that with the ZEDNA at \$0.80 supercritical and a neutron pulse source of 4×10^{15} 14-MeV neutrons at the top of the core, a neutron fluence and pulse width similar to the SPR-III reactor can be achieved. The previous ZEDNA report (Parma, et al., 2007) focused on the technical feasibility of the ZEDNA concept. This report has provided more details on the operational aspects of a ZEDNA device, the MITL design, hypothetical accident conditions, and downwind dose estimates for hypothetical accidents. The conclusion of this report is that a ZEDNA device can be made to operate safely without undue risk to the public, collocated worker, and worker. Control and shutdown of the reactor is straightforward and can be achieved using standard research reactor instrumentation and control methodologies.

A number of major issues, however, still exist and will require further investigation in order to further the pursuit of a ZEDNA device. These major issues include cost effectiveness, safety basis and approval, and D-T target design and effectiveness in operating an ENDNA-type reactor at the Z facility. A cost estimate was presented in the previous report for the design and construction of the ZEDNA. This initial investment cost, in addition to the operational costs associated with a nuclear facility and the Z machine, must be shown to be reasonable and acceptable by the user community. The downwind dose estimates presented in this report show that hypothetical accidents for the reactor would not pose excessive risk to the public. However, the implications in making TA-IV, or a region therein, the site boundary for a nuclear facility, are uncertain, since it is not a new facility and no facilities within TA-IV are nuclear facilities. The fact that the Z facility would not necessarily be treated as a nuclear facility at all times has additional issues that would be required to be addressed and negotiated with the DOE. Also, to operate the ZEDNA, effectively, a D-T source with an extended MITL would be required, which has yet to be tested. Neutron production performance and shot-to-shot reproducibility are two of several important metrics that must be characterized.

8 References

Parma, E. J.; Coats, R. L.; Dorsey, D. J.; Garde, J. M.; Jaramillo, D. M.; Lipinski, R. J.; Mehlhorn, T. A.; Peters, C. D.; Sinars, D. B.; Smith, D. L.; Suo-Anttila, A. J.; Heames, T. J.; Green, T. C.; *An Externally Driven Neutron Multiplier Assembly Concept Using a Z-Pinch 14-MeV Neutron Source (ZEDNA),* SAND2007-1679, Sandia National Laboratories, Albuquerque, NM, March 2007.

Cipiti, B. B.; Cleary, V. D.; Cook, J. T.; Durbin, S.; Keith, R. L.; Mehlhorn, T. A.; Morrow, C. W.; Olson, C. L.; Rochau, G. E.; Smith, J. D.; Turgeon, M. C.; Young, M. F.; El-Guebaly, L.; Grady, R.; Phruksarojanakun, P.; Sviatoslavsky, I.; Wilson, P.; Alajo, A. B.; Guild-Bingham, A.; Tsvetkov, P.; Youssef, M.; Meier W.; Venneri, F.; Johnson, T. R.; Willit, J. L.; Drennen, T. E.; Kamery, W.; *Fusion Transmutation of Waste: Design and Analysis of the In-Zinerator Concept,* SAND2006-6590, Sandia National Laboratories, Albuquerque, NM, November 2006.

Suo-Anttila, A. J., *Dynamic Reactor Modeling With Application to SPR and ZEDNA,* SAND2007-xxxx, Sandia National Laboratories, Albuquerque, NM, September 2007.

Eckerman, K. F., Wolbarst, A., Richardson, A. C.; *Limiting Values for Radionuclide Intake and Air Concentration and Dose Conversion Factors for Inhalation, Submersion, and Ingestion,* Federal Guidance Report 11, EPA 520/1-88-020, second printing with corrections, Environmental Protection Agency, Washington, DC, 1989.

Eckerman, K. F., Ryman, J. C.; *External Exposure to Radionuclides in Air, Water, and Soil,* Federal Guidance Report 12, EPA 402-R-93-081, Environmental Protection Agency, Washington, DC, 1993.

DOE-STD-3009-94, (Change Notice 2, April 2002), *Preparation Guide for U.S. Department of Energy Nonreactor Nuclear Facility Documented Safety Analyses,* U.S. Department of Energy, Washington, D.C., July 1994.

DOE-HDBK-3010-94, (Change 1, March 2000), *Release Fractions/Rates and Respirable Fractions for Nonreactor Nuclear Facilities,* U.S. Department of Energy, Washington D.C., December 1994.

DOE-STD-1027-92, (Change Notice 1, September 1997), *Hazard Categorization and Accident Analysis Techniques for Compliance with DOE Order 5480.23, Nuclear Safety Analysis Reports*, U.S. Department of Energy, Washington, D.C., December 1992.

Croff, A. G., "ORIGEN2: A Versatile Computer Code for Calculating the Nuclide Compositions and Characteristics of Nuclear Materials," *Nuclear Technology,* 62, 335, 1983.

Chanin, D. I., Young, M. L.; *Code Manual for MACCS2: Volume 1, User's Guide,* SAND97-0594, Sandia National Laboratories, Albuquerque, NM, 1997.

Regulatory Guide 1.145, Rev. 1 (Reissued February 1983), *Atmospheric Dispersion Models for Potential Accident Consequence Assessment at Nuclear Power Plants*, U.S. Nuclear Regulatory Commission, Washington, DC, November 1982.

U.S. Code of Federal Regulations, Title 10, Part 50.67, *Domestic Licensing of Production and Utilization Facilities – Accident Source Term,* Office of the Federal Register, Washington, DC.

Bander, T. J., *PAVAN: An Atmospheric Dispersion Program for Evaluating Design Basis Accidental Releases of Radioactive Materials From Nuclear Power Stations,* Pacific Northwest Laboratory, NUREC/CR-2858, PNL-4413, November 1982.

Naegeli, R. E., *A MACCS2 Single Nuclide Downwind Dose Database for Sandia National Laboratories, Technical Area V,* SAND2003-0883, Sandia National Laboratories, Albuquerque, NM, March 2003.

R. Deola, Private Communication, Sandia National Laboratories, July 2007.

Reuscher, J. A. *Thermomechanical Analysis of Fast Burst Reactors*, Proc. National Topical Meeting on Fast Burst Reactors, Albuquerque, NM, pp. 51-74, January 28-29, 1969.

Reuscher, J. A., "Analysis of Internal Heating Shock Effects in Reactor Fuel Components," *Nuclear Engineering and Design*, **18**, 213, 1972.

MCNP (2003) "MCNP - A General Monte Carlo N-Particle Transport Code, Version 5," LA-UR-03-1987, Los Alamos National Laboratory, Los Alamos, NM, April 2003.

A Appendix – ZEDNA Fission Product Activity

For all accidents that involve the reactor, it was assumed that the reactor has been operating in the pulse mode for 30 days prior to the accident. The reactor is assumed to have pulsed every day at 25 MJ per pulse. In order to determine the fission product pre-accident inventory, a power level of 300 W (equivalent to 25 MJ divided by 24 hours per day and 3600 seconds per hour) was assumed over a 29 day period with a 24 hour decay period leading up to the accident condition. The inventory for a 25 MJ pulse was also calculated with a 10 minute decay period. The pulse inventory was then scaled appropriately to reflect the amount of fission energy in the accident event. The fission product inventory was calculated using the computer code ORIGEN2 (Croff 1983). The calculated fission product inventory for the 25 MJ pulse with a 10 minute decay and the 300 W operation for 29 days with a 24 hour decay is shown in Table A-1. This inventory represents the MAR_i values used in determining the source term, RS_i.

Table A-1. Fission Product Activity Following a ZEDNA Pulse.

Isotope	Activity (Ci) 25 MJ Pulse (10 min decay)	Activity (Ci) 300 W for 29 days (1 day decay)
Gases		
Kr-83m	3.79E-01	5.66E-03
Kr-85	3.03E-06	3.48E-03
Kr-85m	1.23E+01	7.91E-02
Kr-87	7.26E+01	1.31E-05
Kr-88	4.90E+01	2.58E-02
Xe-131m	4.53E-07	5.42E-02
Xe-133	2.66E-03	1.48E+01
Xe-133m	5.74E-03	4.44E-01
Xe-135	1.30E+00	5.73E+00
Xe-135m	2.38E+01	1.94E-01
Xe-138	6.32E+02	0.00E+00
Halogens		
Br-82	1.65E-04	2.68E-04
Br-83	7.60E+00	1.46E-03
Br-84	6.08E+01	6.79E-14
I-130	6.02E-04	2.68E-04
I-131	2.68E-02	1.53E-04
I-132	7.92E-01	6.74E+00
I-133	3.80E+00	9.46E+00
I-134	8.73E+01	7.51E+00
I-135	3.57E+01	4.61E-07

Isotope	Activity (Ci) 25 MJ Pulse (10 min decay)	Activity (Ci) 300 W for 29 days (1 day decay)
Semi-Volatiles		
Se-81	2.12E+01	4.01E-10
Se-81m	1.48E-01	2.71E-10
Se-83	1.78E+01	3.06E-20
Ru-103	1.38E-01	3.22E+00
Ru-105	6.45E+00	6.80E-02
Ru-106	2.56E-03	7.48E-02
Te-125m	2.45E-08	1.58E-04
Te-127	1.55E-03	6.52E-01
Te-127m	4.63E-06	1.62E-02
Te-129	1.49E+00	1.65E-01
Te-129m	9.64E-04	1.59E-01
Te-131	6.67E+01	1.24E-01
Te-131m	3.14E-01	5.50E-01
Te-132	2.23E+00	9.17E+00
Te-133	4.79E+02	1.39E-08
Te-133m	8.50E+01	8.31E-08
Te-134	3.11E+02	6.80E-10
Cs-134	8.55E-08	5.38E-06
Cs-135	8.46E-12	3.76E-07
Cs-135m	3.14E-02	1.31E-11
Cs-136	2.38E-03	3.47E-02
Cs-137	8.23E-04	2.77E-02
Cs-138	1.82E+02	9.73E-13
Other Non-Volatiles		
Ag-109m	1.31E+00	9.43E-02
Ag-111	3.65E-03	1.42E-01
Ag-112	2.03E-02	7.27E-02
As-77	1.45E-02	3.71E-02
Ba-139	9.77E+01	1.03E-04
Ba-140	8.90E-01	1.13E+01
Ba-141	5.46E+02	0.00E+00
Ba-142	6.45E+02	0.00E+00
Cd-115	1.61E-02	8.62E-02
Cd-115m	1.54E-04	4.14E-03
Ce-141	1.55E-03	6.75E+00
Ce-143	2.76E+00	8.70E+00
Ce-144	3.10E-02	8.98E-01
Eu-155	1.37E-05	1.47E-03

Isotope	Activity (Ci) 25 MJ Pulse (10 min decay)	Activity (Ci) 300 W for 29 days (1 day decay)
Eu-156	4.05E-05	4.08E-02
Ge-77	2.45E-02	4.00E-03
In-115m	3.25E-04	9.35E-02
La-140	1.03E-02	1.18E+01
La-141	1.94E+01	2.35E-01
La-142	6.75E+01	3.31E-04
La-143	6.07E+02	0.00E+00
Mo-101	5.53E+02	0.00E+00
Mo-99	3.46E+00	1.11E+01
Nb-95	6.94E-06	1.13E+00
Nb-95m	1.80E-05	2.60E-02
Nb-96	9.49E-04	6.82E-04
Nb-97	3.33E+00	5.48E+00
Nb-97m	1.31E+01	5.16E+00
Nd-147	1.45E-01	4.61E+00
Nd-149	2.30E+01	1.85E-04
Nd-151	4.81E+01	0.00E+00
Pd-109	1.31E+00	9.42E-02
Pm-147	3.44E-07	6.91E-02
Pm-148	5.34E-07	1.46E-05
Pm-148m	2.93E-08	4.58E-06
Pm-149	3.70E-02	2.06E+00
Pm-151	2.64E-01	6.07E-01
Pr-143	5.33E-04	1.03E+01
Pr-144	2.72E-02	8.98E-01
Pr-144m	4.33E-03	1.08E-02
Pr-145	2.71E+01	5.91E-01
Pr-147	3.13E+02	0.00E+00
Rb-86	8.99E-06	1.61E-04
Rb-88	1.89E+01	2.88E-02
Rb-89	4.81E+02	0.00E+00
Rh-103m	1.45E-02	2.90E+00
Rh-105	4.90E-02	2.04E+00
Rh-106	2.56E-03	7.48E-02
Sb-125	6.18E-05	4.35E-03
Sb-126	2.46E-04	3.76E-03
Sb-127	4.94E-02	6.80E-01
Sb-128a	1.91E-01	1.71E-02
Sb-129	7.43E+00	5.22E-02
Sb-130	1.40E+01	1.01E-11

Isotope	Activity (Ci) 25 MJ Pulse (10 min decay)	Activity (Ci) 300 W for 29 days (1 day decay)
Sb-131	2.23E+02	1.02E-18
Sm-151	2.14E-08	6.40E-04
Sm-153	1.12E-01	3.40E-01
Sn-119m	3.38E-06	1.53E-04
Sn-121	8.13E-02	7.44E-02
Sn-123	1.77E-04	4.89E-03
Sn-125	4.94E-03	5.80E-02
Sn-128	2.10E+01	6.51E-08
Sr-89	3.60E-02	3.71E+00
Sr-90	9.52E-04	2.59E-02
Sr-91	2.36E+01	2.45E+00
Sr-92	8.25E+01	3.14E-02
Tc-101	2.68E+02	0.00E+00
Tc-104	2.16E+02	0.00E+00
Tc-99m	5.73E-02	1.06E+01
Y-90	1.70E-04	2.65E-02
Y-91	9.66E-04	4.05E+00
Y-91m	1.80E+00	1.56E+00
Y-92	2.93E+00	4.62E-01
Y-93	1.53E+01	3.09E+00
Y-94	5.69E+02	0.00E+00
Y-95	7.77E+02	0.00E+00
Zr-95	8.35E-02	4.24E+00
Zr-97	1.38E+01	5.45E+00

B Appendix – Downwind Dose Conversion Results Using MACCS

The Melcor Accident Consequence Code System Version 2 (MACCS2) computer model (Chanin and Young, 1997) was used in the form of an isotopic database as a function of downwind distance. This database was developed for TA-V nuclear facilities (Naegeli, 2003) and is used exclusively for calculating release estimates in the nuclear facilities documented safety analysis. The assumption in using this database is that the directional wind data and atmospheric stability classes for TA-IV are similar to TA-V. This is believed to be true since the two areas are in relative close proximity to each other. Table B-1 shows a portion of this database for fission product isotopes and downwind distances of 0.35 m to 0.55 m, 0.95 km to 1.05 km, and 1.30 km to 1.40 km. This table presents the results for a ground release (no stack) of the source term, which is conservative. The downwind dose TEDE at the receptor is found by multiplying each value by the corresponding isotope released from the facility.

Table B-1. Downwind Dose Conversion Using MACCS – Ground Release.

Isotope	Dose (Rem/Ci) at 0.35 – 0.55 km	Dose (Rem/Ci) at 0.95– 1.05 km	Dose (Rem/Ci) at 1.30 – 1.40 km
Gases			
Kr-83m	5.69E-10	2.98E-10	2.24E-10
Kr-85	4.58E-08	2.52E-08	1.99E-08
Kr-85m	2.98E-06	1.51E-06	1.14E-06
Kr-87	1.52E-05	7.98E-06	5.92E-06
Kr-88	5.34E-05	2.98E-05	2.26E-05
Xe-131m	1.52E-07	8.27E-08	6.42E-08
Xe-133	6.03E-07	3.25E-07	2.52E-07
Xe-133m	5.58E-07	2.98E-07	2.32E-07
Xe-135	4.57E-06	2.52E-06	1.99E-06
Xe-135m	6.45E-06	2.58E-06	1.37E-06
Xe-138	3.95E-05	1.96E-05	1.24E-05
Halogens			
Br-82	7.05E-04	1.21E-04	1.01E-04
Br-83	1.74E-05	3.40E-06	2.14E-06
Br-84	1.07E-04	2.78E-05	1.19E-05
I-130	8.72E-04	2.09E-04	1.08E-04
I-131	7.05E-03	1.19E-03	9.97E-04
I-132	3.20E-04	7.66E-05	5.11E-05
I-133	1.09E-03	3.09E-04	1.31E-04
I-134	2.13E-04	5.30E-05	3.16E-05
I-135	5.07E-04	1.09E-04	7.15E-05

Isotope	Dose (Rem/Ci) at 0.35 – 0.55 km	Dose (Rem/Ci) at 0.95– 1.05 km	Dose (Rem/Ci) at 1.30 – 1.40 km
Semi-Volatiles			
Se-81	3.35E-06	7.45E-07	3.34E-07
Se-81m	1.74E-05	3.38E-06	2.14E-06
Se-83	1.07E-04	2.29E-05	1.17E-05
Ru-103	2.01E-03	4.76E-04	2.20E-04
Ru-105	2.05E-04	5.11E-05	3.03E-05
Ru-106	1.01E-01	2.15E-02	1.11E-02
Te-125m	1.13E-03	3.25E-04	2.05E-04
Te-127	6.91E-05	1.17E-05	7.85E-06
Te-127m	4.17E-03	1.04E-03	5.40E-04
Te-129	2.05E-05	5.03E-06	2.21E-06
Te-129m	5.04E-03	1.08E-03	7.05E-04
Te-131	1.03E-04	2.10E-05	1.07E-05
Te-131m	1.29E-03	3.37E-04	2.11E-04
Te-132	2.05E-03	5.08E-04	3.02E-04
Te-133	3.37E-05	1.00E-05	5.12E-06
Te-133m	3.02E-04	7.10E-05	3.31E-05
Te-134	2.01E-04	5.07E-05	3.02E-05
Cs-134	1.01E-02	2.15E-03	1.11E-03
Cs-135	9.87E-04	2.12E-04	1.09E-04
Cs-135m	1.10E-04	3.13E-05	2.00E-05
Cs-136	1.96E-03	4.38E-04	2.20E-04
Cs-137	7.05E-03	1.19E-03	9.97E-04
Cs-138	1.15E-04	3.24E-05	2.06E-05
Other Non-Volatiles			
Ag-109m	3.20E-09	5.12E-10	1.86E-10
Ag-111	1.08E-03	3.07E-04	1.21E-04
Ag-112	2.09E-04	5.20E-05	3.06E-05
As-77	2.07E-04	5.16E-05	3.05E-05
Ba-139	3.26E-05	7.63E-06	5.06E-06
Ba-140	7.70E-04	2.02E-04	1.05E-04
Ba-141	5.02E-05	1.04E-05	5.32E-06
Ba-142	5.73E-05	1.12E-05	7.35E-06
Cd-115	9.20E-04	2.10E-04	1.09E-04
Cd-115m	8.72E-03	2.08E-03	1.08E-03
Ce-141	1.74E-03	4.00E-04	2.18E-04
Ce-143	7.22E-04	1.51E-04	1.02E-04
Ce-144	7.36E-02	1.89E-02	1.03E-02
Eu-155	8.40E-03	2.05E-03	1.07E-03
Eu-156	3.07E-03	7.28E-04	3.39E-04

Isotope	Dose (Rem/Ci) at 0.35 – 0.55 km	Dose (Rem/Ci) at 0.95– 1.05 km	Dose (Rem/Ci) at 1.30 – 1.40 km
Ge-77	3.43E-04	1.00E-04	5.24E-05
In-115m	5.04E-05	1.08E-05	7.06E-06
La-140	1.10E-03	3.16E-04	2.01E-04
La-141	1.07E-04	3.01E-05	1.17E-05
La-142	3.09E-04	7.38E-05	4.18E-05
La-143	1.12E-05	3.05E-06	1.14E-06
Mo-101	5.34E-05	1.10E-05	7.24E-06
Mo-99	8.40E-04	2.05E-04	1.06E-04
Nb-95	1.09E-03	3.12E-04	1.72E-04
Nb-95m	5.08E-04	1.09E-04	7.14E-05
Nb-96	8.72E-04	2.08E-04	1.08E-04
Nb-97	7.59E-05	2.01E-05	1.05E-05
Nb-97m	1.36E-06	2.56E-07	1.19E-07
Nd-147	1.11E-03	3.20E-04	2.03E-04
Nd-149	8.74E-05	2.08E-05	1.07E-05
Nd-151	3.08E-05	7.06E-06	3.18E-06
Pd-109	2.09E-04	5.23E-05	3.07E-05
Pm-147	7.70E-03	2.02E-03	1.05E-03
Pm-148	2.20E-03	5.29E-04	3.12E-04
Pm-148m	5.08E-03	1.08E-03	7.09E-04
Pm-149	5.94E-04	1.14E-04	7.50E-05
Pm-151	3.78E-04	1.02E-04	5.30E-05
Pr-143	1.39E-03	3.35E-04	2.12E-04
Pr-144	7.57E-06	1.17E-06	7.49E-07
Pr-144m	2.04E-06	5.98E-07	3.23E-07
Pr-145	1.11E-04	3.16E-05	2.00E-05
Pr-147	3.08E-05	7.05E-06	3.17E-06
Rb-86	1.10E-03	3.15E-04	2.01E-04
Rb-88	3.27E-05	7.45E-06	3.62E-06
Rb-89	7.24E-05	1.21E-05	9.40E-06
Rh-103m	1.01E-06	2.10E-07	1.08E-07
Rh-105	2.05E-04	5.11E-05	3.02E-05
Rh-106	1.04E-07	1.22E-08	4.00E-09
Sb-125	5.08E-04	1.09E-04	7.16E-05
Sb-126	1.12E-03	3.23E-04	2.05E-04
Sb-127	6.11E-04	1.15E-04	7.57E-05
Sb-128a	5.06E-05	1.03E-05	5.17E-06
Sb-129	3.13E-04	7.49E-05	5.00E-05
Sb-130	2.20E-04	5.31E-05	3.15E-05
Sb-131	1.10E-04	3.14E-05	2.01E-05

Isotope	Dose (Rem/Ci) at 0.35 – 0.55 km	Dose (Rem/Ci) at 0.95– 1.05 km	Dose (Rem/Ci) at 1.30 – 1.40 km
Sm-151	6.11E-03	1.15E-03	7.55E-04
Sm-153	3.79E-04	1.02E-04	5.29E-05
Sn-119m	1.08E-03	3.09E-04	1.22E-04
Sn-121	1.02E-04	2.19E-05	1.13E-05
Sn-123	6.91E-03	1.18E-03	9.04E-04
Sn-125	3.10E-03	7.38E-04	3.41E-04
Sn-128	2.36E-04	5.87E-05	3.23E-05
Sr-89	1.09E-03	3.12E-04	1.71E-04
Sr-90	5.04E-02	1.08E-02	7.05E-03
Sr-91	3.23E-04	9.64E-05	5.22E-05
Sr-92	3.05E-04	7.29E-05	3.40E-05
Tc-101	1.10E-05	2.71E-06	1.11E-06
Tc-104	7.55E-05	2.02E-05	1.03E-05
Tc-99m	2.27E-05	5.39E-06	3.19E-06
Y-90	1.50E-03	3.38E-04	2.15E-04
Y-91	1.02E-02	2.17E-03	1.11E-03
Y-91m	5.07E-05	1.07E-05	7.10E-06
Y-92	2.01E-04	4.60E-05	2.19E-05
Y-93	4.48E-04	1.05E-04	5.42E-05
Y-94	5.27E-05	1.08E-05	7.11E-06
Y-95	2.21E-05	5.22E-06	3.02E-06
Zr-95	3.14E-03	7.51E-04	4.98E-04
Zr-97	1.04E-03	2.51E-04	1.16E-04

C Appendix – Dispersion Coefficients Calculated Using PAVAN

Wind Rose Data

A meteorological tower has been in place 1 km north of the Z-machine facility in TA-IV for several years. The hourly data from this tower has been made available for the years 2001 through 2005 from SNL (Deola, 2007). The data has been used to generate two wind rose diagrams shown in Figure C-1. A wind rose diagram shows the frequency of the wind speed and direction over a time period. The diagram on the left covers all 24 hrs of each day in the 5 year period. The dominant wind condition is from the east. The wind rose on the right covers the daytime hours from 6 AM until 8 PM. During the period when there would likely be workers in the area, the dominant wind direction is from the west. This is the normal pattern for winds in this area due to the presence of mountains and passes a few miles to the east of the site. This implies that a release would generally go in a direction away from the parking lot, office buildings, and areas where people would normally traverse on the westerly side of the site.

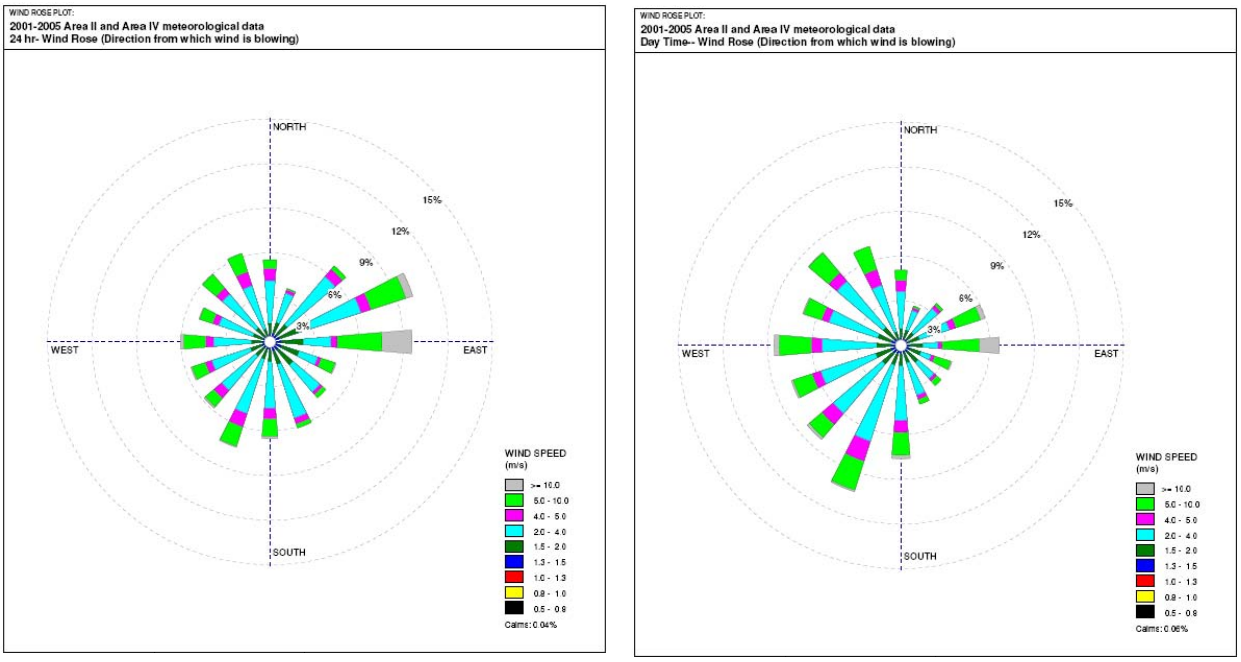

Figure C-1. Wind Rose Displays of TA-IV Meteorological Data.

PAVAN Results

In this analysis, the meteorological data from the site was input into the PAVAN code to determine the site boundary location dilution value as well as a maximum directional independent value. The results from the code as a function of the site boundary are shown in Table C-1. The maximum X/Q at all time intervals occurs in the southerly direction primarily due to the proximity of the fence to the building perimeter. Note that the X/Q in the direction of the parking lot gate is less than 25% of the maximum value. One could alternatively use a

constant site boundary distance of 100 m to perform the analysis in which case the maximum X/Q occurs in the westerly direction, primarily due to the low wind speeds. The maximum X/Q value in the constant 100 m site boundary case is 0.00465 s/m^3, which is half the maximum value given in the Table C-1.

Table C-1. Site Boundary Atmospheric Dilution Coefficients (s/m3)

SECTOR	DISTANCE (m)	0 - 2 HOURS	0 - 8 HOURS	8 - 24 HOURS	1 - 4 DAYS	4 - 30 DAYS
N	235	8.47E-04	4.47E-04	3.24E-04	1.62E-04	5.98E-05
NNE	227	7.54E-04	3.95E-04	2.85E-04	1.41E-04	5.15E-05
NE	298	5.16E-04	2.65E-04	1.89E-04	9.17E-05	3.24E-05
ENE	189	8.48E-04	4.51E-04	3.29E-04	1.66E-04	6.21E-05
E	97	1.76E-03	9.81E-04	7.33E-04	3.89E-04	1.57E-04
ESE	82	2.52E-03	1.41E-03	1.05E-03	5.56E-04	2.23E-04
SE	63	7.14E-03	3.75E-03	2.71E-03	1.35E-03	4.95E-04
SSE	68	1.18E-03	6.26E-04	4.55E-04	2.27E-04	8.41E-05
S	62	9.27E-03	4.72E-03	3.37E-03	1.62E-03	5.65E-04
SSW	80	6.00E-03	3.21E-03	2.35E-03	1.19E-03	4.51E-04
SW	101	4.40E-03	2.46E-03	1.84E-03	9.78E-04	3.95E-04
WSW	227	1.08E-03	5.99E-04	4.46E-04	2.36E-04	9.44E-05
W	221	1.18E-03	6.29E-04	4.58E-04	2.31E-04	8.61E-05
WNW	149	2.15E-03	1.14E-03	8.24E-04	4.12E-04	1.52E-04
NW	194	1.37E-03	7.41E-04	5.46E-04	2.81E-04	1.08E-04
NNW	255	8.27E-04	4.37E-04	3.18E-04	1.59E-04	5.90E-05

A similar calculation was performed for the Low Population Zone (LPZ) distances from the Z-machine facility. The results of this analysis are shown in Table C-2. In this case the maximum X/Q value is found is in the south westerly direction (0.000308 s/m^3) due to the minimum distance to Pennsylvania Avenue (500 m) used in the calculation.

Table C-2. Low Population Zone Atmospheric Dilution Coefficients (s/m3)

SECTOR	DISTANCE (m)	0 - 2 HOURS	0 - 8 HOURS	8 - 24 HOURS	1 - 4 DAYS	4 - 30 DAYS	
N	1600	5.80E-05	2.72E-05	1.86E-05	8.18E-06	2.51E-06	Schiff Auditorium
NNE	2500	2.79E-05	1.25E-05	8.39E-06	3.52E-06	1.01E-06	Eubank Gate
NE	3000	2.55E-05	1.10E-05	7.26E-06	2.93E-06	7.93E-07	4-Hills Housing
ENE	1600	4.06E-05	1.89E-05	1.29E-05	5.62E-06	1.70E-06	
E	1600	2.88E-05	1.38E-05	9.58E-06	4.31E-06	1.37E-06	
ESE	1600	2.87E-05	1.39E-05	9.72E-06	4.44E-06	1.44E-06	
SE	1600	4.85E-05	2.32E-05	1.61E-05	7.22E-06	2.29E-06	
SSE	1800	1.12E-05	5.05E-06	3.39E-06	1.43E-06	4.13E-07	Golf Course
S	1600	6.24E-05	2.97E-05	2.05E-05	9.18E-06	2.89E-06	
SSW	1600	6.34E-05	3.19E-05	2.26E-05	1.08E-05	3.69E-06	
SW	500	3.08E-04	1.74E-04	1.31E-04	7.05E-05	2.90E-05	Pennsylvania Rd
WSW	1600	6.62E-05	3.38E-05	2.41E-05	1.16E-05	4.07E-06	
W	750	1.55E-04	8.20E-05	5.97E-05	3.00E-05	1.11E-05	Wyoming Rd
WNW	1600	6.48E-05	3.17E-05	2.21E-05	1.02E-05	3.33E-06	
NW	10000	1.00E-05	4.25E-06	2.77E-06	1.10E-06	2.89E-07	Downtown
NNW	2100	4.73E-05	2.21E-05	1.51E-05	6.60E-06	2.01E-06	Base Housing

Distribution

1	MS0736	John Kelly, 6770
1	MS0748	Gary Rochau, 6763
1	MS0748	Benjamin Cipiti, 6763
1	MS1056	Samuel Myers, 1112
1	MS1136	Paul Pickard, 6771
1	MS1136	Curtis Peters, 6771
1	MS1136	Terence Heames, 6771
10	MS1136	Edward Parma, 6771
1	MS1141	Richard Coats, 1383
1	MS1141	Michael Gregson, 1383
1	MS1142	Darren Talley, 1381
1	MS1146	Patrick Griffin, 1384
1	MS1146	Ahti Suo-Anttila, 1384
1	MS1159	James Bryson, 1344
1	MS1167	Frederick Hartman, 1343
1	MS1169	James Lee, 1300
1	MS1178	Finis Long, 1637
1	MS1178	Randall McKee, 1639
1	MS1178	David Smith, 1639
1	MS1179	Mark Hedemann, 1340
1	MS1186	Thomas Mehlhorn, 1674
1	MS1193	Daniel Sinars, 1673
1	MS1415	Charles Barbour, 1120
2	MS9018	Central Technical Files, 8944
2	MS0899	Technical Library, 4536


Sandia National Laboratories